AD

USAAVLABS TECHNICAL REPORT 67-9E

IN-FLIGHT MEASUREMENT OF ROTOR BLADE AIRLOADS, BENDING MOMENTS, AND MOTIONS, TOGETHER WITH ROTOR SHAFT LOADS AND FUSELAGE VIBRATION, ON A TANDEM ROTOR HELICOPTER

VOLUME V

INVESTIGATION OF BLADE STALL CONDITIONS

By

Richard R. Pruyn

April 1968

U. S. ARMY AVIATION MATERIEL LABORATORIES

FORT EUSTIS, VIRGINIA

CONTRACT DA 44-177-AMC-124(T)

VERTOL DIVISION

THE BOEING COMPANY

MORTON, PENNSYLVANIA

Disclaimers

The findings in this report are not to be construed as an official Department of the Army position unless so designated by other authorized documents.

When Government drawings, specifications, or other data are used for any purpose other than in connection with a definitely related Government procurement operation, the United States Government thereby incurs no responsibility nor any obligation whatsoever; and the fact that the Government may have formulated, furnished, or in any way supplied the said drawings, specifications, or other data is not to be regarded by implication or otherwise as in any manner licensing the holder or any other person or corporation, or conveying any rights or permission, to manufacture, use, or sell any patented invention that may in any way be related thereto.

Disposition Instructions

Destroy this report when no longer needed. Do not return it to the originator.

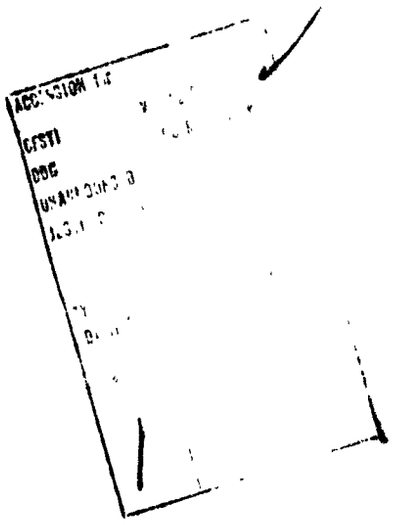

DEPARTMENT OF THE ARMY
U. S. ARMY AVIATION MATERIEL LABORATORIES
FORT EUSTIS, VIRGINIA 23604

This report has been reviewed by the U. S. Army Aviation Materiel Laboratories and is considered to be technically sound. The work was performed under Contract DA 44-177-AMC-124(T) for the purpose of measuring the dynamic air pressures on the blades of a tandem-rotor helicopter and the resulting blade and shaft stresses and fuselage vibrations during flight. The report is published for the dissemination and application of information and the stimulation of ideas.

Task 1F125901A14604
Contract DA 44-177-AMC-124(T)
USAAVLABS Technical Report 67-9E
April 1968

IN-FLIGHT MEASUREMENT OF ROTOR BLADE AIRLOADS, BENDING MOMENTS, AND MOTIONS, TOGETHER WITH ROTOR SHAFT LOADS AND FUSELAGE VIBRATION, ON A TANDEM ROTOR HELICOPTER

VOLUME V

INVESTIGATION OF BLADE STALL CONDITIONS

D8-0382-5

by

Richard R. Pruyn

Prepared by

VERTOL DIVISION
THE BOEING COMPANY
Morton, Pennsylvania

for
U.S. ARMY AVIATION MATERIEL LABORATORIES
FORT EUSTIS, VIRGINIA

BLANK PAGE

SUMMARY

A brief analysis of the tandem rotor dynamic airloads data has been made to isolate the sources of the high dynamic rotor loads which are commonly associated with blade stall. Blade section airload pressure data were reduced to normal force and pitching moment coefficients for this investigation. Blade stall, compressibility, and radial flow effects are shown to contribute to these high dynamic loads. Aerodynamic evidence of blade stall occurs at significantly less severe conditions than those conditions which produce excessive loads.

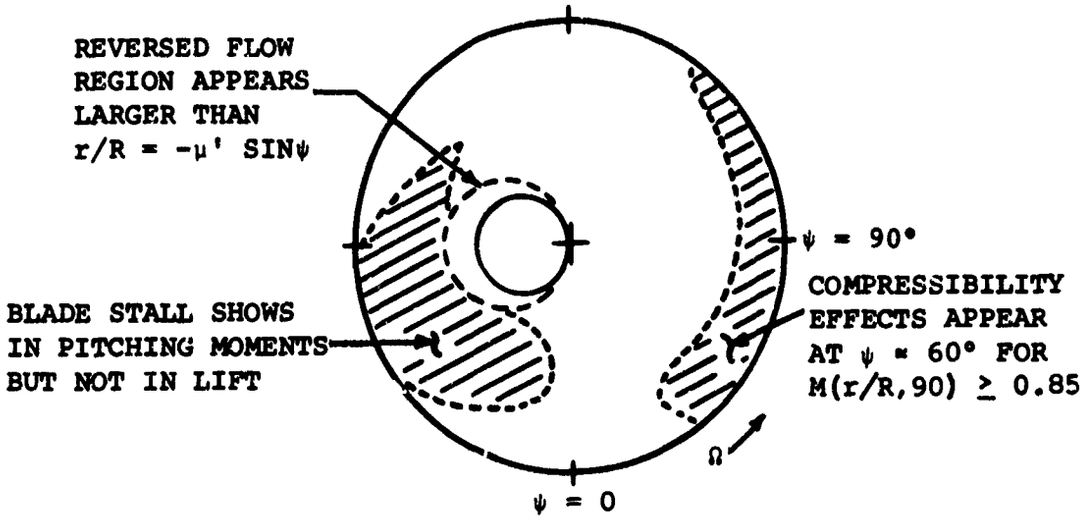

Blade section aerodynamic pitch moment damping is shown to give a positive identification of blade stall. This criterion is required since there is little variation in the blade section lift data which can be attributed to stall. Aerodynamic pitch moment damping is shown to be a predominantly first-harmonic phenomenon and is predicted with reasonable accuracy by potential flow theory for conditions with no stall, small blade section sweep, and small compressibility effects. This damping becomes negative over a portion of the azimuth due to stall.

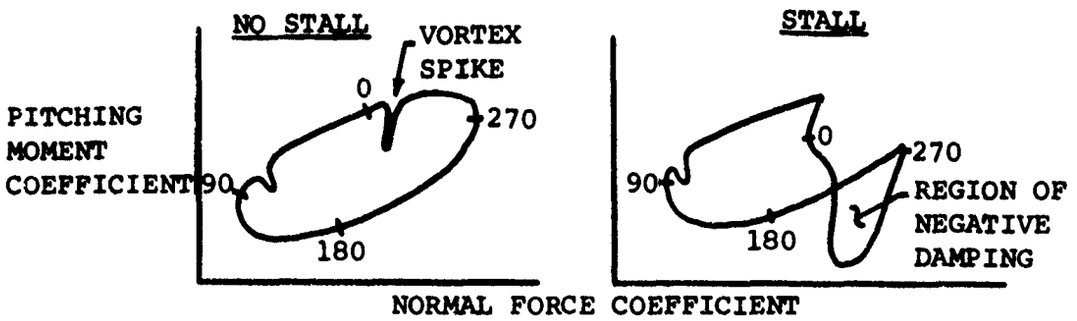

Blade stall effects are shown to be significantly delayed by the local sweep angle produced by the radial component of the local resultant velocity.

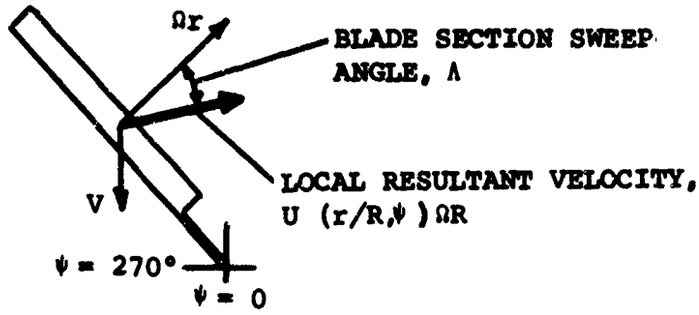

For inboard sections of the blade which experience larger sweep angles, normal force (= lift) coefficients larger than 2.0 were measured with no evidence of stall showing in the pitching moment coefficients. However, there is an indication that sweep also produces an aerodynamic pitch moment instability.

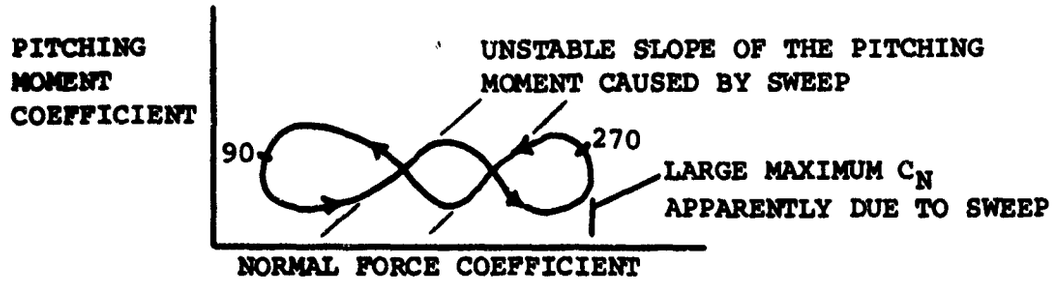

Blade stall indications from the aerodynamic pitch damping data show a complicated relationship to the retreating blade tip angle of attack calculated with the assumption of uniform downwash and rigid blades. Variations in blade stall due to gross weight and rpm changes are not adequately reflected in the calculated angle of attack. This approximate angle of attack has been evaluated in spite of its known inaccuracies since it is convenient and is used in most of the contemporary criteria for blade stall. Establishment of a single value of maximum allowable angle of attack which could be used to ensure that stall will not occur would be excessively restrictive on the operation of the helicopter. The widely used criterion of 14 degrees angle of attack appears to be overly optimistic with most instances of stall occurring at about 10 degrees.

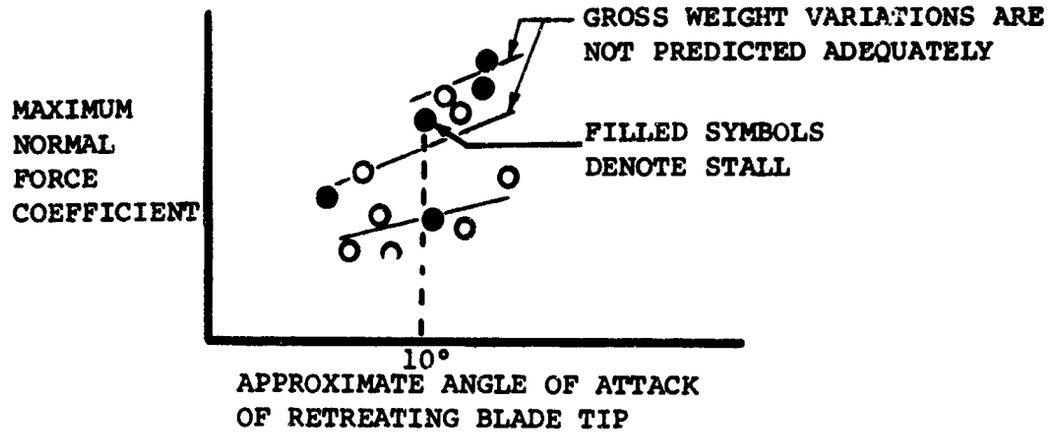

The bottom of scatter of the blade stall test points shows a strong dependence of stall on the local Mach number of the retreating blade sections. Confidence in this relation is somewhat limited by the small amount of data which have been analyzed; however, a greater sensitivity to compressibility of the aft rotor data can be noted. Static airfoil data are shown to give a fair prediction of the Mach number dependence of rotor blade sections. The usefulness of this prediction is limited, since the available rotor theories cannot presently predict the maximum normal force coefficient. It should be noted that increases in rotor rpm apparently can increase the Mach number enough to increase stall even though the thrust coefficient of the rotor is reduced.

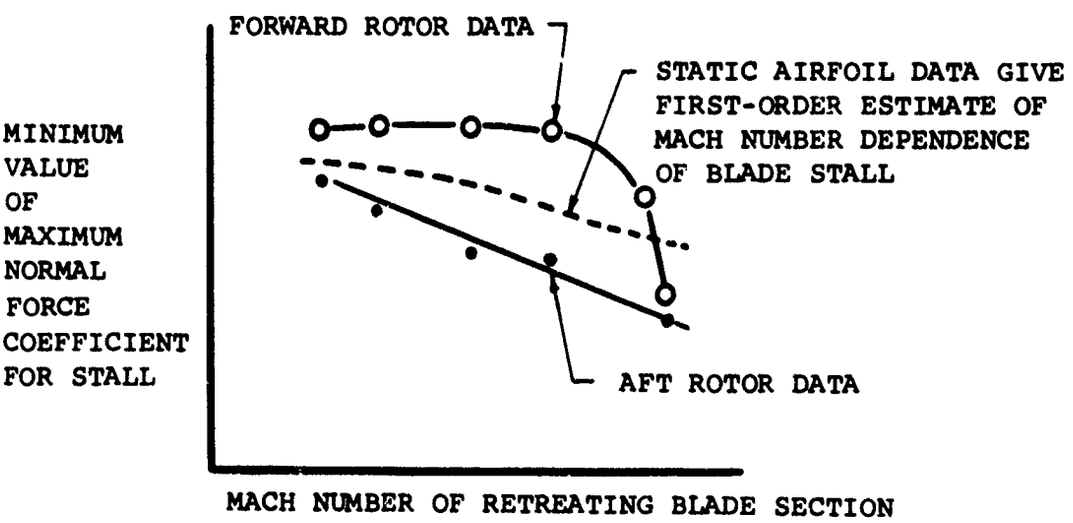

It is suggested that this initial effort be expanded to formulate a reliable stall criterion from the analysis of airloads data. Such a criterion apparently must account for nonuniform downwash, blade bending, and the variations due to blade radius of the following parameters:

1. Maximum angle of attack and possibly the maximum slope of angle of attack with azimuth prior to reaching the maximum angle of attack

2. Local blade sweep angle and the rate of change of sweep

3. Local Mach number of the retreating blade

This criterion can be developed from purely aerodynamic considerations based on the available rotor airloads measurements. Such a pure aerodynamic criterion for stall will be of value, but the practical limitations to rotor operations due to blade and control dynamics should also be considered. Rotor systems can usually tolerate a significant amount of aerodynamic stall.

Compressibility effects are shown to contribute significantly to blade loads. Pitching moment coefficient-normal force coefficient plots show that compressibility produces negative aerodynamic damping on the advancing blade. From a brief study it appears that this phenomenon occurs when the blade section advancing Mach number, M(r/R, 90), exceeds 0.85. Further analysis of all of the available rotor airloads data should be made to define the effects of compressibility.

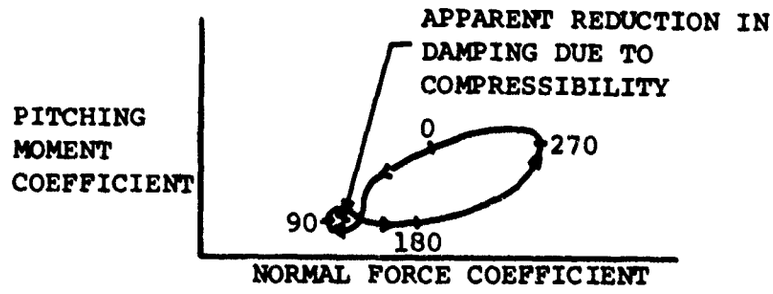

A further effort toward synthesis of airfoil data from rotor airloads measurements has been made as part of this analysis. It was believed that the prediction of the instantaneous angle of attack would be a limiting restraint on this synthesis, so three methods of predicting angle of attack from nonuniform downwash analyses are evaluated in this report. It is shown

that the theoretical quasi-static angle of attack which includes blade bending effects gives a good prediction of the azimuthal variations of the normal force coefficients of the forward rotor. For the aft rotor, the azimuthal variation of the angle-of-attack prediction is shown to be poor. It is suggested that the use of a theoretical angle of attack in the synthesis is unnecessary and that the angle of attack should be estimated from the normal force coefficients. A method of utilizing the airloads data to prepare synthesized airfoil data based on this assumption is outlined.

FOREWORD

This report describes the results of an extension to the Dynamic Airloads Program to obtain data under extreme operating conditions and to isolate the evidence of blade stall from the resulting data. The entire project was performed under Contract DA 44-177-AMC-124(T) through the period from June 1964 to January 1967. The reports covering the basic program consist of four volumes as follows:

Volume	I,	Instrumentation and In-Flight Recording System
Volume	II,	Calibrations and Instrumented Component Testing
Volume	III,	Data Processing and Analysis System
Volume	IV,	Summary and Evaluation of Results

The project was conducted under the technical cognizance of William T. Alexander, Jr., of the Aeromechanics Division of USAAVLABS. The author of this report, Richard R. Pruyn, also served as Dynamic Airloads Project Engineer for The Boeing Company, Vertol Division.

The author acknowledges the aid of F. D. Harris of the Vertol Division for his explanation of the effects of blade sweep and for his suggestion of the normal force coefficient-to-angle of attack relation which led to the aerodynamic damping presentations of this report. Dr. M. I. Young was also of great help for his consultations on blade stall. The Dynamic Airloads Project staff included A. B. Meyer, J. C. Fries, and E. C. Haren when the data evaluation and analysis were performed.

CONTENTS

ILLUSTRATIONS

SYMBOLS

a_o	azimuthal average value of any parameter
A	arbitrary coefficient used in time-dependence study
b	number of blades per rotor
B	arbitrary coefficient used in time-dependence study
c	rotor blade chord, inches
C_d	drag coefficient obtained from two-dimensional airfoil data
C_ℓ	lift coefficient obtained from two-dimensional airfoil data
C_m	pitching moment coefficient obtained from two-dimensional airfoil data
C_{MC}	pitching moment coefficient obtained from the airload pressures and corrected for the mean aerodynamic center shift
C_{MP}	pitching moment coefficient calculated from pressure measurements using theoretical local resultant velocity (uniform downwash-rigid blades)
$C_{MP}(0.25c)$	pitching moment coefficient with respect to the quarter-chord calculated from pressure measurements using theoretical local resultant velocity (uniform downwash-rigid blades)
C_{MPT}	pitching moment coefficient calculated from pressure measurements using tangential component of the blade section velocity, $(r/R + \mu'\sin\psi)\Omega R$
C_n	normal force coefficient obtained from two-dimensional airfoil data
$\overline{C_n}$	azimuthal average value of normal force coefficients obtained from two-dimensional airfoil data

C_{NP}	normal force coefficient calculated from pressure measurements using theoretical local resultant velocity (nonuniform downwash-rigid blades)
$\overline{C_{NP}}$	azimuthal average value of normal force coefficients obtained from pressure measurements
$(C_{NP})MAX$	largest magnitude of the normal force coefficient obtained at a particular radius for a given test point
C_{NPT}	normal force coefficient calculated from pressure measurements using tangential component of the blade section velocity, $(r/R + \mu'\sin\psi)\Omega R$
$\lvert C_{NPT} \rvert_N$	normal force coefficient calculated from the Nth harmonic resultant amplitude of the pressure measurements using the azimuthal average tangential velocity, Ωr
C_P	rotor power coefficient
C_{TW}	thrust coefficient based on run gross weight - for mid-cg, $C_{TW} = RGW/2\rho\pi R^2(\Omega R)^2$
$dC_m/d\alpha$	rate of change of a pitching moment coefficient with respect to angle of attack
$d\Lambda/d\psi$	rate of change of Λ with ψ
f	helicopter equivalent parasite drag area, square feet
h	nondimensional vertical distance between successive loops of the rotor wake vorticity, equal to $(4\pi/cb\Omega)$ (inflow velocity)
$k_{\theta\Omega}$	reduced frequency of an oscillation of the blade about the pitch axis at the natural frequency of the control spring
k_{1V}	reduced frequency of the first harmonic airload oscillation with azimuth based on the forward flight velocity of the helicopter

$k_{1\Omega}$	reduced frequency of the first harmonic airload oscillation with azimuth based on the rotor rotational speed
K_1, K_2	constants obtained from potential flow theory
$\left(\frac{L}{D}\right)_r$	rotor lift-to-effective drag ratio
m	ratio of a frequency of interest to the rotor rotational frequency
M	a local Mach number
$M(r/R, \psi)$	functional notation for the local Mach number at the r/R blade radius and at azimuth position ψ; e.g., M(1.0,270) is the Mach number at r/R = 1.0 and ψ = 270 degrees
N	harmonic number based on rotor rotational frequency
q	dynamic pressure, pounds per square foot
r	distance from the center of rotation to a particular blade station, inches
R	rotor blade tip radius, inches
RGW	run gross weight, pounds
RHDL	region of high dynamic loads
$\lvert S_{A1} \rvert$	longitudinal first harmonic shaft shear to rotor lift ratio; for mid-cg as tested rotor lift was assumed to be one-half of the run gross weight
TPN	test point number
V	resultant velocity, feet per second
α	local angle of attack, degrees
α_{CN}	blade section angle of attack calculated from C_{NP} coefficient using potential flow theory, degrees

$\dot{\alpha}_{CN}, \ddot{\alpha}_{CN}$	first and second time derivatives of α_{CN}, degrees per second and degrees per second^2, respectively
α_{da}	blade section angle of attack calculated from α(SNUD-E) by the addition of an angle-of-attack rate term, degrees
α (NUD-R)	blade section angle of attack calculated assuming nonuniform downwash and rigid blades, degrees
α (SNUD-E)	blade section angle of attack calculated assuming a simplified nonuniform downwash and elastic blades, degrees
$\approx\alpha$ (1.0,270)	approximate angle of attack of the retreating blade tip as calculated assuming uniform downwash and rigid blades
β_{A1}	longitudinal first harmonic blade flapping amplitude with respect to the shaft axis, degrees
β_{A1C}	longitudinal first harmonic blade flapping amplitude with respect to the control axis, degrees
$\Delta\alpha$	apparent error in α(SNUD-E), degrees
θ	blade section pitch angle, degrees
θ_{B1}	longitudinal cyclic blade pitch (longitudinal cyclic trim control on tandem helicopter), degrees
Λ	local blade section sweep angle produced by the radial component of the forward flight velocity of the helicopter, degrees
μ'	rotor advance ratio, calibrated true airspeed of helicopter divided by the rotational tip speed of the rotors
ρ	mass density of air, slugs per cubic foot
σ	rotor solidity, $\sigma = bc/\pi R$

ψ	rotor azimuth angle, measured in direction of rotation from position over the centerline of the helicopter when blade tip is pointing aft
Ω	rotor rotational speed, radians per second
$\frac{\partial \beta_{A1C}}{\partial \mu}$	partial derivative of the longitudinal-first harmonic-control axis blade flapping with respect to the advance ratio
1/rev.,3/rev.,etc.	one per revolution, three per revolution, etc.

Note: A consistent symbol definition has been used in this report to designate the flight which was the source of the data. The symbols used are as follows:

Symbol	Flight Number
◊	384
◺	386
⌂	389
◇	390
△	391
◊	393
◺	394
◇	395
○	397
□	398

INTRODUCTION

Discussions of blade stall apparently must start with a strong reminder that rotor blade stall and the stall of an airplane wing result in greatly different consequences. The buffeting, poor control, and sudden lift loss which the fixed-wing aerodynamicist identifies with stall do not apply to the helicopter. From model testing, the rotor aerodynamicist's point of view is given in reference 6 as, " . . . to . . . the fixed wing aerodynamicist the thought is that stall is in fact a response to boundary layer separation and that visibility of this boundary layer separation is most widely publicized with curves of airfoil lift and drag coefficients versus angle of attack. These barometers of the state of the boundary layer always show a maximum lift coefficient and increase in airfoil drag as 'stall' occurs. The rotary wing aerodynamicist, although familiar with this classical stall background, must determine what the 'response to boundary layer separation' is for a rotor. In short, 'blade stall' has today the connotation of blade lift loss and drag rise; . . . (rotor model test data) . . . indicate that a 'lift stall' did not occur. The profile plus induced power coefficient indicates a drag stall did occur." From a helicopter flight testing point of view, the situation is further masked by the relacive sizes of the parasite drag power and the profile drag power, which make it very difficult to determine the increase in profile power due to stall. Flight testing of helicopters to determine the effects of blade stall has therefore been performed many times with uncertain results. This is due generally to the smoothing nature of rotors and to the gradual onset of the conditions associated with stalling.

Tandem rotor helicopters tend to be difficult to test for blade stall because stall-induced vibration and the expected deterioration of flying qualities are difficult to isolate. The lack of stall vibration is apparently due to the masking of stall-induced vibration by the rotor-airframe-rotor coupling and by vibration absorbers. Flying qualities are not impaired because of the strong longitudinal control characteristics that are obtained from differential collective pitch with the tandem rotor helicopter. Tandem rotor helicopters are therefore flown routinely in blade stall conditions with no apparent deleterious effects, until the dynamic rotor loads approach such magnitudes that the fatigue life of the rotor system components becomes seriously affected. This situation makes the establishment of a blade stall boundary almost

impossible, since the magnitude of the load which can be endured depends upon the design of the component, which can nearly always be changed to increase strength. To avoid this problem, it is suggested that blade stall be considered only as a situation which tends to cause high blade loads, those loads in particular which are at frequencies above the third harmonic, or which increase sharply from the usual square-of-the-advance-ratio trend. These loads apparently are caused by rapidly changing aerodynamic loads of large magnitude, or are due to a reduction of aerodynamic damping which makes the inertia loads more significant. In either case, the cause is aerodynamic in origin and is associated with high angle of attack or rapidly changing angle-of-attack conditions. The analysis of the dynamic airloads measurements presented in this report has been made to define the parameters of this problem.

It is probably fortunate that early attempts at optimizing rotor design, like that of reference 18, were made by rotor aerodynamicists. It is doubly fortunate that these aerodynamicists had inadequate techniques, such as the nonuniform downwash theory, available to define the rotor loads which would have resulted from their optimizations. The helicopter industry would have lost considerable enthusiasm and optimism if this were not the case. More recent rotor optimization studies, like that of reference 14, or the more extensive study of reference 22, have shown the uncertainty that results when rotor loads are considered in the optimization. However, since helicopters are now commonly accepted as proven vehicles, the real practical limitations of rotor loads can now be faced objectively. Rotor optimization for minimum rotor loads is required. Airfoil sections which produce minimum rotor loads with reasonable performance should be developed for rotors. Blade planforms, stiffness and mass distributions, twist distributions, and rotor hub geometries which produce minimum loads should be devised. It is expected that these efforts will indicate rotor designs which can operate at high speed and high lift, under stall conditions, without incurring significant dynamic loads.

DISCUSSION OF THE PROBLEM

As mentioned in the introduction, blade stall investigations can easily digress from an investigation of the practical limitations to the operation of rotors. To avoid this situation, the limitations of rotor performance are discussed and a background of the static airfoil data available to predict this performance is presented. Some of the meager dynamic airfoil section performance data available are presented and discussed.* The general inadequacy of the tools for predicting rotor loads in extreme operating conditions is illustrated.

ROTOR PERFORMANCE LIMITATIONS

It should be emphasized that, while blade stall tends to increase the power required for a rotor, the power increase is generally moderate and does not pose a limitation. This situation is illustrated by the rotor performance data which are available in the literature. Some of these data have been compiled and prepared as lift-to-effective-drag ratios at constant propulsive force coefficient as shown in Figure 1. It should be noted in these data that even the relatively unsophisticated H-21 rotor had a lift-drag ratio of six at an advance ratio of 0.42. This lift-drag ratio is the same as that which would be expected at the normal H-21 operating advance ratio of about 0.23. Since the H-21 rotor performance was quite satisfactory at an advance ratio of 0.23, it should also be satisfactory at any other speed which gives an equal or better lift-drag ratio. Therefore, operation to advance ratios of at least 0.42 appears to be practical from a performance consideration, even with the rotor providing all the propulsion of a relatively high-drag helicopter. With reduced drag this situation improves considerably.

---

* Since this report was written, the lack of dynamic airfoil data was alleviated slightly by the publication of the following paper: Carta, F.O., An Analysis of Stall Flutter Instability of Helicopter Rotor Blades, Paper No. 130 presented at the 23rd Annual National Forum of the American Helicopter Society, May 1967.

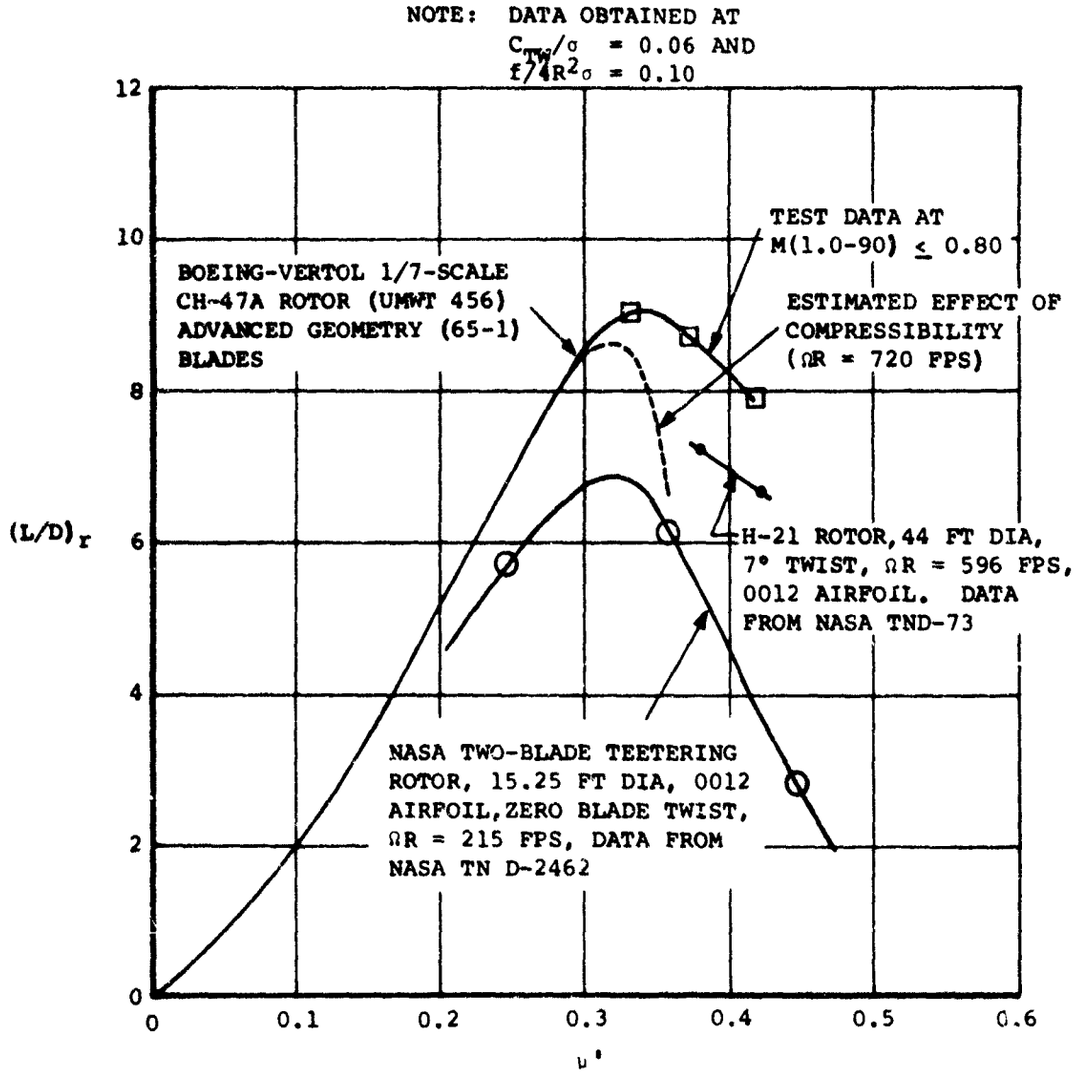

Figure 1. Effect of Advance Ratio on Isolated Rotor Efficiency When Producing Propulsive Force.

Figure 1 also contains advanced geometry model rotor data which reached a lift-drag ratio of nine when operating at advancing tip Mach numbers of less than 0.8. A calculated correction to these data for operation at a constant rotational speed is also shown in the figure and illustrates the serious effects of compressibility on rotor performance. It appears that blade stall losses are much less severe. Since both stall and compressibility produce high rotor loads, it is believed that rotor design efforts should emphasize the minimization of stall effects on rotor loads in combination with reduced rotor speeds to avoid compressibility effects.

STATIC AIRFOIL SECTION PERFORMANCE

The aerodynamic environment of a rotor is neither static nor quasi-static, so that the consideration of static airfoil section performance in rotor stall studies is of extremely limited value. As noted in the introduction to Volume IV of this report, dynamic airfoil tests show that, even for conditions similar to the first harmonic variations of the rotor environment, time-dependent effects on airfoil performance are very significant. However, the available dynamic airfoil data are extremely limited and considerable static data have been compiled so that some discussion is warranted.

The airfoil section of the CH-47A blades as tested in this program was an NACA 0012 which was increased in chord with a symmetrical leading edge cap and a flat plate trailing edge extension. Typical performance data for this airfoil section measured at a Mach number such as would be expected for a section of a retreating blade are shown in Figure 2. It should be noted that these data were obtained from semispan wing wind tunnel testing and should be corrected for the loss of maximum lift coefficient due to wing tip effects. An increase of about 10 percent of the measured maximum lift coefficient is apparently required for truly two-dimensional static airfoil data; however, this correction to the data has not been made due to the overshadowing effects of the rotor dynamic environment. Within these limitations a stall criterion for defining the likelihood of a change in blade loads with angle of attack is illustrated in Figure 3. Two criteria for a boundary of pitching moment divergence at stall are shown as a function of Mach number. Due to the unknowns produced by the dynamic environment, the boundaries suggested by these data are probably not applicable to rotors; however, the strong dependence on local Mach number will be shown to apply to the rotor case. It is

NOTES:
1. DATA OBTAINED WITH FULL-SIZE SEMISPAN (ASPECT RATIO 6) MODEL AT M=0.405, REFERENCE 8
2. THE CH-47A AIRFOIL IS A 0011-1.43 SECTION.
3. C_m CURVE WAS SHIFTED -0.002 FOR C_m =0 AT C_ℓ=0.

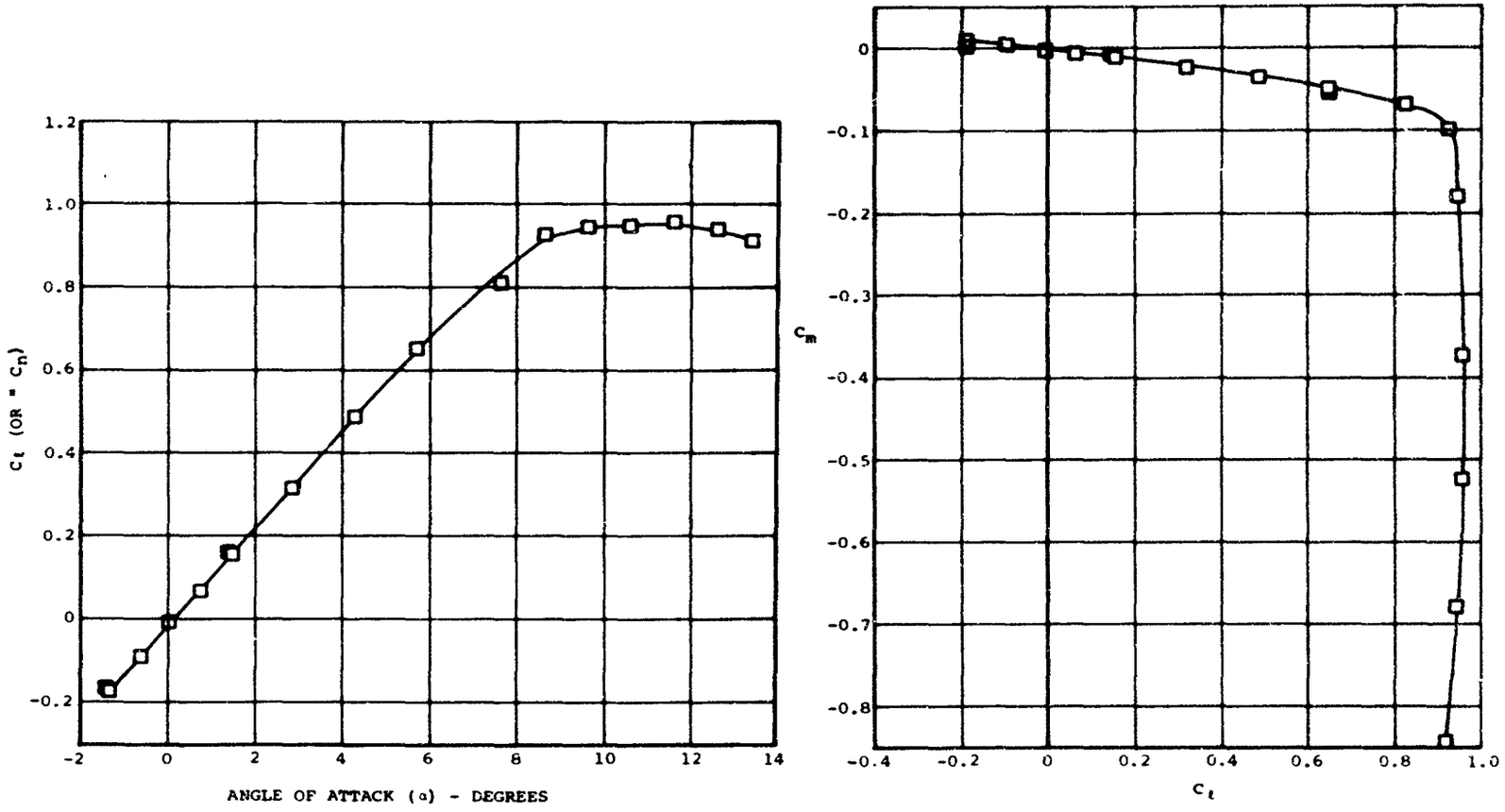

Figure 2. Static Aerodynamic Characteristics of the CH-47A Airfoil for Retreating Blade Operating Conditions.

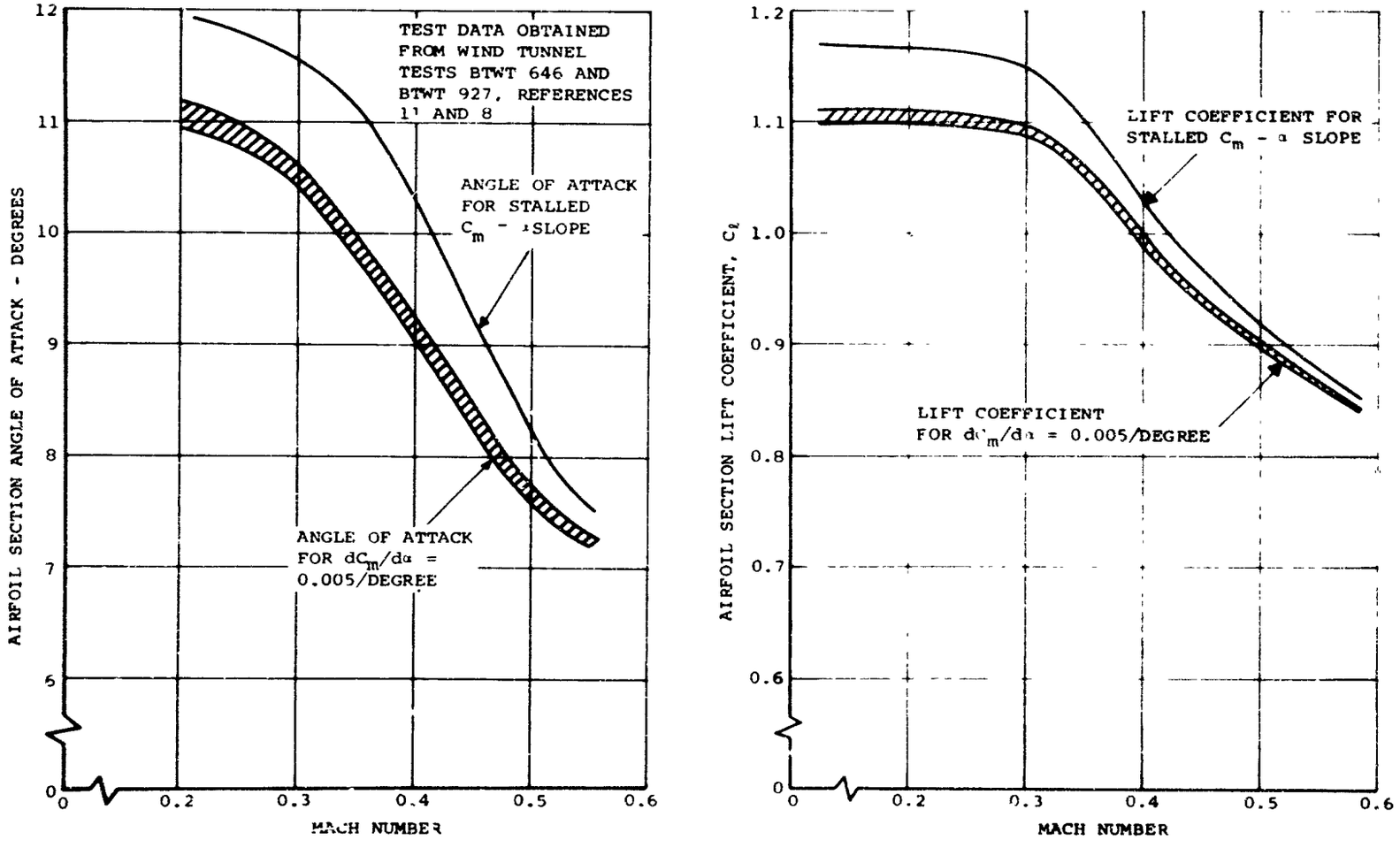

Figure 3. Boundaries for Pitching Moment Divergence of CH-47A Airfoil Section (0011-1.43) from Wind Tunnel Static Test.

also of interest that the rotor aerodynamicist's usual stall limit of 14 degrees is considerably beyond the limit which would be established based on pitching moment divergence. The 14-degree criterion apparently is a carryover from the lift-stall concept and does not apply to rotors.

DYNAMIC-AERODYNAMIC EFFECTS OF THE ROTOR ENVIRONMENT

At present there is no way to simulate the complicated azimuthal variations in velocity, angle of attack, and rate of heave produced by rotors. The only dynamic wind tunnel data available are steady-state oscillating airfoil tests. The most applicable of these data to the rotor situation are the data of reference 20. In this reference the significant reduction in the negative damping due to stall which is produced by airfoil camber is shown. It is also suggested that the influence of heave motions on stall flutter is negligible. These types of data show considerable differences between the starting cycle and steady-state cycles. For rotors, stall oscillations as evidenced by blade torsion and control loads start and stop during each revolution, starting on the retreating side of the rotor disk and stopping near the zero azimuth angle. The magnitude of the damping of oscillations through stall as measured in the steady-state tests is apparently much larger than that which occurs for the starting-stopping situation of the rotor environment.

There are some data available on rotor airloads during hovering stall flutter. This situation is of some special interest since it is similar to fixed-wing stall flutter and steady-state oscillating wind tunnel testing. One test point obtained by Ham at M.I.T. has received considerable attention, with some of the data published in reference 5. A somewhat expanded presentation of these data is included in this report as Figure 4. It can be noted in this figure that the normal force coefficient ($\approx C_\ell$) is influenced only slightly by stall, with the aerodynamic lift damping predicted reasonably well by the potential flow (Theodorsen) theory. Pitching moment data from this test are shown to be significantly influenced by stall. As shown in the right plot of Figure 4, the first quarter of the pitching oscillation gives a moment-to-pitch-angle relationship which is predicted by the potential flow theory. When the pitch angle has increased beyond 15 degrees, the moment does not follow the prediction but remains at a fairly constant and relatively large negative value. As the pitch angle starts to decrease, the moment breaks sharply, reaching a value similar to a fully

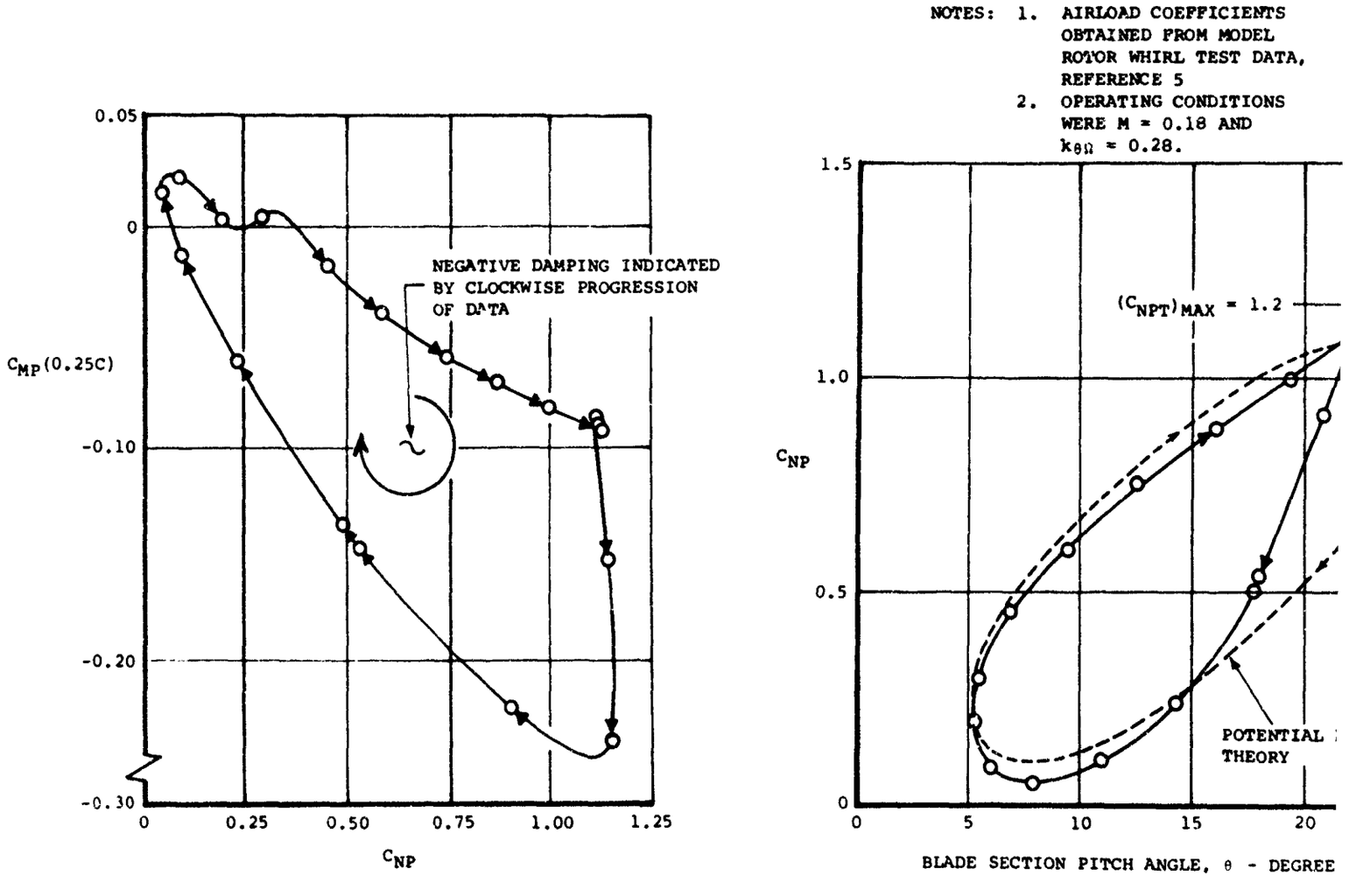

Figure 4. Illustration of Time-Dependent Effects Which Can Occur in Rotor Section Performance.

ES: 1. AIRLOAD COEFFICIENTS OBTAINED FROM MODEL ROTOR WHIRL TEST DATA, REFERENCE 5
2. OPERATING CONDITIONS WERE M = 0.18 AND $k_{\theta\Omega} = 0.28$.

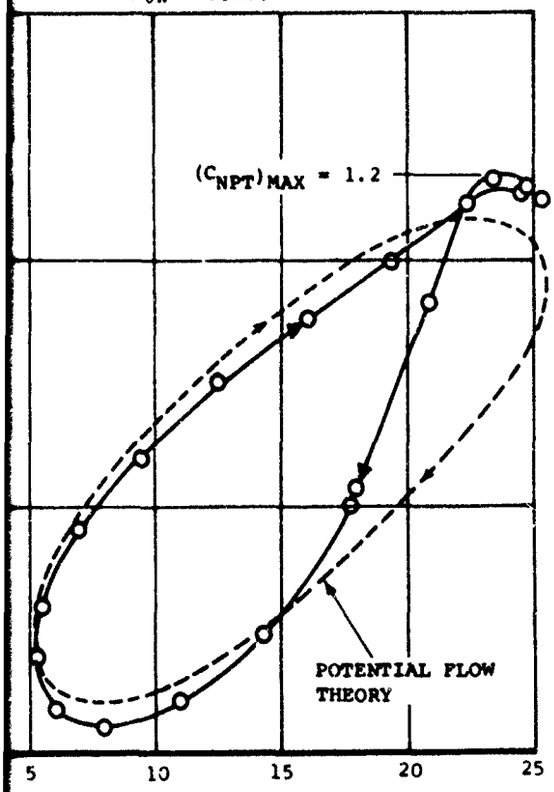

DE SECTION PITCH ANGLE, θ - DEGREES

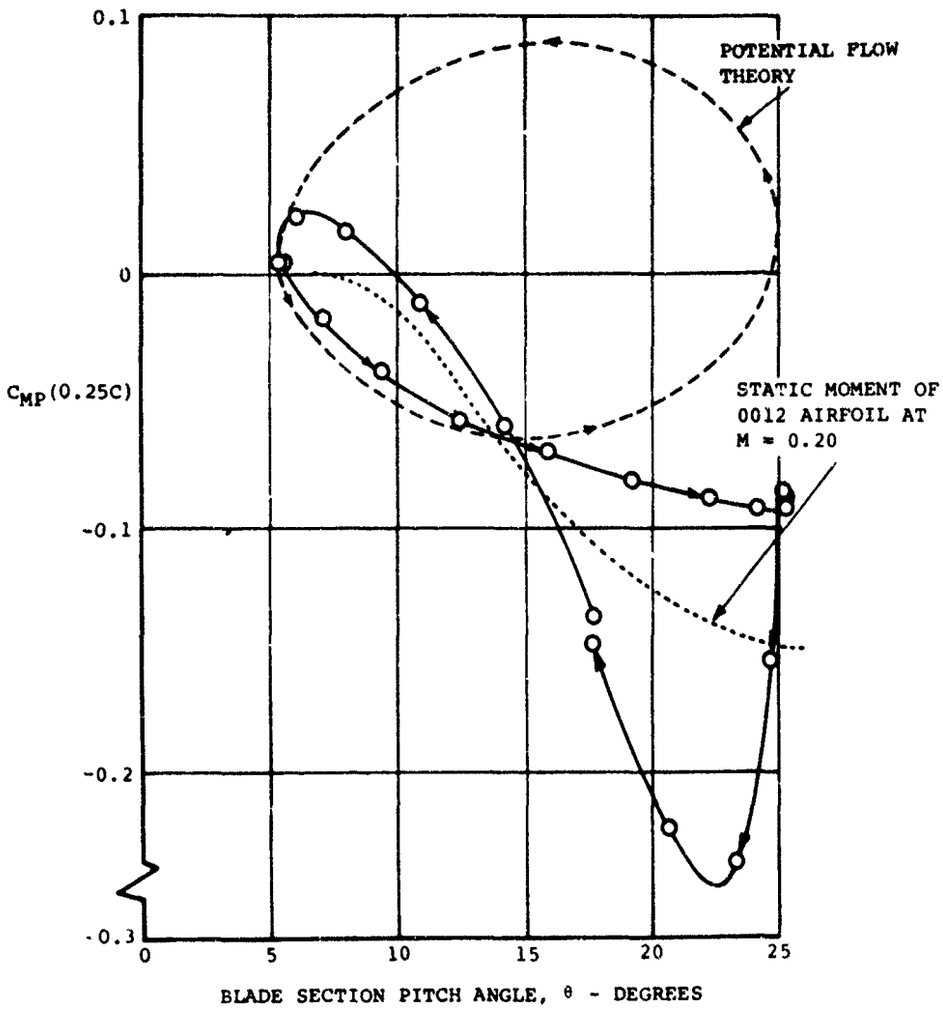

BLADE SECTION PITCH ANGLE, θ - DEGREES

stalled thin plate; that is, with the center of pressure at the midchord. Further reductions of the pitch angle cause the pitch moment to return to zero as the minimum pitch angle is reached

The data presentation shown in the uppermost plot of Figure 4 is used later in this report to indicate the aerodynamic damping relationships of the rotor airloads measurements obtained in this program. This presentation depends only on the measured normal force and pitching moment coefficients, C_{NP} and C_{MP}. Except for a time delay which can be shown to be small for the rotor situation, C_{NP} is almost linearly equal to the angle of attack. Therefore, the C_{MP} versus C_{NP} plot is essentially a C_{MP} versus angle-of-attack plot, and shows the presence of aerodynamic damping if an area is enclosed by a counterclockwise progression of the data. As shown in Figure 4, a negative aerodynamic damping is indicated for this stall flutter test point.

It is emphasized in this report that, whenever damping is discussed, it will always be the aerodynamicist's concept of damping. This is not necessarily the rotor dynamicist's damping, since blade motions due to blade pitch, bending, or twisting are not linearly equivalent to angle-of-attack variations. It is therefore possible (but unlikely) for positive aerodynamic damping to appear in the control system equations of motion as a negative damping. The resolution of this complication is beyond the scope of the present study.

RADIAL FLOW EFFECTS

The blade section sweep angle produced by the radial component of the helicopter's forward velocity has been shown in reference 6 to be a further explanation for the stall delay of rotors. Static wind tunnel data obtained with a yawed wing were reduced to two-dimensional data which show a significant lift-stall relief due to sweep angle. At higher advance ratios, rotor blades experience sweep angles of 30 to 35 degrees at the three-quarter radius and probably experience much larger sweep angles near the reversed flow region. As shown in Figure 5, increases in the maximum lift coefficient of about 30 percent should be expected due to 30 degrees of sweep. While it is not shown in this figure, it should be noted that the lift-stall delay does not apply to the pitching moments. The stall-induced divergence of the pitching moments is almost independent of the sweep angle.

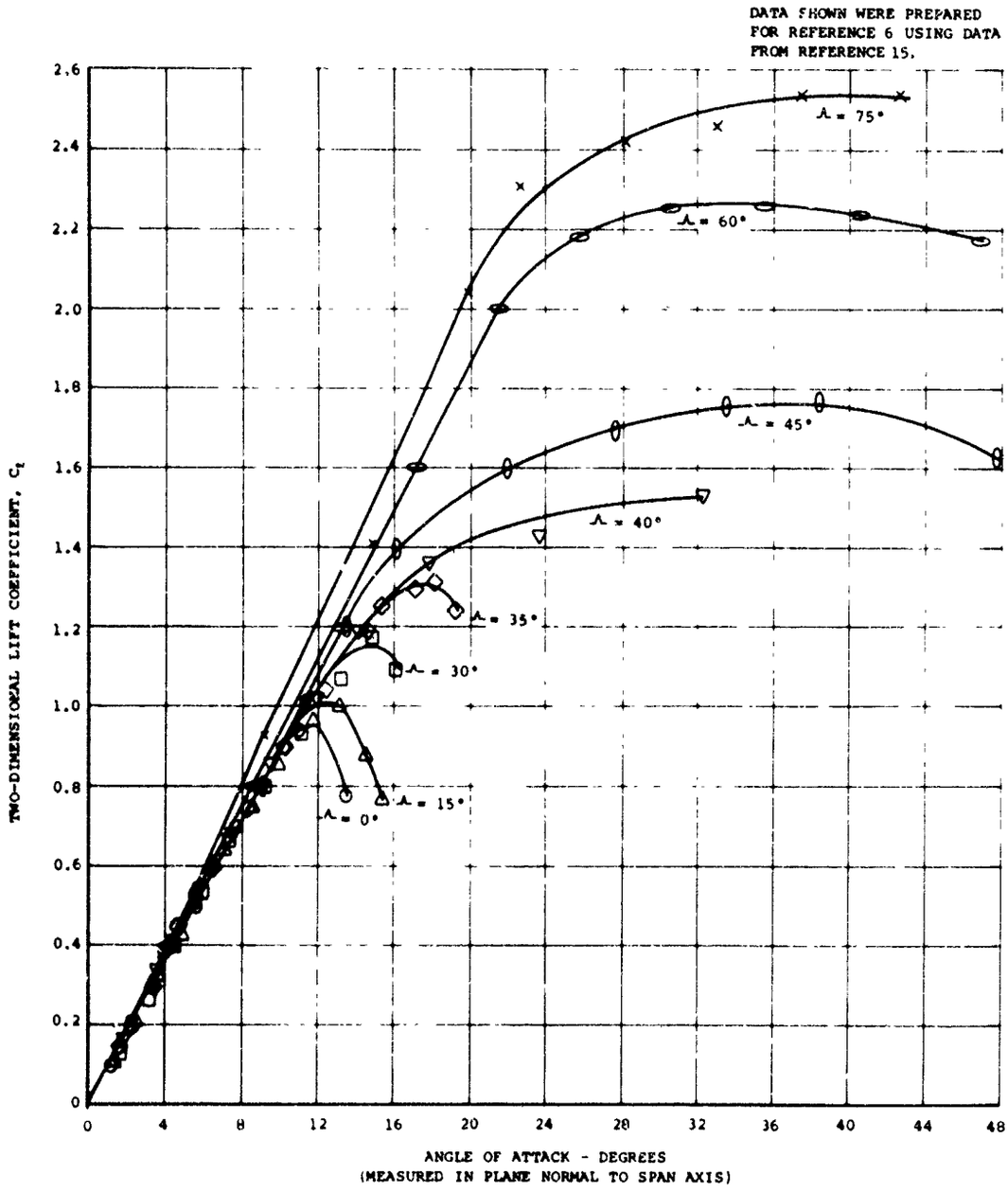

Figure 5. Delay of Lift-Stall Due to Local Blade Section Sweep Angle.

TESTS AT THE HIGH DYNAMIC LOADS BOUNDARY

The tandem rotor airloads measurement program included a wide range of operating conditions, with approximately 40 test points obtained near the high dynamic loads (HDL) boundary. These test points are illustrated in Figure 6. Due to the relatively unproven nature of the highly instrumented rotor blades, a reasonable margin was maintained from the HDL boundary. Test points (TPN) 224, 225, and 226 were flown at higher altitudes and were specifically intended to investigate stall effects. Penetration of the HDL boundary was not possible with the test aircraft due to high loads and excessive vibration. Test points were also flown to achieve a maximum advance ratio, with test point 217 reaching an advance ratio of 0.37 at 158 knots. This testing was also limited by excessive vibration.

An indication of the severity of the operating conditions tested can be obtained from the calculated retreating blade tip angle of attack based on uniform downwash, $\alpha(1.0,270)$. These data are presented in Figure 7 and show a reasonable correlation of proximity to the HDL boundary and an angle of attack which would be near the pitching moment divergence boundary of Figure 3. Later in this report it will be shown that this situation is quite uncertain, and that a more rigorous criterion for the high loads due to large retreating blade tip angle of attack is required. In particular, the relative positions of test points 226 and 217 in this plot should be noted, with larger angles of attack shown for test point 217. Test point 217 data will be shown to evidence no significant effects of stall.

The measured azimuthal average airload normal force and pitching moment distributions are shown in Figures 8 and 9 for some typical test points obtained at high speed. Only small differences in average loading are shown, with a small increase in loading reflecting the increased propulsion required at higher speed. The significant difference in the average rotor loading distribution between the forward and aft rotors, discussed in Volume IV, is shown to continue at light weights and high speed. The forward rotor data continue to show fairly uniform loading distribution with radius, but the average loading is reduced somewhat inboard, apparently due to the download in the reversed flow region. Reversed flow effects apparently cause the large positive average pitching moment at the inboard end of the forward rotor. The aft rotor data

presented in Figure 9 show the more usual rotor load distribution of the aft rotor, with the largest load carried near the blade tips. This load distribution apparently makes the aft rotor considerably more sensitive to stall. It is believed that differences in the stalling pattern cause the peculiar variations in average pitching moment with radius shown at the outboard end of the aft rotor. The indications of the effects of reversed flow are also considerably different for the two rotors, with the forward rotor behaving as expected. As also shown in Figure 9, the average pitching moment for the inboard end of the aft rotor blade is a fairly large negative value. These data cannot be explained; however, later data presentations also show other significant differences in the indications of reversed flow effects of the two rotors. The study of the airloads data to isolate the effects of reversed flow appears warranted but is beyond the scope of the present study.

The practical potential of helicopter rotor operation at high speeds has been subject to question and is believed to be somewhat supported by the data shown in Figures 10 and 11. These data are the harmonic coefficients of the aft rotor airload normal force data for typical nonstalled test conditions at various advance ratios. It is shown that the airload coefficients generally decrease continually with increased advance ratio, with almost negligible harmonic coefficients shown at an advance ratio of 0.37. These data are believed to indicate that, when the dynamic system of the rotor is properly tuned and if stall can be avoided or properly handled, rotor operation to advance ratios of at least 0.37 can be accomplished with less vibration than is experienced at lower speeds. Nonuniform downwash-aeroelastic rotor analyses generally support this conclusion.

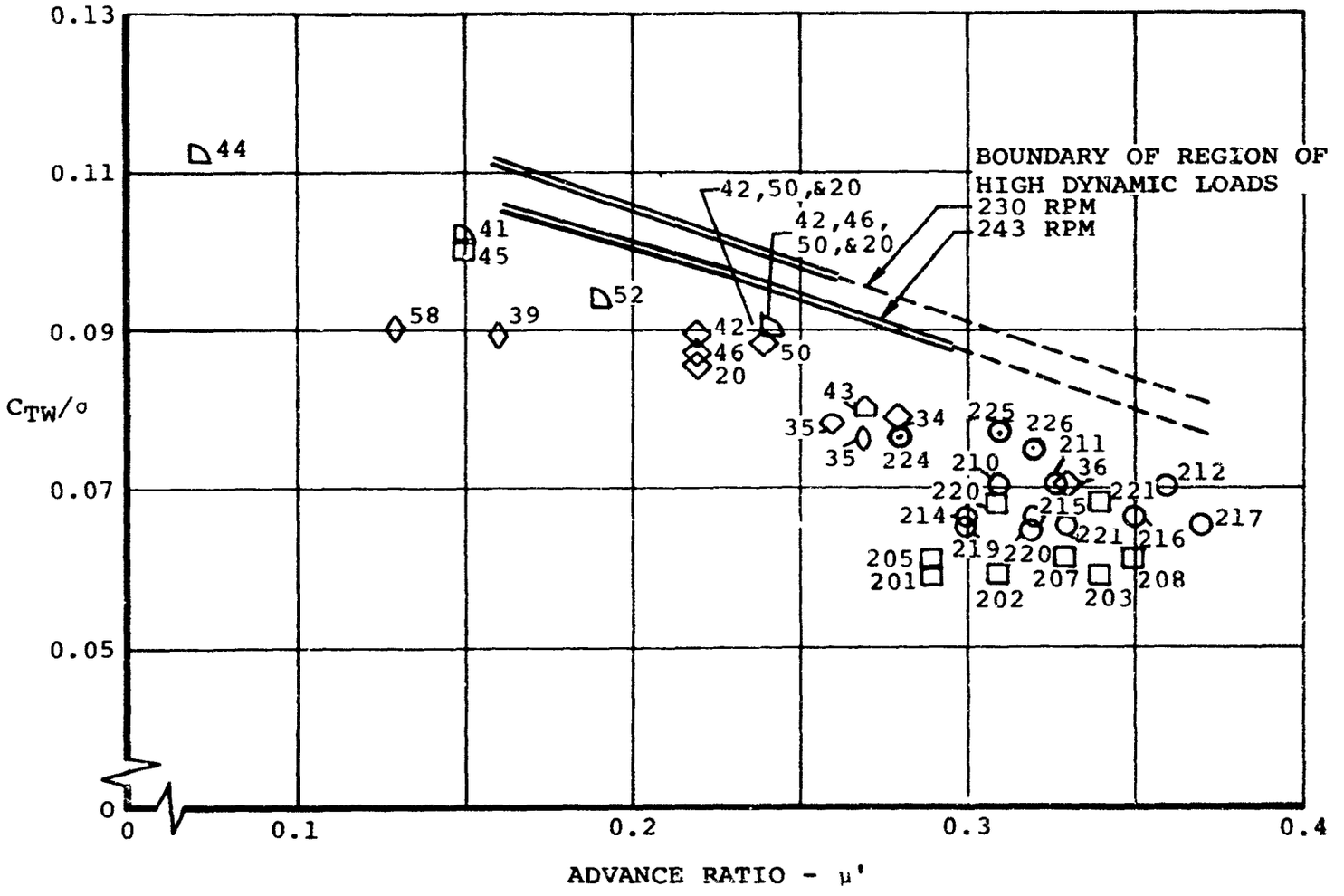

Figure 6. Test Points Obtained Near Boundary of High Dynamic Loads Region.

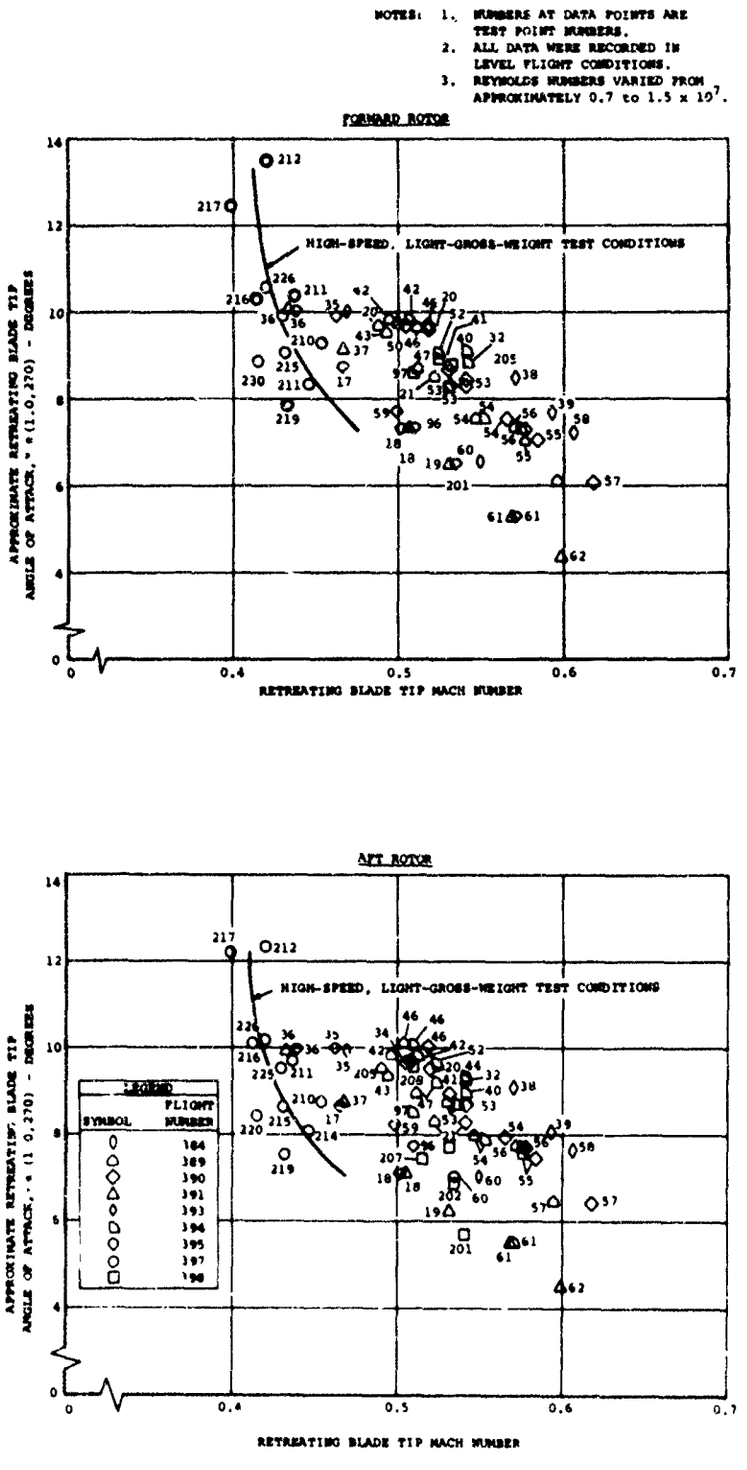

Figure 7. Retreating Blade Tip Operating Conditions Tested, Based on Uniform Downwash and Rigid Blades.

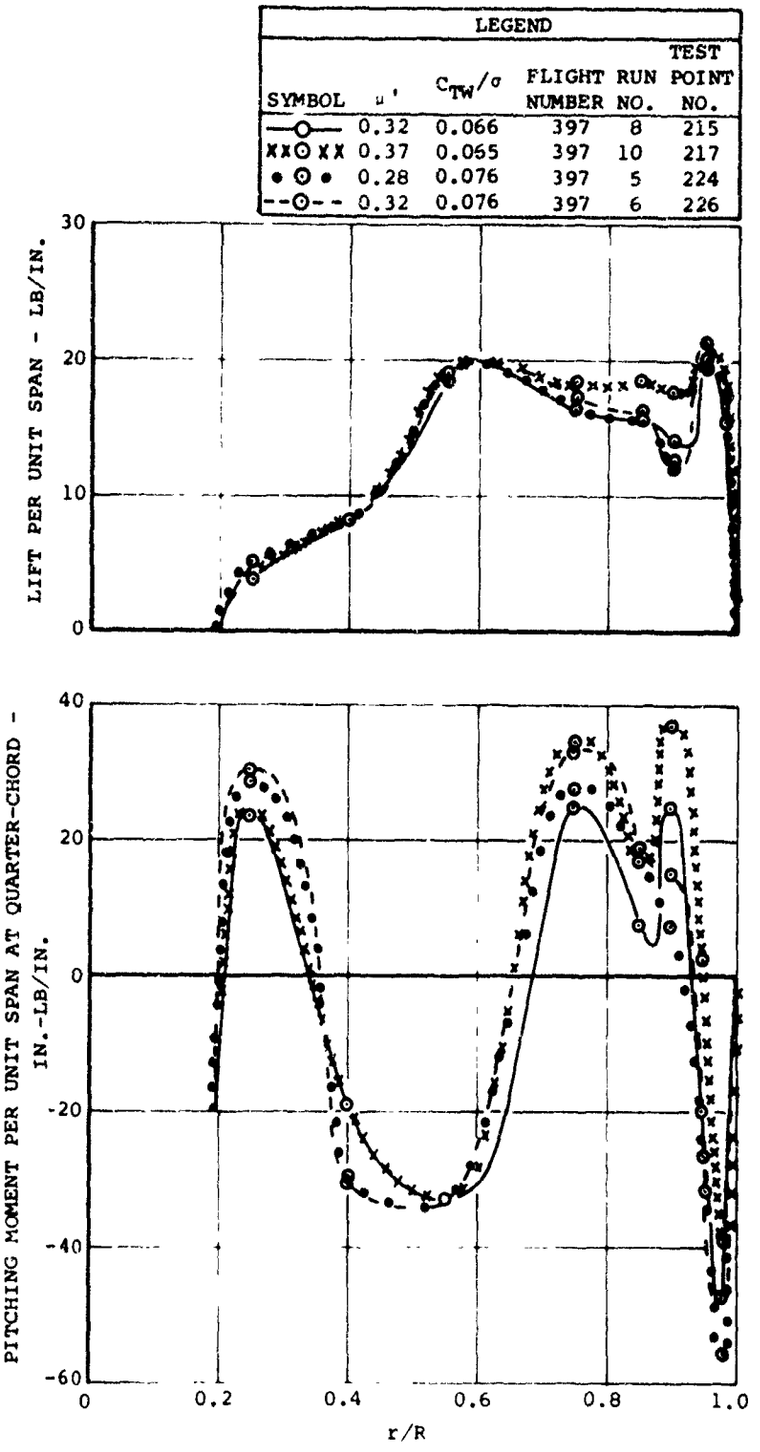

Figure 8. Azimuthal Average Normal Force and Pitching Moment Loading on the Forward Rotor at High Speed.

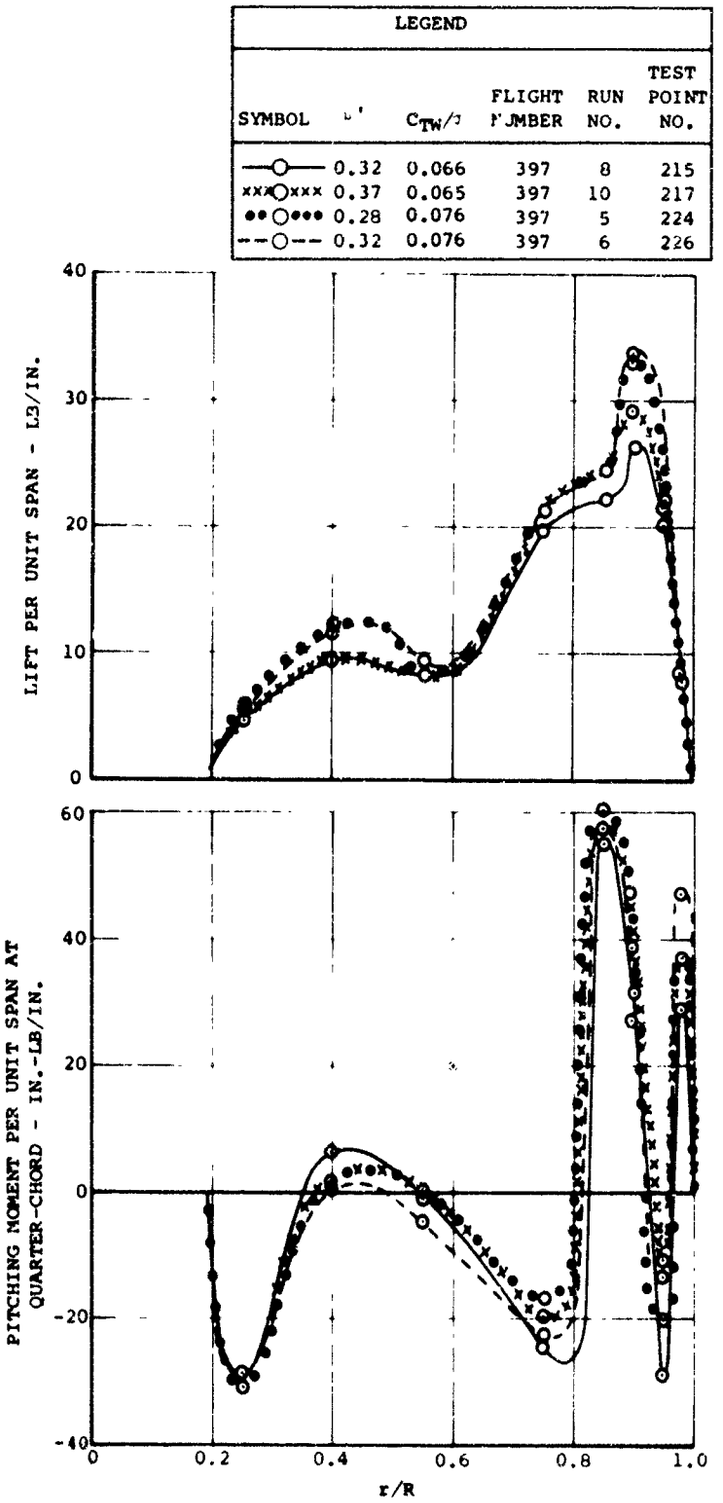

Figure 9. Azimuthal Average Normal Force and Pitching Moment Loading on the Aft Rotor at High Speed.

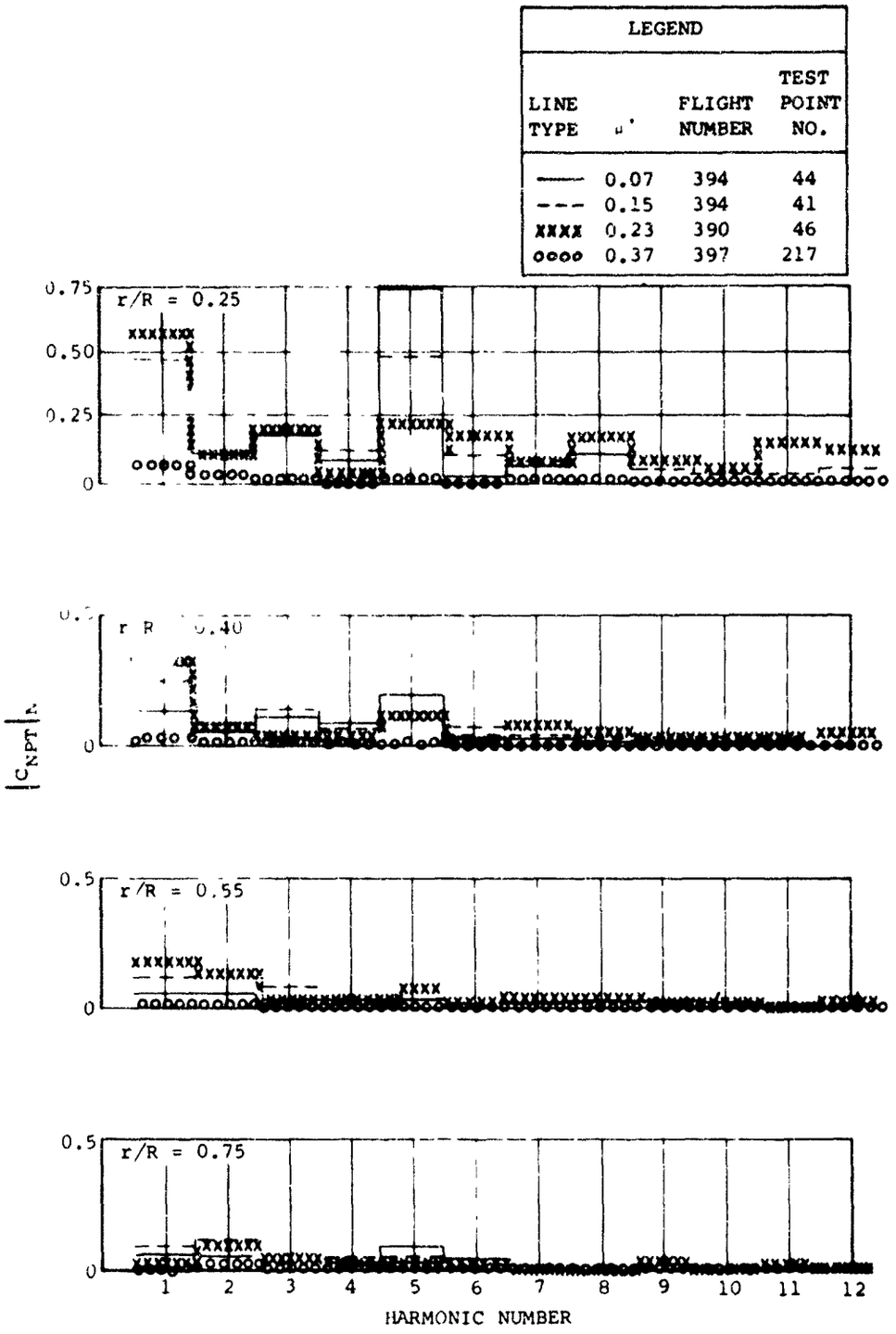

Figure 10. Effect of Advance Ratio on Airload Harmonics for Test Points Near HDL Boundary - Inner Portion of Aft Rotor.

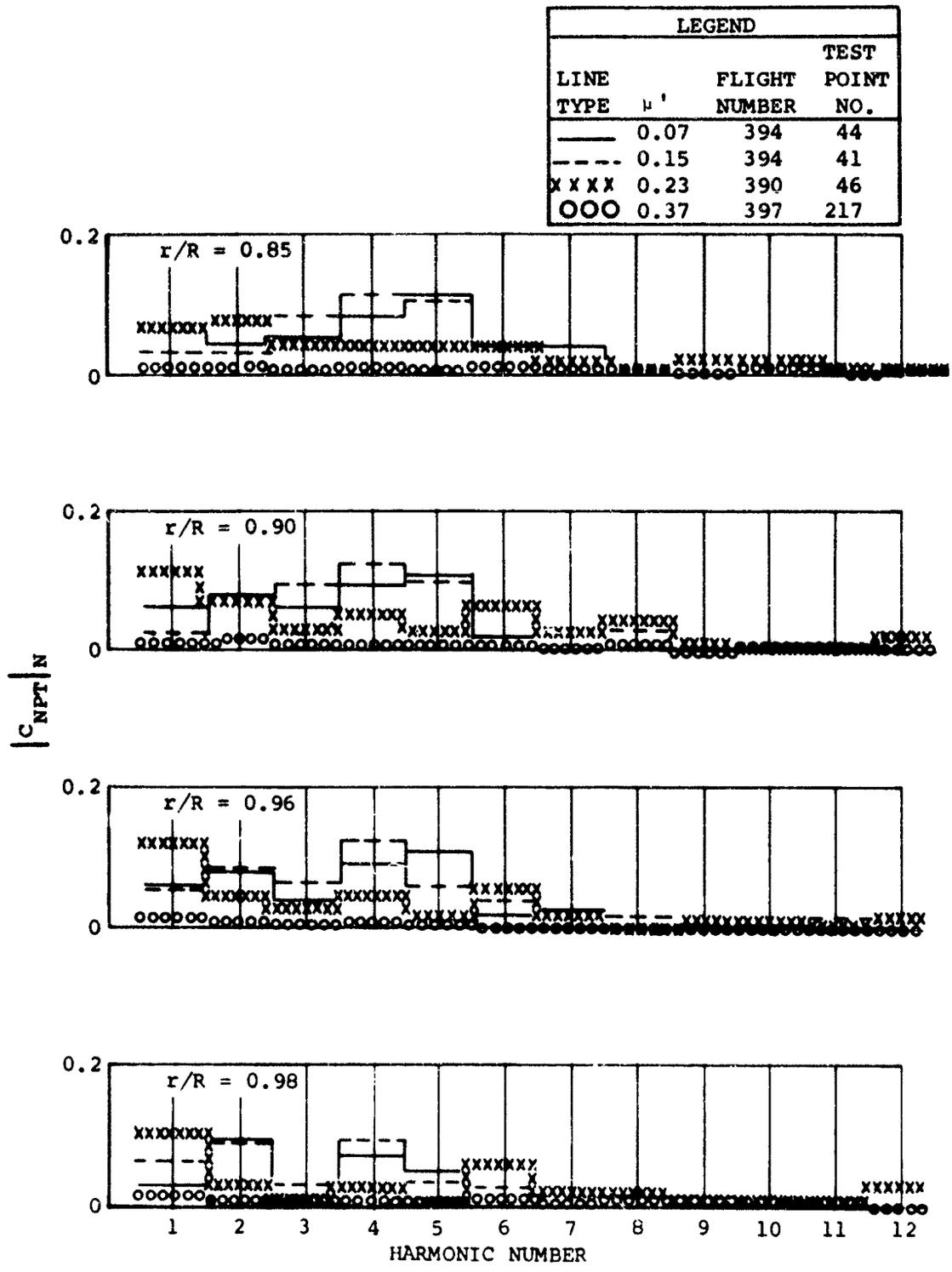

Figure 11. Effect of Advance Ratio on Airload Harmonics for Test Points Near HDL Boundary - Outer Portion of Aft Rotor.

EVIDENCE OF STALL IN ROTOR LOADS AND BLADE MOTION DATA

In a later section of this report (Indications of Negative Aerodynamic Damping, Stall Effects, page 54), it will be shown that at least 14 test points of this program had aerodynamic evidence of blade stall. The rotor loads data which are presented in this section do not show evidence of stall effects except for one somewhat more severe test point (TPN 226). This contradiction is emphasized since the relation between aerodynamic stall and the practical evidence of the phenomenon called "stall" is highly dependent on the dynamic response of the rotor system. An explanation of how aerodynamic stall can occur without causing the loads which are commonly associated with stall is beyond the scope of this report.

There has been considerable conjecture that one of the more serious effects of blade stall is an increase in the longitudinal component of the first harmonic blade motions about the flap hinge. On the tandem helicopter, an increase in this component of blade flapping can result in excessive rotor shaft bending stresses, reduced fuselage-to-rotor clearance, or excessive cyclic trim requirements. To study this problem, the blade motion data have been corrected for cyclic trim and normalized by the thrust coefficient for a large variety of level flight test points. If reversed flow effects and downwash nonlinearities are neglected, and if the blade section aerodynamics are assumed to be linear, this normalized control axis flapping angle is expected to be linear with advance ratio. The forward rotor data, shown in Figure 12, show a somewhat nonlinear variation with advance ratio, but these data are generally within the band of values predicted by the contemporary uniform-downwash rigid-blade rotor theory. These data do not appear to show any effects of stall. The aft rotor data, Figure 13, are similar to the forward rotor data with the exception of test point 226. These test data show a somewhat larger flapping than expected. It is believed that blade stall may have caused an increase of about one degree in flapping of the aft rotor for this test point. Further analysis of these data, not illustrated in this report, shows that a large increase in the eighth harmonic blade flap hinge motion also occurs for this test point. This eighth harmonic hinge motion is apparently due to a significant increase in the third mode flapwise bending of the stalling rotor blade.

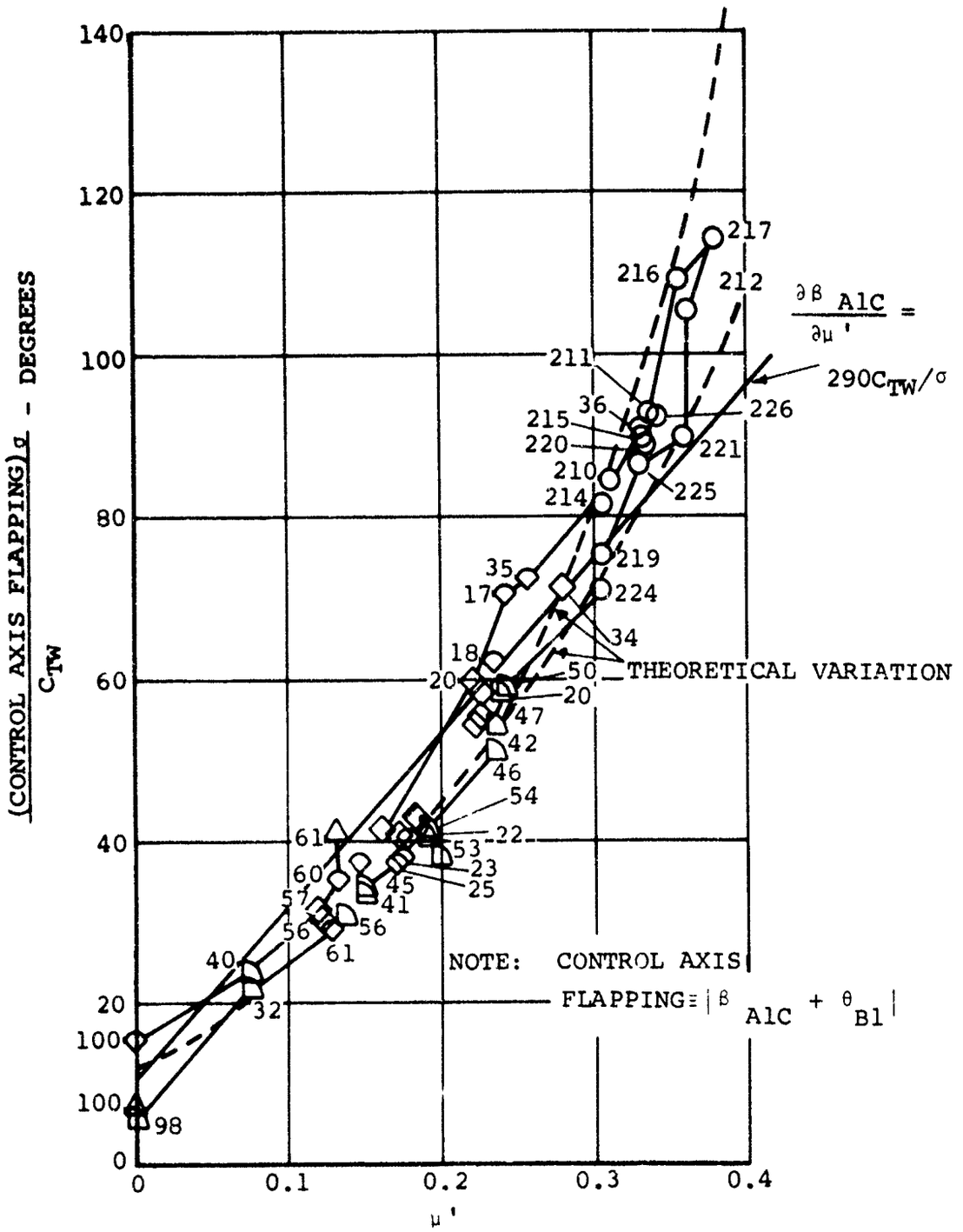

Figure 12. Forward Rotor Flapping Data, Compared with Theory, Showing No Stall Effect.

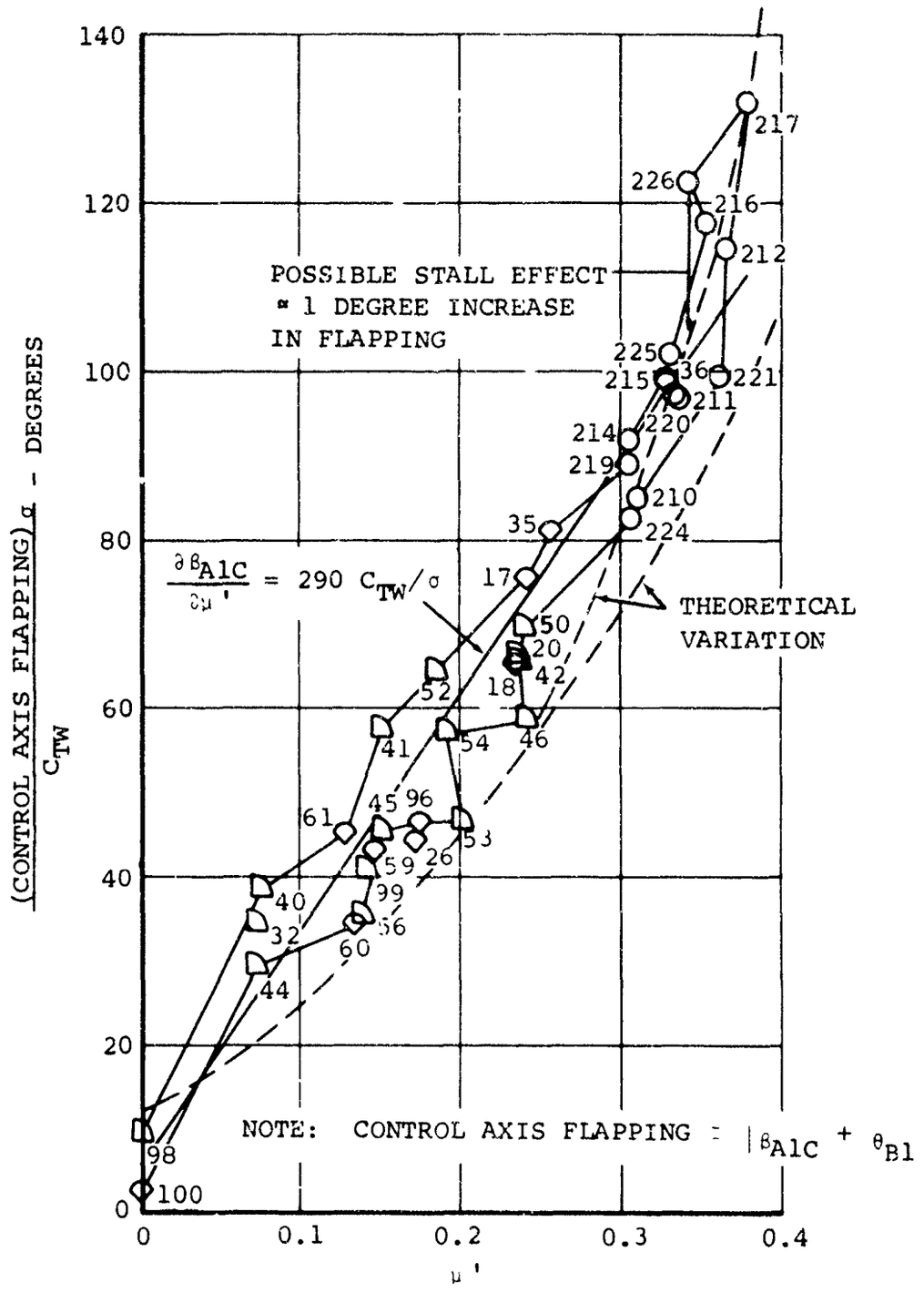

Figure 13. Aft Rotor Flapping Data Showing Possible Stall Effect at Most Extreme Condition Tested.

It is predicted by rotor analysis and model tests that significant amounts of blade stall will cause a sizable increase in rotor drag. This effect, of course, causes the decrease of the lift-effective drag ratio of rotors with advance ratio shown in Figure 1. The rotor shaft shear data measured in this program show the rotor and hub drag as the longitudinal component of the first harmonic amplitude of shear. These data are presented in Figure 14 and show that test points 224, 225, and 226 are at the top of the scatter. This trend may be due to stall being more fully developed for these test points.

Since the effects of what appears to be stall can be seen in the rotor drag measurements, it is not surprising that a similar effect can also be seen in the rotor power data of Figure 15. Again the data points obtained for the aft rotor at higher thrust coefficients are shown to be at the top of the scatter of data. These data indicate that the power increase from this amount of stalling has a small effect on performance, with an advance ratio penalty of about 0.04 (or about 2 knots) required to have a specific power coefficient of 0.12 with and without stall.

The concept of drag increase and lift decrease with stalling leads one to expect that blade bending data would also reflect the effects of blade stall. Figures 16 through 19 show that this situation does occur, with blade bending and torsion loads increasing apparently due to stall. In every case it is only the aft rotor which shows effects of "stall"; the data points with the highest thrust coefficient show the divergence of the "stall" effect, and the extreme point is test point 226. The alternating flapwise bending (one-half peak-to-peak) data shown in Figure 16 are believed to increase with stall due to an increased excitation of the third mode flapwise bending. Eighth-harmonic oscillations are prevalent in the blade flap hinge motions and in the blade airloads for stalled conditions due to this effect. It is noted that the Figure 16 data were measured at the most outboard antinode (85-percent radius) and would be most sensitive to third-mode blade bending. The midspan chordwise blade bending data of Figure 17 show the expected results of a blade drag increase due to stall. An expected finding of the alternating blade loads data is the sensitivity of alternating blade torsion to stall, Figure 18. The blade pitching moments which are expected from stall are also apparent in the alternating pitch link loads, Figure 19.

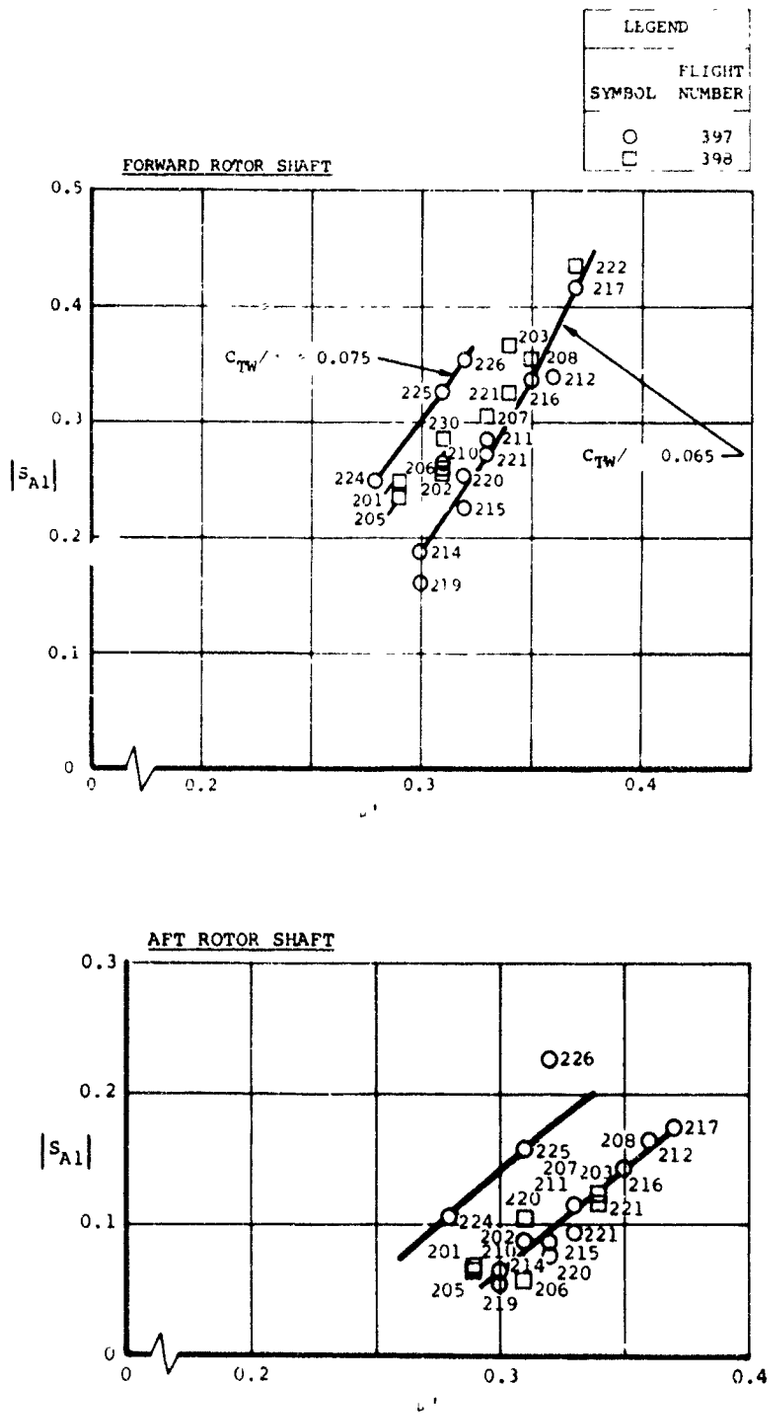

Figure 14. Rotor and Hub Drag for Test Points at High Speed and Light Gross Weight.

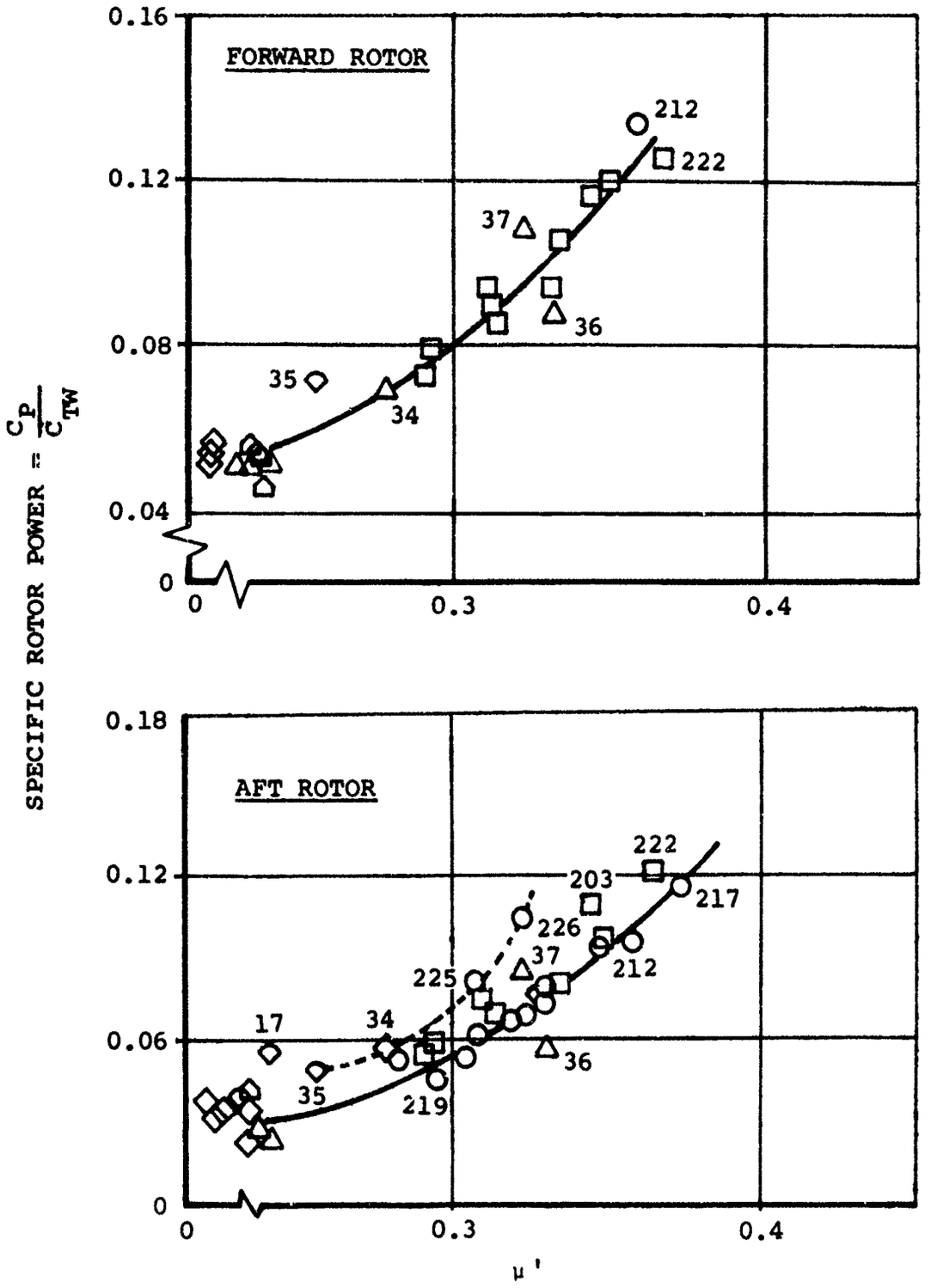

Figure 15. Rotor Specific Power Data Showing Aft Rotor Power Increase Due to Stalling.

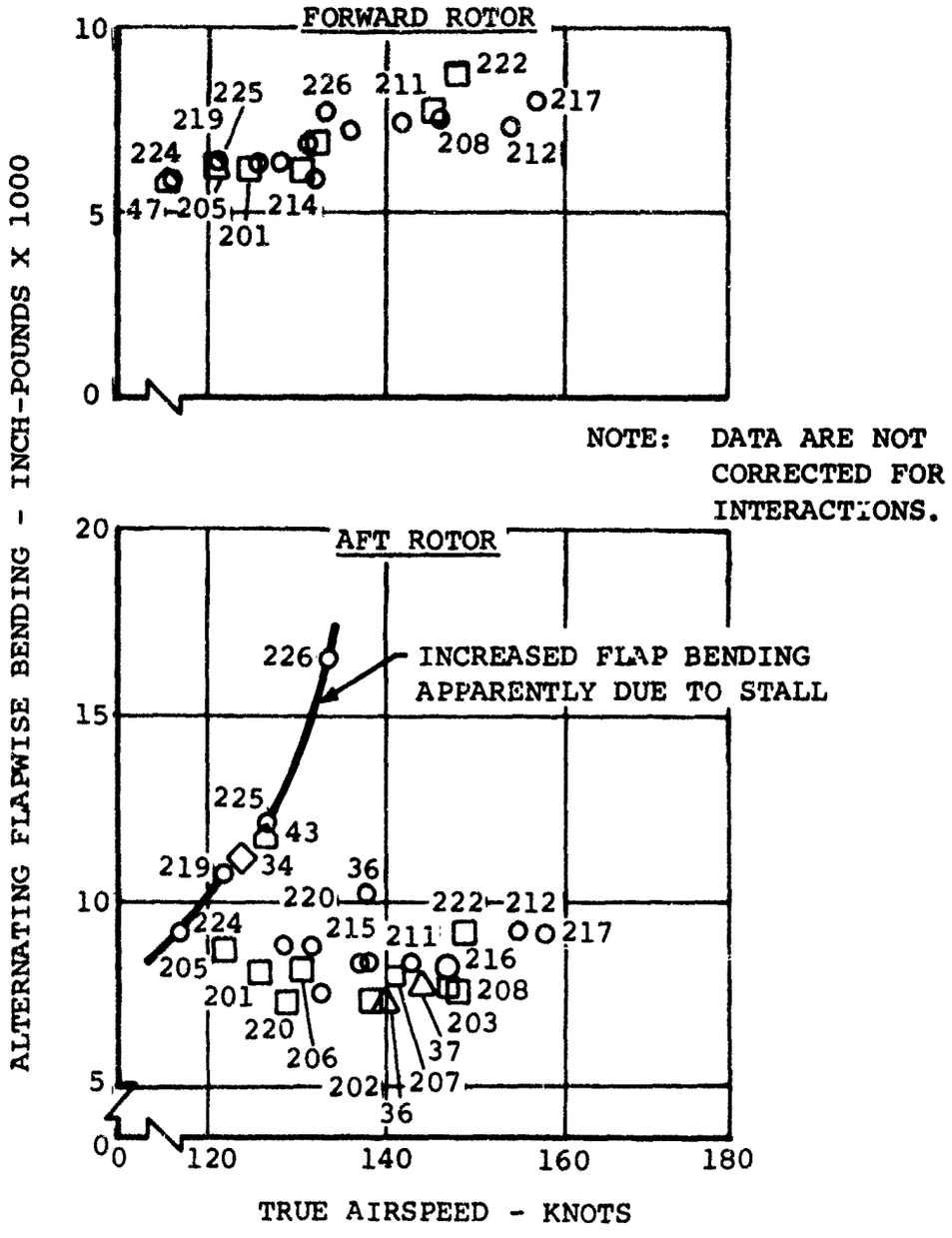

Figure 16. Alternating Flapwise Blade Bending at 85-Percent Radius for High-Speed, Light-Gross-Weight Test Points.

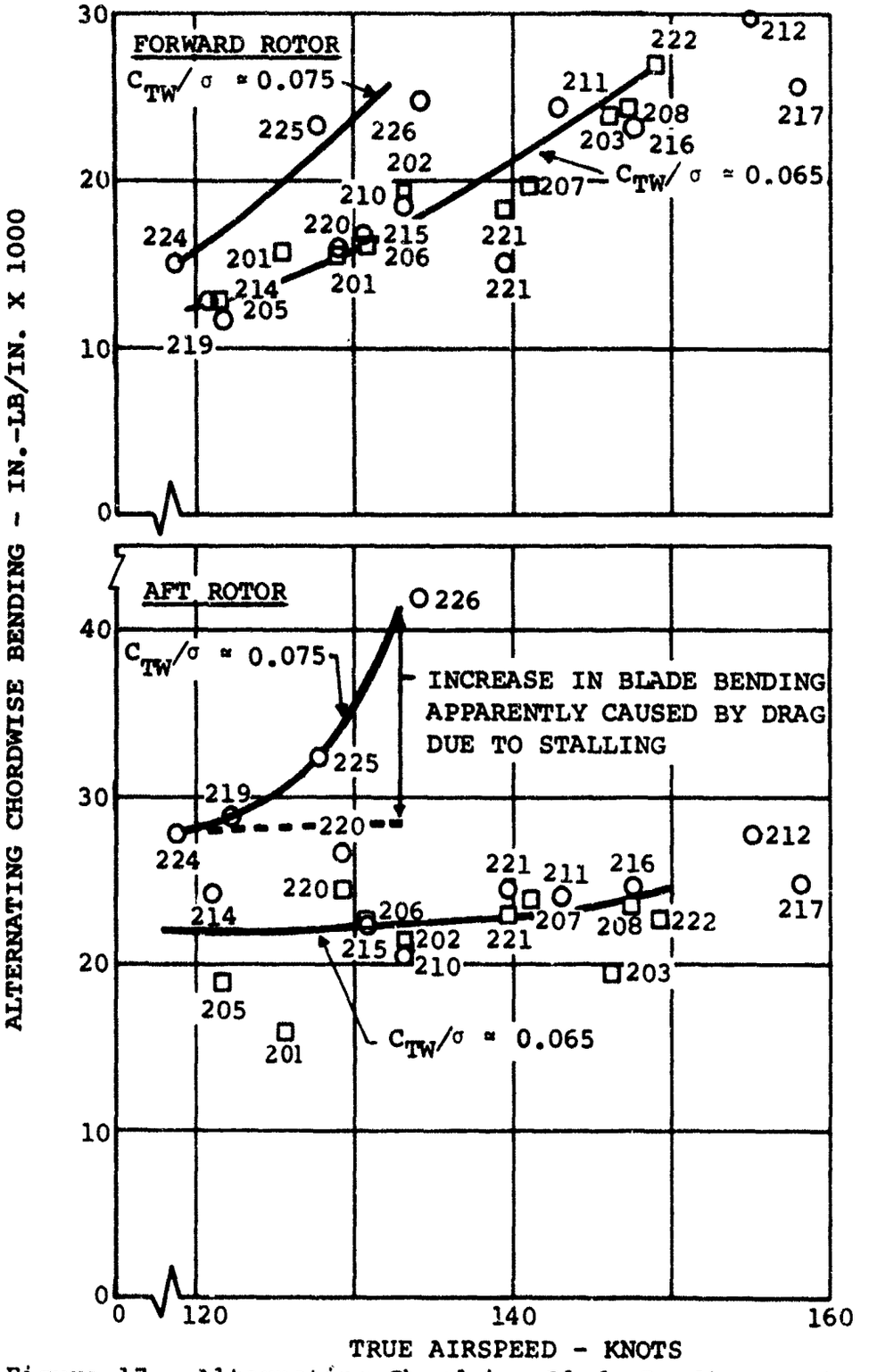

Figure 17. Alternating Chordwise Blade Bending at 65-Percent Radius for High-Speed, Light-Gross-Weight Test Points.

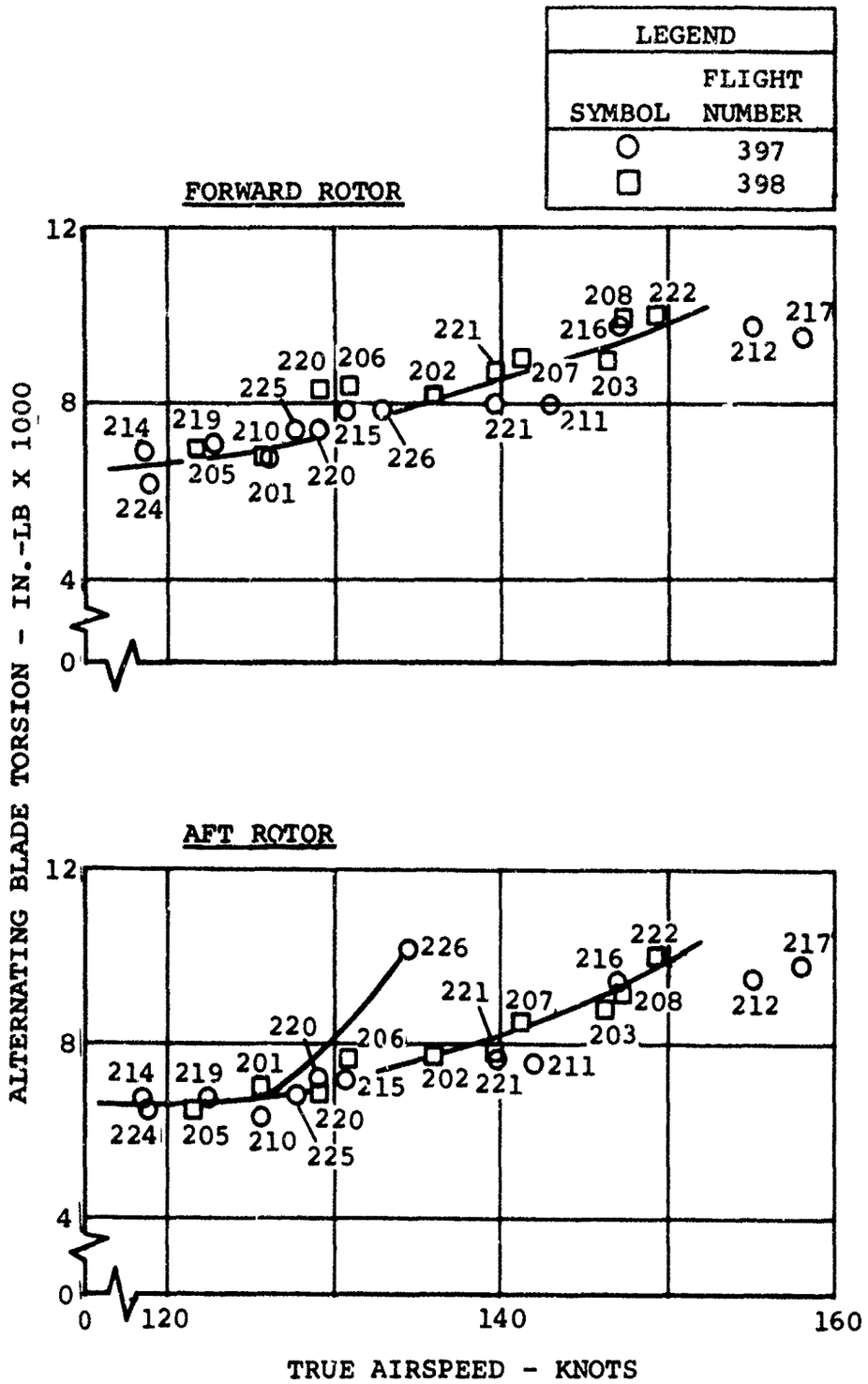

Figure 18. Alternating Blade Torsion at 13-Percent Radius for High-Speed, Light-Gross-Weight Test Points.

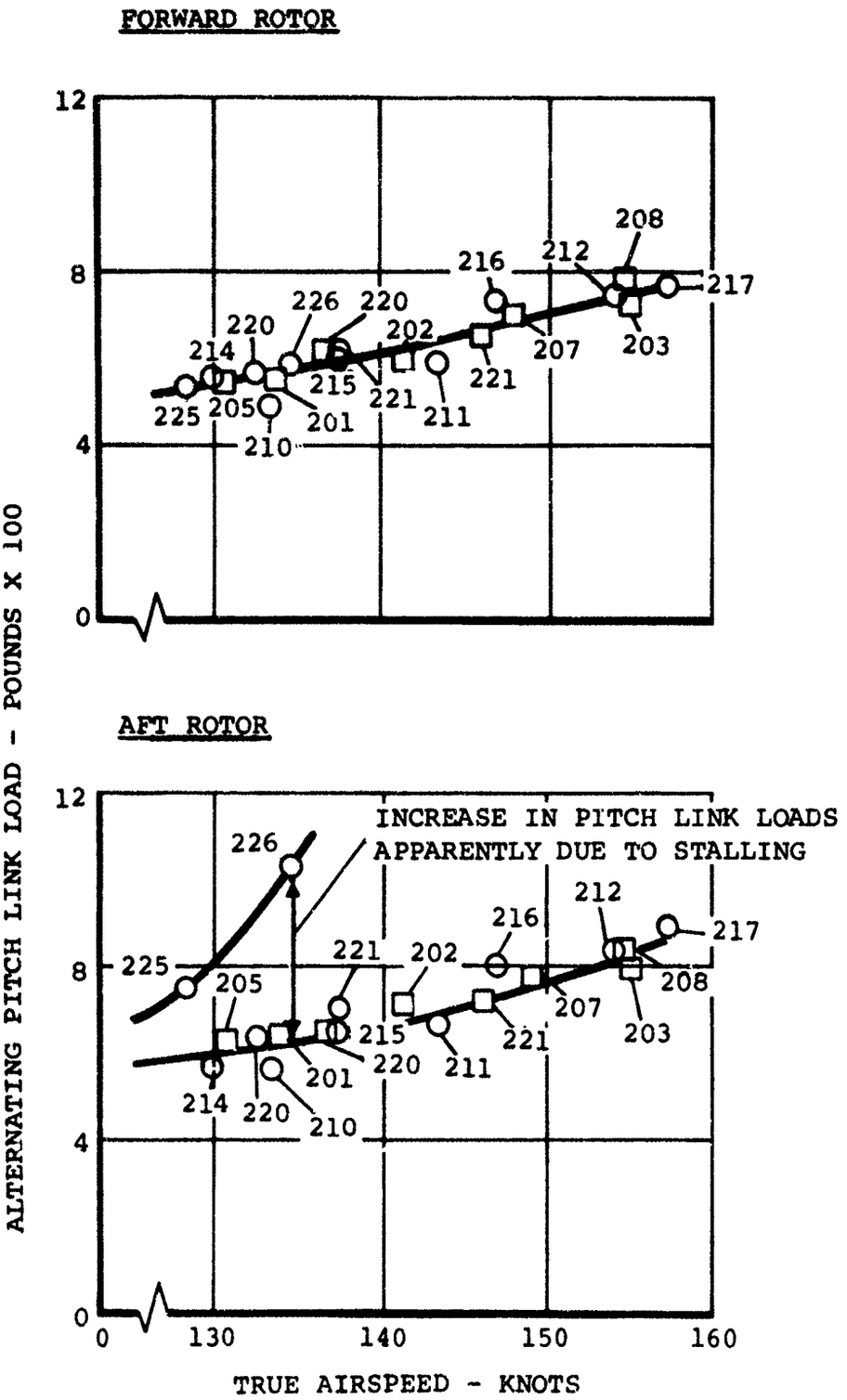

Figure 19. Pitch Link Loads at High-Speed, Light-Gross-Weight Test Points.

The azimuthal waveforms of the blade torsion measurements and the pitch link loads are shown in Figures 20 and 21. The forward rotor data, Figure 20, show no evidence of stall or other unexpected phenomena, and the torsion data are directly equivalent to the pitch link loads. Almost identical waveforms are shown for the two thrust coefficients tested. Aft rotor loads are similar to the forward rotor loads at the lower thrust coefficient, showing a similar, predominantly second-harmonic waveform. Test point 226, obtained at the higher thrust coefficient, shows a nose-down moment and an equivalent compression load in the pitch link at about 50 degrees azimuth. These data also show sixth- and eighth-harmonic variations on the retreating side of the rotor disk. It is believed that the higher harmonic oscillations on the retreating side are due to stall; the load spike in the first azimuthal quadrant is believed to be due to compressibility effects.

These phenomena may be coupled, in that stall loads make the blade twist, which then results in a larger angle of attack on the advancing side. With a larger angle of attack, compressibility effects would be greater. It is significant to note in the data of Figure 21 that, if the compressibility spike did not occur, the oscillations due to stall would have reduced the peak-to-peak variations of the blade torsion and pitch link loads. The blade twisting due to stalling apparently causes a considerable readjustment in the rotor blade loading and reduces the first- and second-harmonic control loads. This situation is confused by the evidence of compressibility effects, which may also be influenced by the blade twisting due to stalling.

The pronounced coupling of these phenomena is illustrated by the azimuthal waveform of the airload pitching moments for test point 226. These data, Figure 22, show that for the unstalled forward rotor, the pitching moments contain an eighth-harmonic ripple but are essentially constant with azimuth (except for some intersting inboard data variations). The aft rotor data show a region of pronounced nose-down pitching moments due to stalling betwee the 200-degree and 350-degree azimuth positions. The eighth-harmonic variation is also much more pronounced on the aft rotor. There does not appear to be any evidence of the compressibility spike in the airloads, unless it is due to the phase coincidence of the airload moments which occurs at this azimuth. Except for the 85-percent radius data, each of the airload moment measurements is

nose-down when the nose-down load spike occurs. The significance of compressibility is more obvious in the airload coefficients which are presented later in this report.

In summation, the rotor loads and blade motion data are believed to show little of the expected evidence of "blade stall" except for one test point. The high rotor loads and increased blade motions associated with "blade stall" that are shown appear to be related to eighth-harmonic variations produced by third-mode flapwise blade bending. Stall and compressibility appear to be coupled through blade twisting. Chordwise blade loads also reflect the effects of stall and/or compressibility. The coupling and the relatively high frequency of these phenomena are believed to be the prime contributors to the prevalent lack of understanding of the rotor loads caused by stall and compressibility.

NOTE:

FORWARD ROTOR BLADE TORSION DATA AT STATION 140 ARE NOT AVAILABLE FOR THESE FLIGHTS DUE TO AN INSTRUMENTATION MALFUNCTION.

LEGEND			
LINE TYPE	FLIGHT NUMBER	RUN NO.	TEST POINT NO.
———	397	6	226
– – –	398	9	207

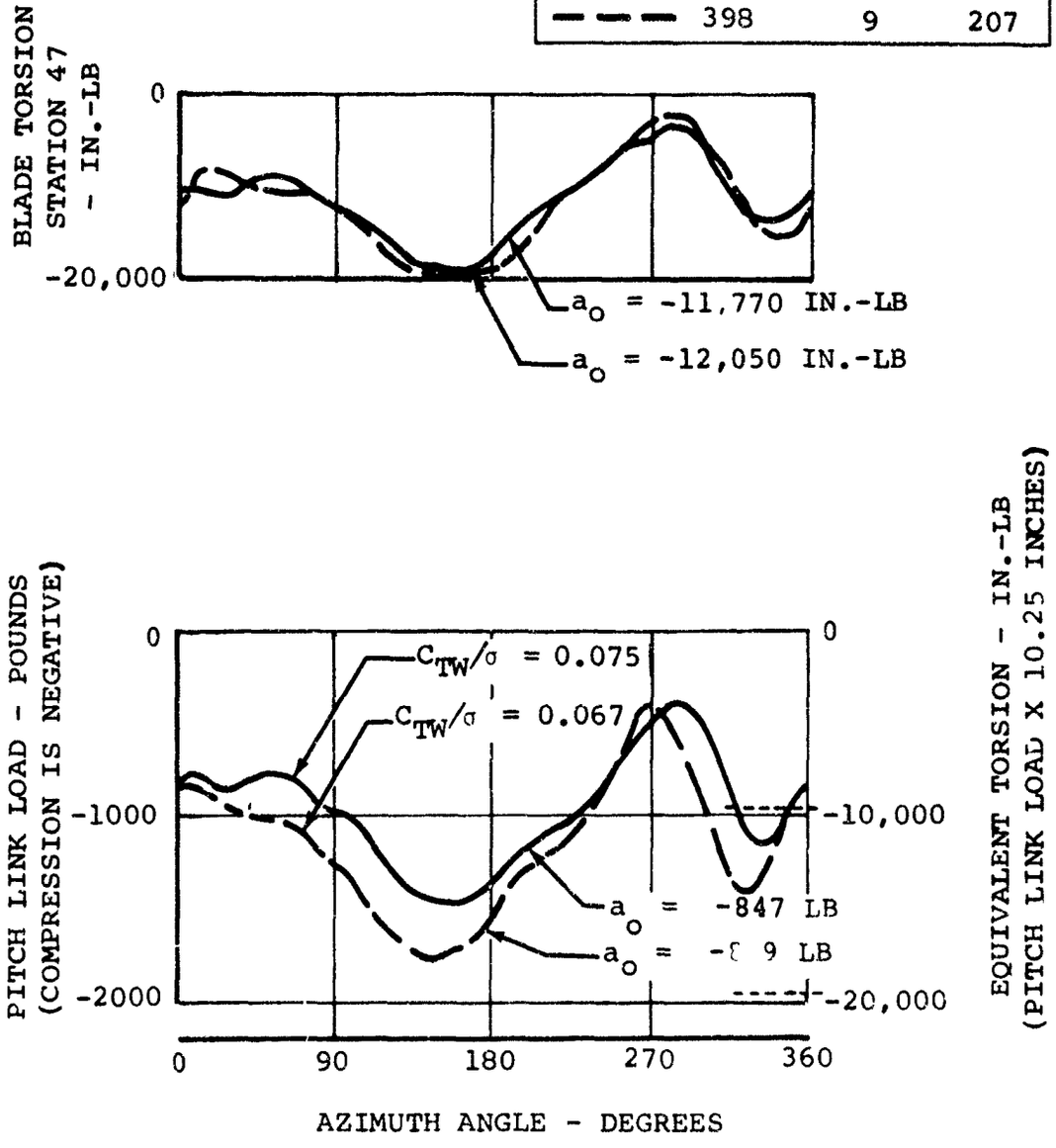

Figure 20. Azimuthal Variation of Blade Torsion and Control Load of Forward Rotor for Two High-Speed, Light-Gross-Weight Test Points.

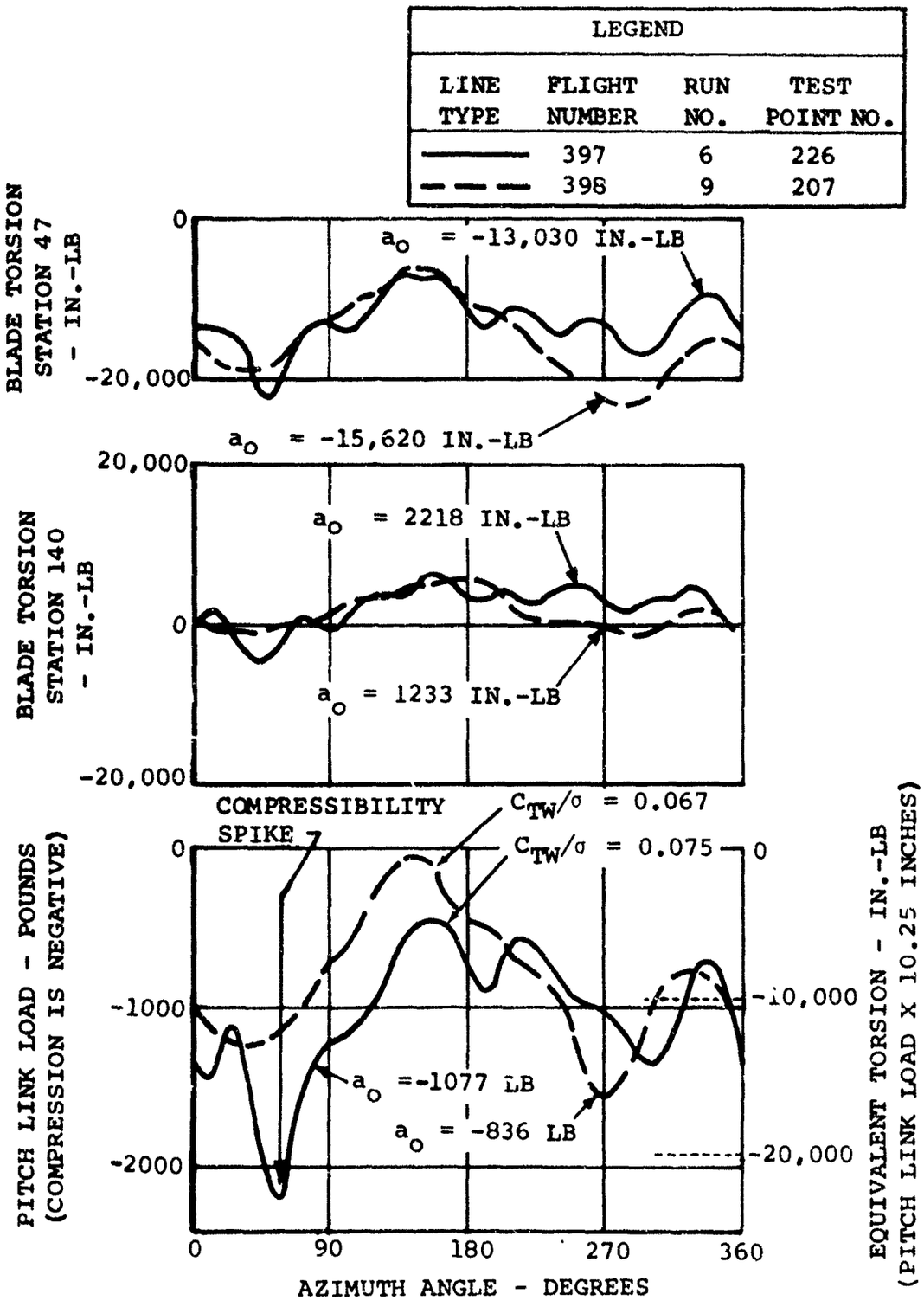

Figure 21. Azimuthal Variation of Blade Torsion and Control Load of Aft Rotor for Two High-Speed, Light-Gross-Weight Test Points.

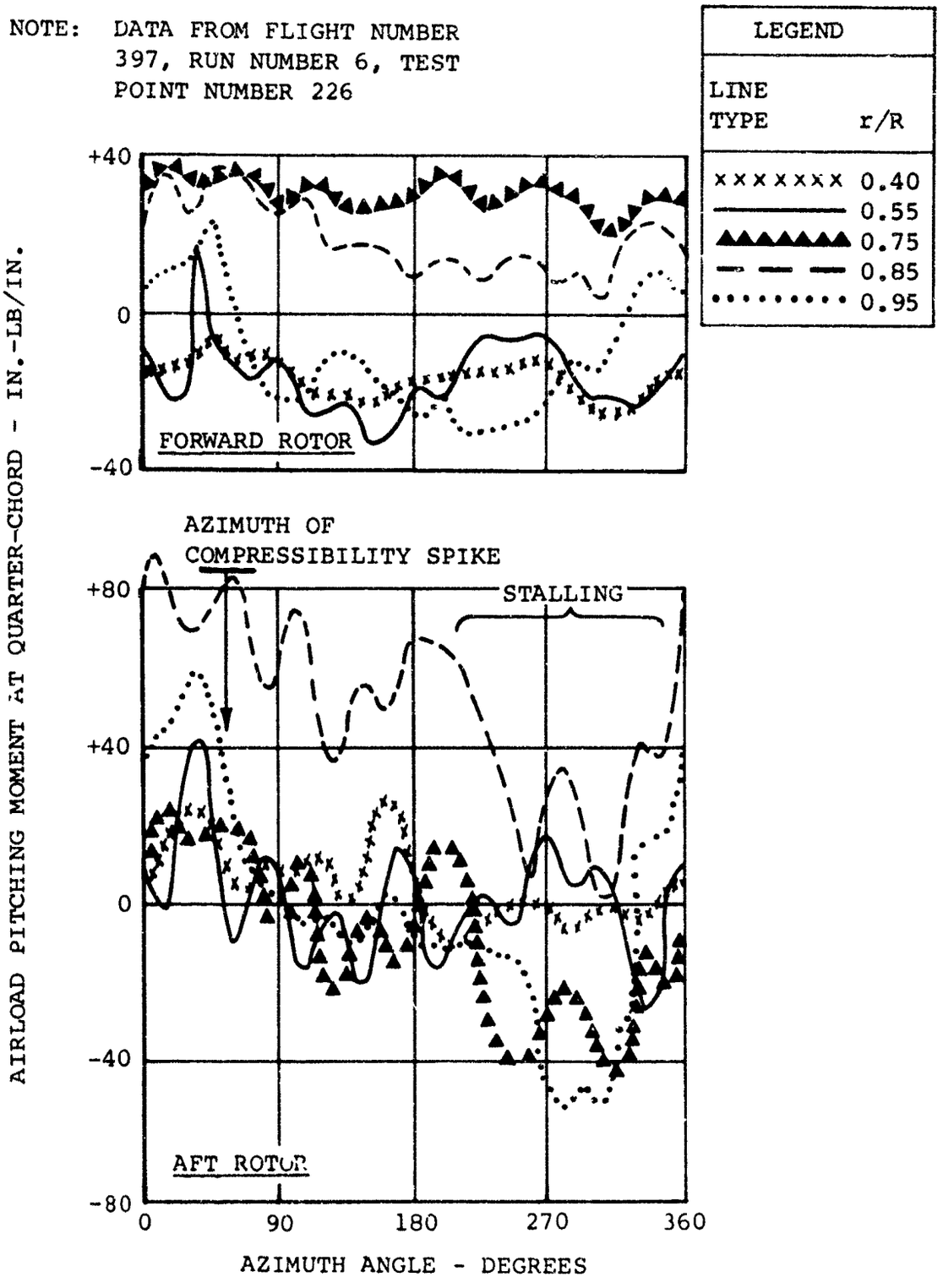

Figure 22. Airload Moments for Most Extreme Condition Tested.

COEFFICIENTS OF ROTOR AIRLOADS NEAR HDL BOUNDARY

The analysis of airloads data is considerably simplified when the airloads data are reduced to coefficient form, since the concepts of airfoil section aerodynamics can then be applied to aid in understanding the results. In coefficient form the airloads data generally show good comparison, among radii and among considerably different flight conditions. Typical examples of the azimuthal variations of the normal force and pitching moment coefficients are presented in this section. These data generally show consistency and repeatability.

There is some uncertainty as to the assumptions which should be made to determine the velocity for calculating the airload coefficients. Later in this report it will be shown that neglecting the out-of-plane component of the rotor blade section velocities produces relatively large coefficients. This assumption is probably too great a simplification. It is believed that use of the uniform-downwash rigid-blade analysis is adequate to calculate the local resultant velocities. The inflow component of the local velocities can be calculated once the theoretical trim is calculated. However, for this project it was desired to have the nonuniform-downwash rigid-blade angle-of-attack values available, so this rather complicated theory was also used to calculate the local resultant velocities. The use of this sophisticated analysis for the velocities is believed to give more confidence in the airload coefficients determined near the reversed-flow region, but it probably does not have much influence on the data for the remainder of the disk. Since the data for blade sections near the reversed-flow region lack credulity due to the very large maximum normal force coefficients obtained, the use of the nonuniform-downwash theory for this exploratory study was probably warranted.

It should also be noted that, in preparing coefficients from the rotor blade airload pressure data, the normal force coefficient is obtained - not the lift coefficient. For airfoils at angles of attack of about 12 degrees or less (such as shown in Figure 2), the difference between the coefficients of normal force and lift is negligible. At angles of attack which cause pronounced stalling, the drag component becomes significant; however, if the angle of attack were known, the normal force coefficient could be related to the lift and drag as follows:

$$C_n = C_\ell \cos\alpha + C_d \sin\alpha \quad . \tag{1}$$

The chordwise airload coefficient is usually small, so that the normal force coefficient is nearly the resultant of C_ℓ and C_d. This minor limitation to the use of the airloads data is probably of little consequence except in the reversed-flow region, which has large, inadequately defined angles of attack. For the present study of blade stall, the differences between C_n and C_ℓ could be neglected; however, to avoid later confusion, the notation "normal force coefficient" is used in this report.

NORMAL FORCE COEFFICIENTS

The normal force coefficients measured at the stations on the outboard quarter of the blades show very little that was not expected. Typical azimuthal variations of the normal force coefficients for the forward and aft rotors at the 85-percent radius are shown in Figure 23. These data show a small bump at 30 degrees azimuth, apparently due to proximity of the tip vortex from the preceding blade of the same rotor. Both rotors have a C_{NP} value on the advancing blade of about 0.1, which is a desirable maximum value for minimum compressibility problems. Both rotors reach a maximum C_{NP} value at about 260 degrees azimuth with no significant discontinuity. There is a discontinuity in the forward rotor data at 290 degrees azimuth which is somewhat more typical of the larger C_{NP} values than are the aft rotor data. This discontinuity is not stall since, as will be noted later, there is no appropriate variation in the blade section pitching moments.

The normal force coefficient data are more repeatable than was expected. This repeatability is illustrated in Figure 24, which shows the comparison of a repeated test point which was obtained in two different test flights. The maximum discrepancy between these two sets of data is about 0.04 except near the maximum C_{NP} value. Rotor blade sections are apparently sensitive to small variations in conditions at high incidence which produce larger variations in the region of large C_{NP}. However, even in this region the discrepancy between these data is only 0.10. This repeatability is considered excellent for this type of data.

Figure 25 was prepared to show the effect of a thrust coefficient variation on the normal force coefficient data obtained

NOTES: 1. ALL DATA FROM FLIGHT NUMBER 390, RUN NUMBER 14, TEST POINT NUMBER 34, AT THE 85-PERCENT RADIUS
2. RUN GROSS WEIGHT = 32,600 LB
$\mu' = 0.28$
$C_{TW}/\sigma = 0.078$

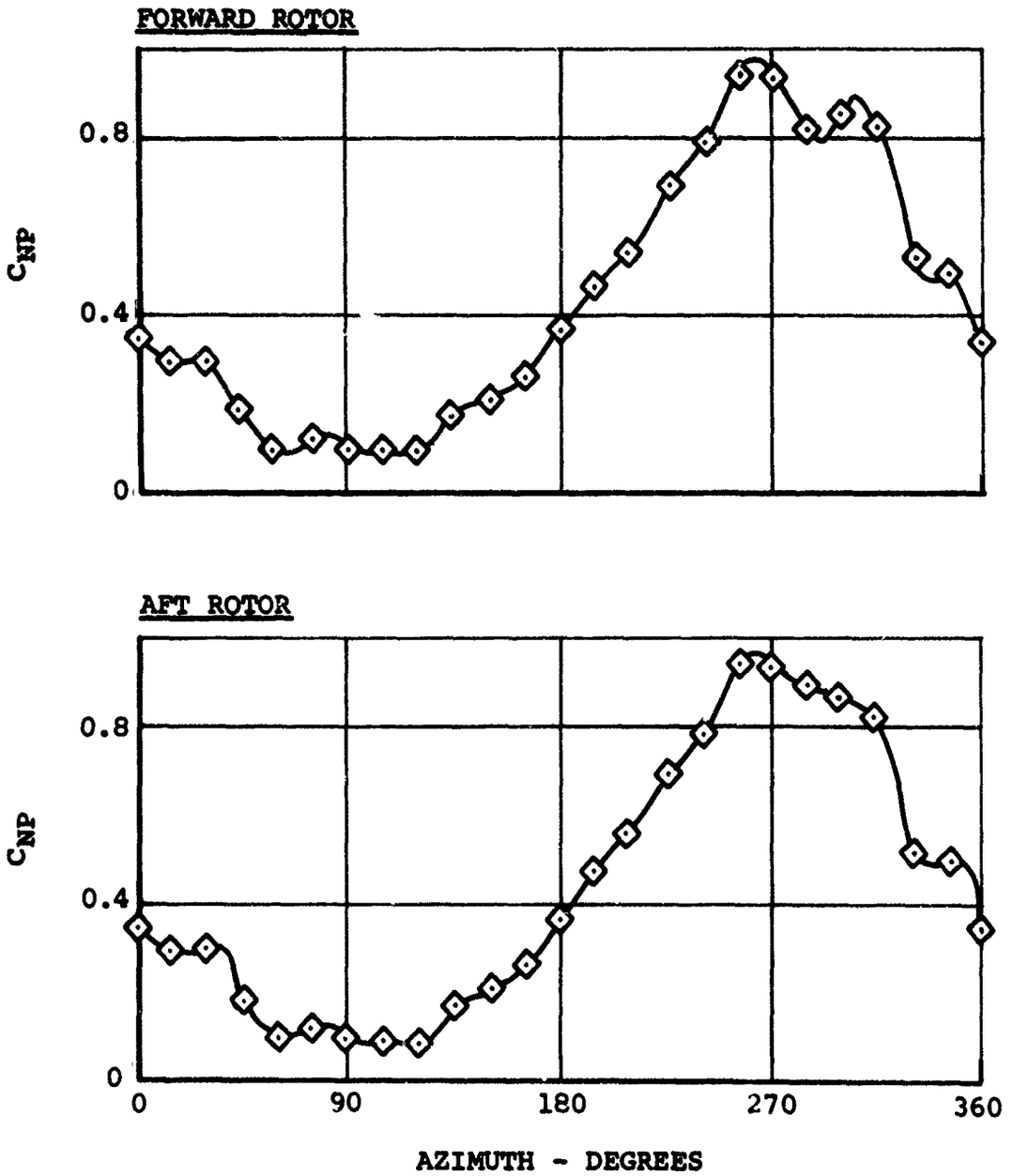

Figure 23. Typical Normal Force Coefficient Data for a Test Point Near the HDL Boundary.

NOTE: ALL DATA OBTAINED AT THE 85-PERCENT RADIUS WITH $\mu' = 0.24$ AND $C_{TW}/\sigma = 0.09$

LEGEND		
SYMBOL	FLIGHT NUMBER	RUN NO.
◇	390	5
▷	394	2

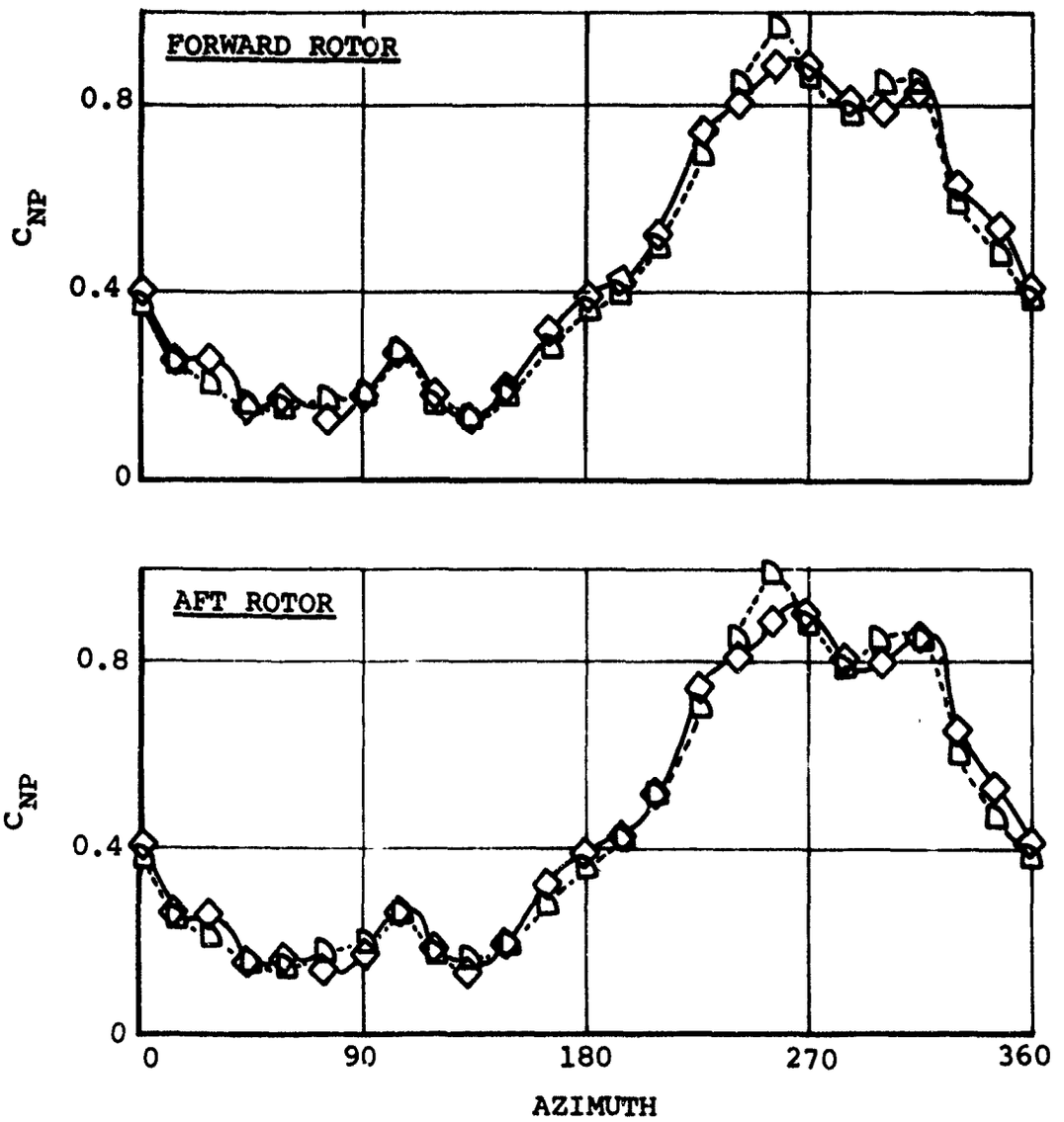

Figure 24. Repeatability of the Normal Force Coefficient Data for the Same Test Point (TPN 46) Obtained in Different Flights.

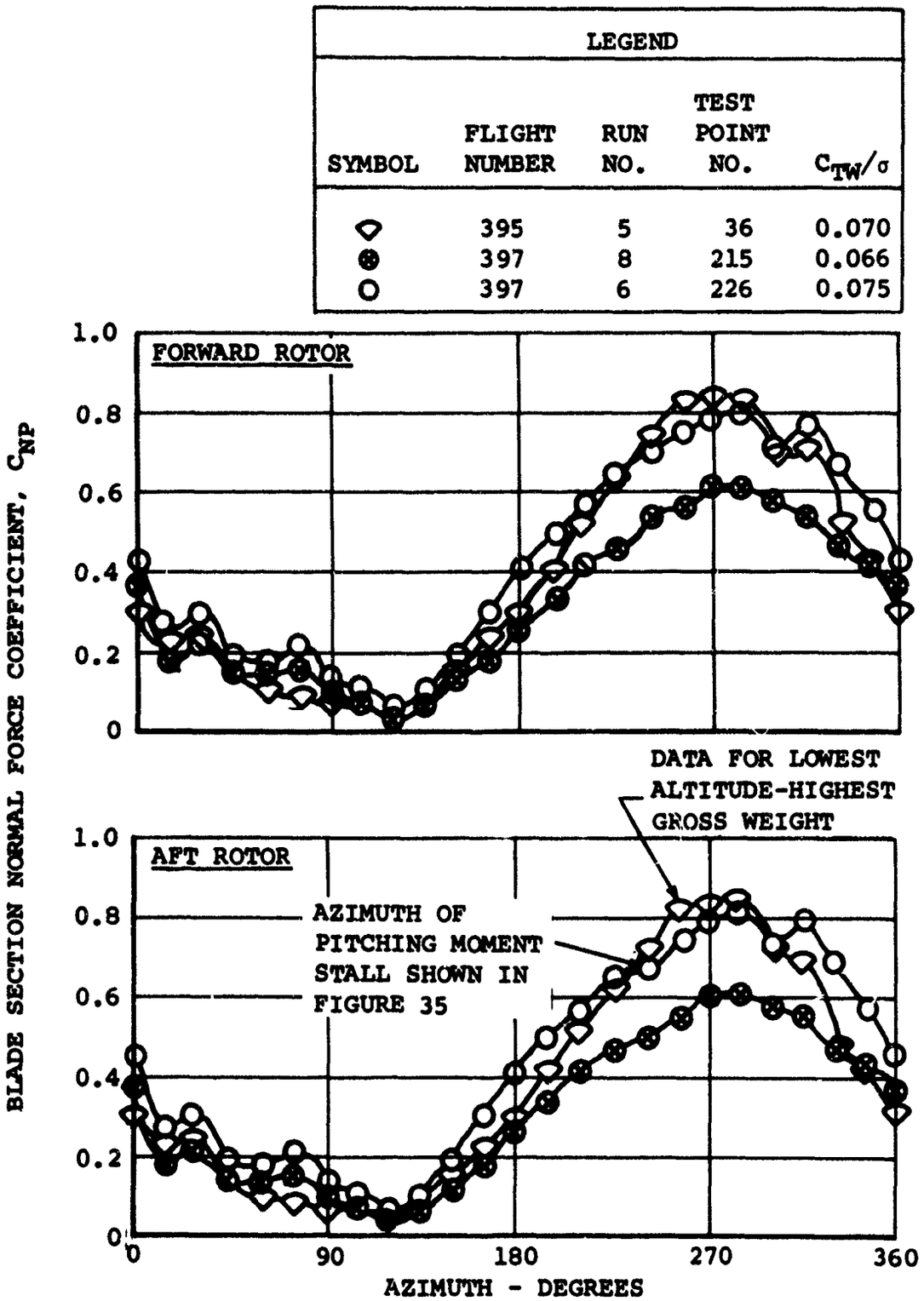

Figure 25. Effect of Thrust Coefficient on Normal Force Coefficients Measured at 95-Percent Radius with an Advance Ratio Near 0.31.

at a constant advance ratio. These data appear to show an azimuthal average C_{NP} value which varies directly with the thrust coefficient; however, the higher gross weight, low-altitude data have a larger first-harmonic variation. This larger azimuthal variation at the higher gross weight results in a larger maximum value of C_{NP}. It can also be noted in this figure that the test data at the higher gross weight have fewer irregularities in the C_{NP} waveform throughout the azimuth but especially near the maximum value of C_{NP}. This relatively more uniform variation may be a reflection of the lack of stall of this test point as compared to test point 226, which will be shown later to be stalled. However, the general trend of more consistent C_{NP} data and larger values of $(C_{NP})_{MAX}$ with increased gross weight is characteristic of the airloads coefficient data. This trend is of much greater significance in the data obtained at the inboard stations of the aft blade.

The only variation in the normal force data which can be attributed to stall with any certainty is also shown in Figure 25. It will be shown later that the airload pitching moments clearly indicate stall, and from this evidence the aft rotor stalled at the 95-percent radius when the azimuth angle reached about 250 degrees for test point 226. Figure 25 shows a slight drop in the azimuthal variation of C_{NP} at this azimuth which is apparently the effect of stall. The data also show many other considerably larger bumps which cannot be explained, so this apparent relation could be coincidence. It appears to be rather certain that if stall has an influence on the normal force coefficient data, this effect is small.

In studying blade stall, the distribution of the normal force coefficients with radius is believed to be important, since blade stall is probably not a two-dimensional phenomenon. Radial distributions of normal force coefficient at 270 degrees azimuth for three typical high-speed test points are shown in Figure 26. These data show a fairly consistent radial distribution for the forward rotor. The normal force coefficients generally increase with decreased blade radius until a peak at the 40-percent radius is reached. At 40-percent radius the C_{NP} values are considerably larger than expected, probably due to the poor definition of the reversed-flow region. It appears from this and from other airload coefficient data that the reversed-flow region is apparently about 0.2 of the radius larger than the expected $r/R=-\mu' \sin\psi$ circle. The use of data

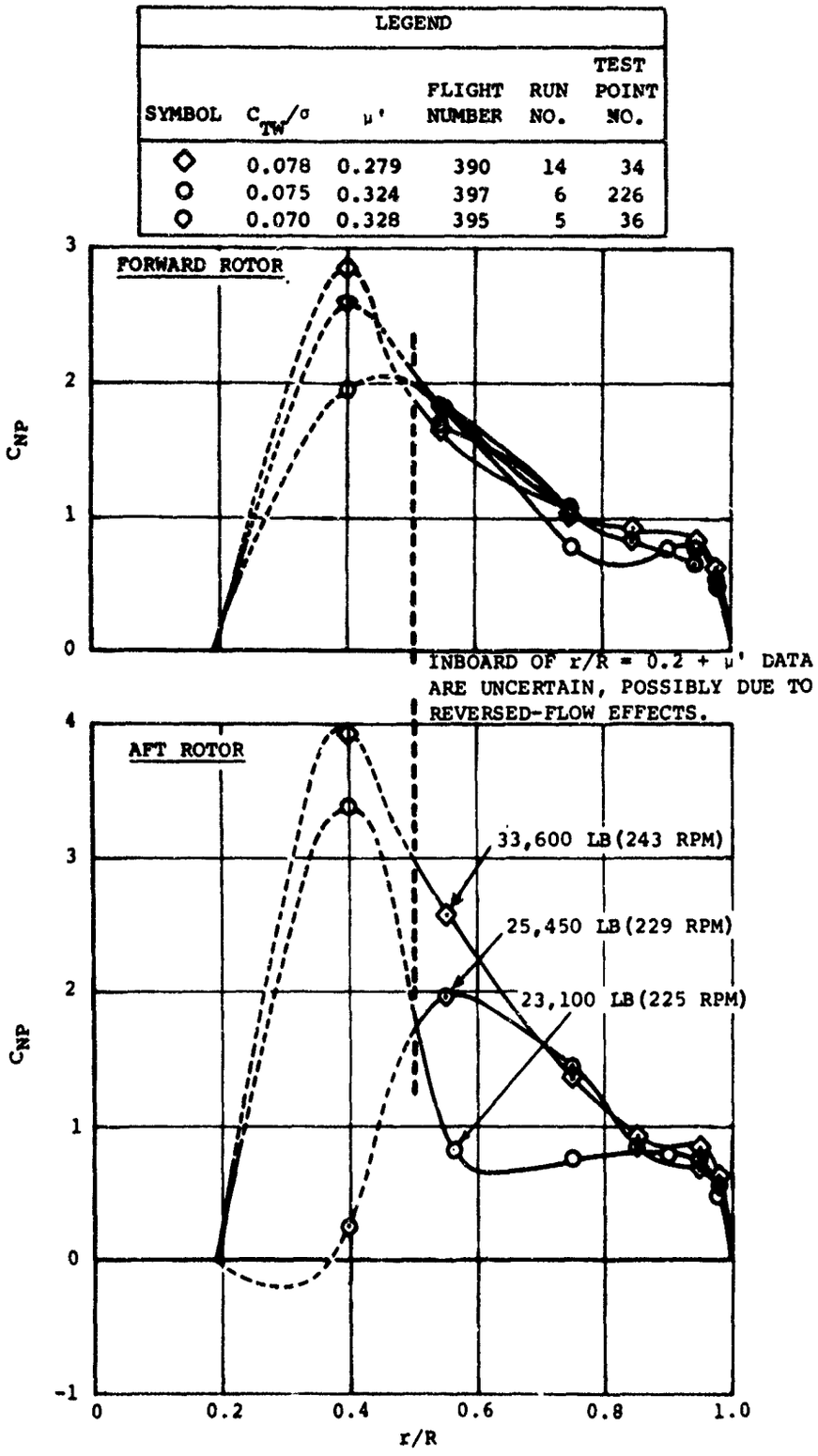

Figure 26. Radial Distribution of Normal Force Coefficient at 270 Degrees Azimuth for Three Test Conditions.

obtained on the retreating blade inboard of the $100(0.2 + \mu')$-percent radius should be made with considerable caution. It is believed that the airload measurements probably have large scatter due to the small loads in the reversed-flow region, and this effect is probably compounded by the uncertain definition of the velocities in this region.

Figure 26 also shows a rather significant increase in the normal force coefficient at the inboard stations of the aft rotor at higher gross weight. This increase presently cannot be explained. A variation like that shown for the forward rotor was expected.

It was anticipated that the occurrence of blade stall would be related to the maximum value of the normal force coefficient which was obtained. These values of $(C_{NP})MAX$ and the azimuth angles at which $(C_{NP})MAX$ occurred vary with blade radius and are considerably different for the forward and aft rotors. Typical values of these data are shown in Figures 27 and 28. Again the higher gross weight, lower-altitude test points produced the expected high values on the forward rotor and higher-than-expected values on the aft rotor. The azimuth angles at which $(C_{NP})MAX$ occurs are distributed as expected for the forward rotor, with the midradius of the blade reaching $(C_{NP})MAX$ earlier than the outboard stations. The aft rotor data show considerable disparities between the values of ψ for $(C_{NP})MAX$. Test points 220, 225, and 226 are shown to reach $(C_{NP})MAX$ much earlier at the inboard stations. It appears that this is related to stalling of the inboard portions of the aft blades for these test points.

Unfortunately the relation between $(C_{NP})MAX$ and stalling is not simple and well defined, as will be shown in the next section of this report. The situation is affected at least by blade section sweep angle and local Mach number. The increased rate of onset of angle of attack which is produced by increased gross weight appears, from the C_{NP} data, to be beneficial in reducing stall effects. Generally for the outboard stations there is almost no evidence of stall in the C_{NP} data. The midradius of the aft blade reaches $(C_{NP})MAX$ much earlier in the azimuth than expected, which may be evidence of stall.

PITCHING MOMENT COEFFICIENTS

The calculation of the airload pitching moments by integrating the first moment of the airload pressure distribution provides

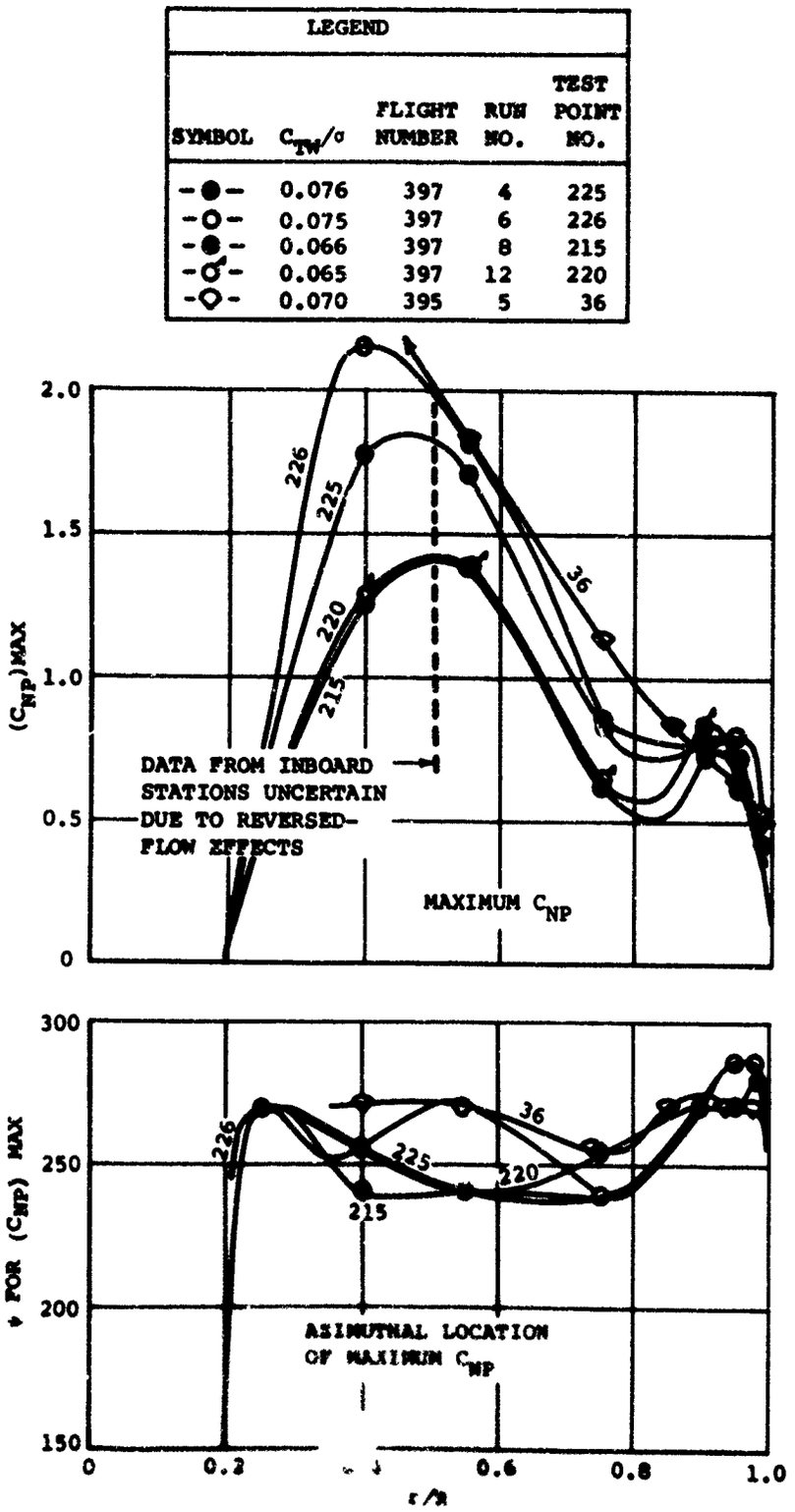

Figure 27. Typical Maximum Normal Force Coefficient Data for the Forward Rotor at an Advance Ratio Near 0.31.

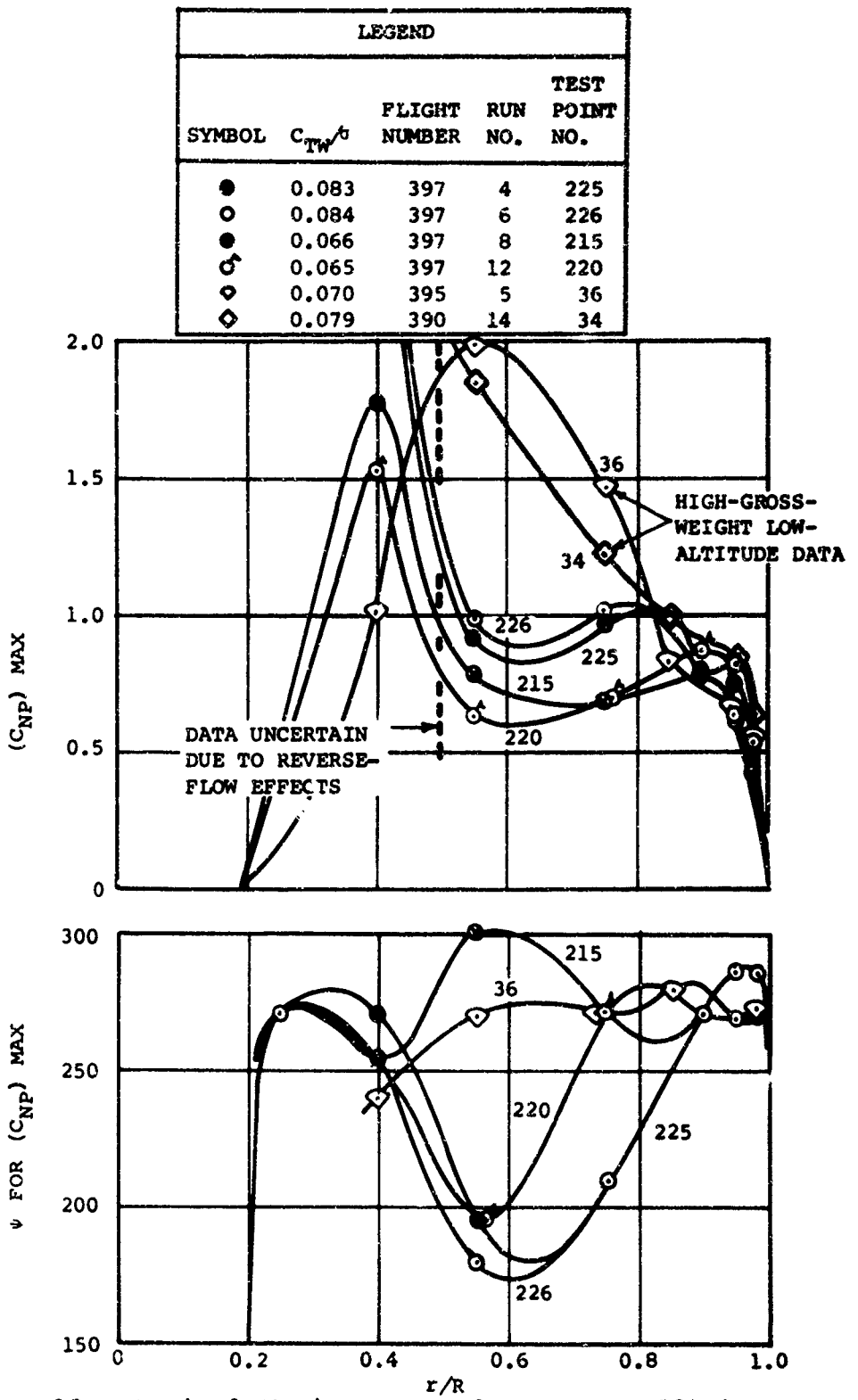

Figure 28. Typical Maximum Normal Force Coefficient Data for the Aft Rotor at an Advance Ratio Near 0.31.

a very sensitive indication of the aerodynamic moment response. These data are acknowledged to be less consistent and less repeatable than is desired; however, the relatively small spurious variations appear to occur as a steady moment variation. This steady moment variation was not unexpected, due to the tendency of the airload instrumentation to have small drifts. In airload coefficient form, a steady pitching moment causes a first-harmonic variation due to the predominantly first-harmonic variation in the local velocity. The moment coefficient data reflect this first-harmonic variation as an aerodynamic center offset. As will be shown, the airloads data generally indicate that the aerodynamic center is forward of the quarter-chord. A statistical evaluation of all the data would be required before a quantitative measure of the aerodynamic center position could be established with confidence.

Typical variations of the airload pitching moments at 95-percent radius for 4 test points at an advance ratio near 0.31 are shown in Figure 29. A rather gentle first-harmonic variation is typical, reflecting the rather sizable first-harmonic angle-of-attack and Mach number variation experienced. The most significant variation shown in these data is the moment break due to stall, which is shown for test point 226 at 260 degrees azimuth in the aft rotor data. This moment coefficient variation is not large as compared with severely stalled blade sections and as compared to the effects of blade sweep and reversed flow. The identification of this variation as stall is based on the C_{MP}-C_{NP} relationship presented in the next section of this report.

As compared to the relatively well-behaved outboard data, the inboard pitching moment coefficients vary greatly, as illustrated in Figure 30. The 40- and 55-percent radius data, which are usually highly suspect due to the uncertainties of the reversed-flow region, show large variations but generally behave as expected. It is rather surprising that the inboard C_{MP} data for the aft rotor are more consistent and show fewer reversed-flow effects than the forward rotor data, since the opposite situation was shown in the normal force data. This situation is typical of the tandem rotor airloads data and is believed to be due to an induced upwash at the forward rotor which is produced by the aft rotor.

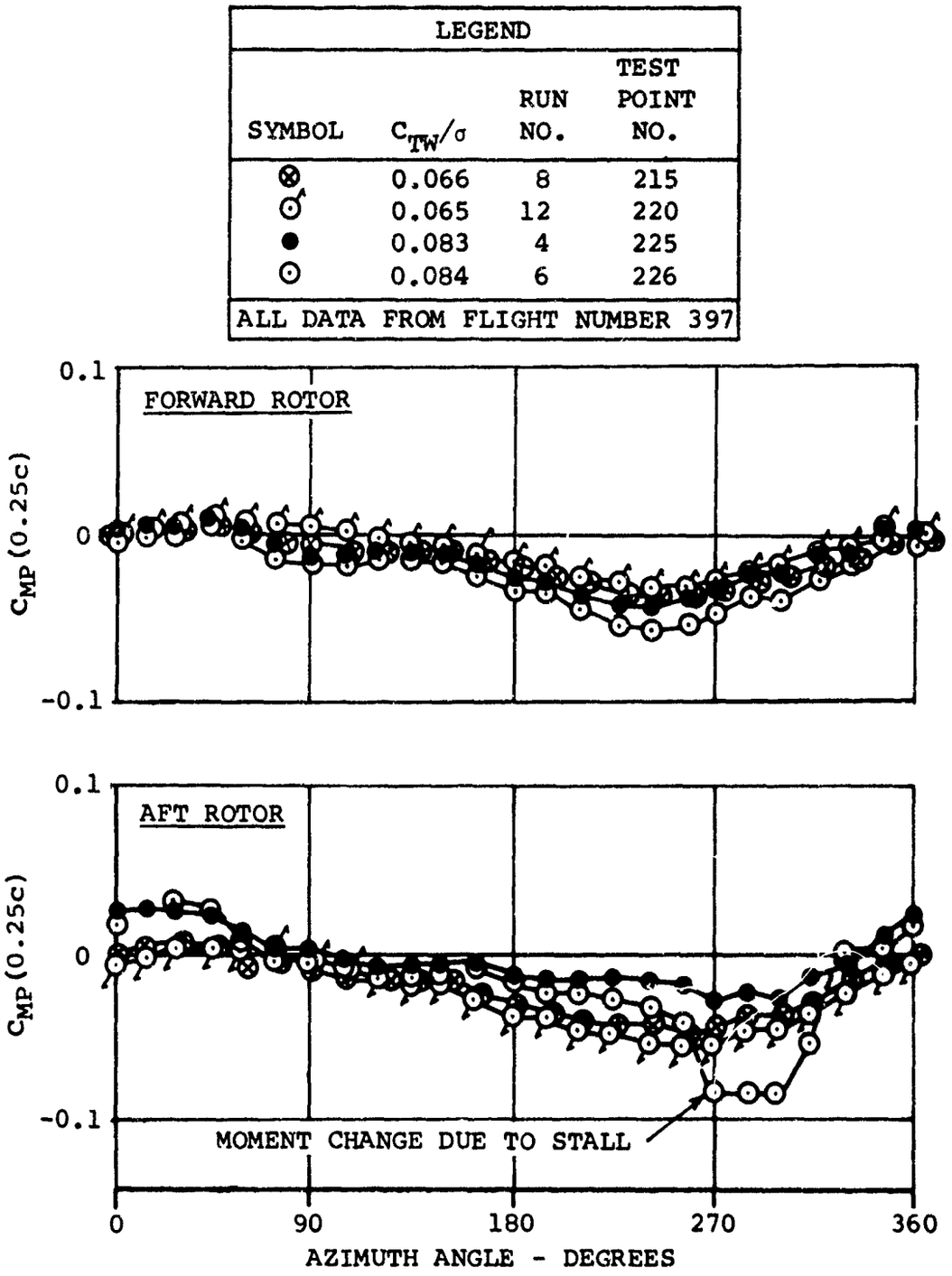

Figure 29. Effect of Thrust Coefficient on Pitching Moment Coefficient Measured at 95-Percent Radius with an Advance Ratio Near 0.31.

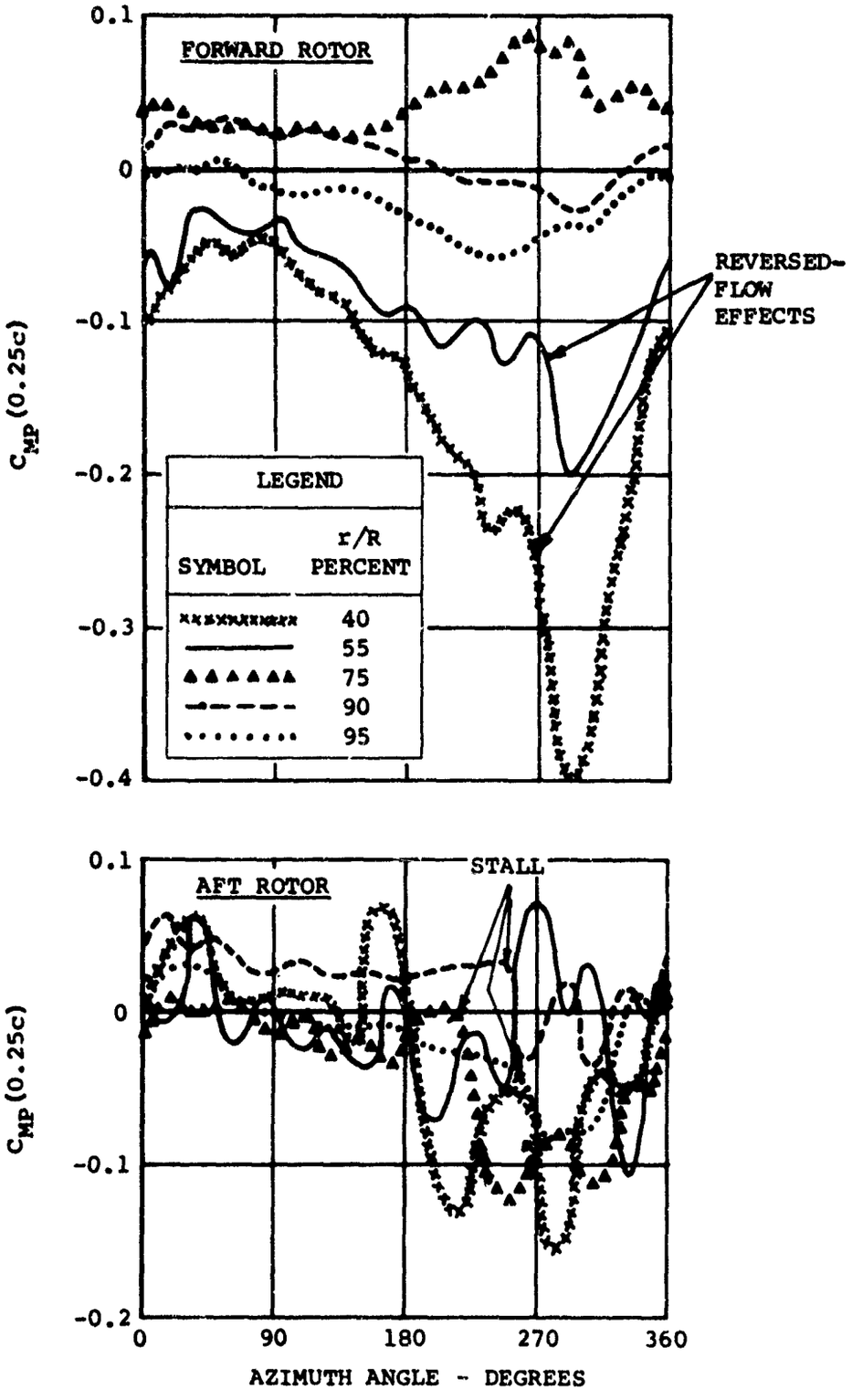

Figure 30. Pitching Moment Coefficients for the Most Extreme Operating Condition Tested.

It should be noted that the data for the 75-percent radius of the forward rotor shown in Figure 30 seem to be inverted. This inversion of the first-harmonic variation of C_{MP} with azimuth is evidence either of an aerodynamic center position which is forward of the quarter-chord or of a steady moment shift in the data. The test data shown in Figure 31 substantiate the test data of Figure 30, since a similar moment coefficient variation is shown at the 85-percent radius of the forward rotor for two other flights. This variation seems to indicate that there is a shift of the effective aerodynamic center which is due to the dynamic-aerodynamic environment. The lack of a similar shift on the aft rotor cannot be explained.

The data of Figure 31, which are plotted to an expanded moment scale, show typical azimuthal variations in the pitch moment coefficient. These data show a fairly pronounced C_{MP} ripple of the forward rotor data and a pronounced C_{MP} break of the aft rotor data for test point 46 which are due to stall. Test point 36 data do not show these variations and, as will be noted in the next section, this point does not show any effects of stall. Figure 31 also shows that test point 46, which was obtained at a significantly lower speed than test point 35, was influenced to a much greater extent by the downwash non-uniformities. There is in particular a pronounced bump in the C_{MP} curve for test point 46 at about 80 degrees azimuth. This bump is probably due to tip vortex interference.

It is believed that the airload coefficient data are shown to be reasonably consistent and repeatable. The normal force coefficient data show the expected azimuthal variations except for the inboard stations of the aft rotor; these stations show significantly different maximum normal force coefficients depending on the gross weight of the helicopter. Blade stall does not appear to influence the normal force coefficient data significantly but is quite pronounced in the pitching moment data.

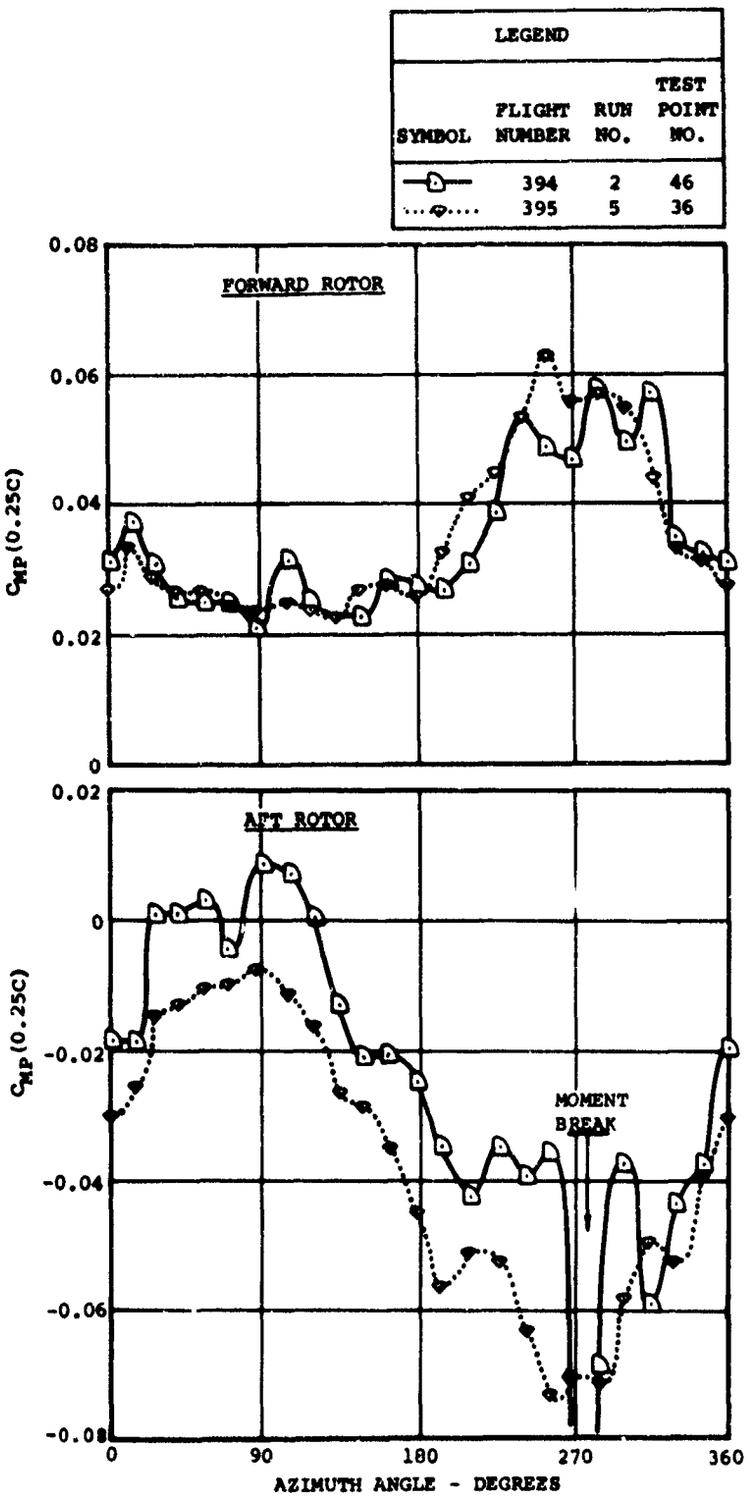

Figure 31. Azimuthal Variation of Typical Pitching Moment Coefficient Data Measured at 85-Percent Radius.

INDICATIONS OF NEGATIVE AERODYNAMIC DAMPING

Rotor blade stability theory indicates that the most serious consequence of stalling is the negative pitch moment damping which is produced. While there is a rather large change in pitching moment due to stall, the reduction of the blade torsional stability is apparently the more significant effect. Without the phase shift resulting from the change in pitch moment damping, the pitching moment due to stall usually does not result in excessive loads. It was therefore decided to use the occurrence of negative aerodynamic damping at large values of C_{NP} as the criterion for stall. This criterion prevented the misidentification of pitching moment variations due to tip vortex proximity bumps, etc., as stall. It also showed unexpectedly that advancing blade compressibility effects can also produce an aerodynamic negative pitch moment damping. This approach is believed to be a key to the analysis of rotor blade airloads data.

The means of identification of negative aerodynamic damping in the airloads data is not obvious and warrants some discussion. While the available pitch moment data, such as shown in Figure 31, indicate rather large oscillations and a moment break apparently due to stall, this evidence is not conclusive. The plot of C_{MP} versus C_{NP} such as shown in Figure 4 does show positive indication of the aerodynamic damping for typical rotor operating conditions. This indication is based on the relatively small time dependence of the normal force coefficient at the frequencies considered for the rotor. The normal force coefficient is therefore almost equal to the angle of attack. The differences between C_{NP} and the local instantaneous angle of attack are largest through stall when this relation is of greatest interest; however, this limitation is not significant, since only an indication of negative damping is desired, not detailed quantitative values. For detailed analyses of stall, these effects should be considered. For the present qualitative review, the use of the C_{MP}-C_{NP} relationship gives a good barometer of aerodynamic damping. This damping indication gives a good criterion for stall and compressibility effects.

When there are no stall, compressibility, or local sweep effects of consequence, the C_{MP}-C_{NP} relation is similar to that shown in Figure 32. The generally elliptical figure is typical and indicates that the first-harmonic damping is predominant. Two irregularities which are apparently due to tip vortex proximity are shown at the 15 and 60 degrees azimuth positions. The

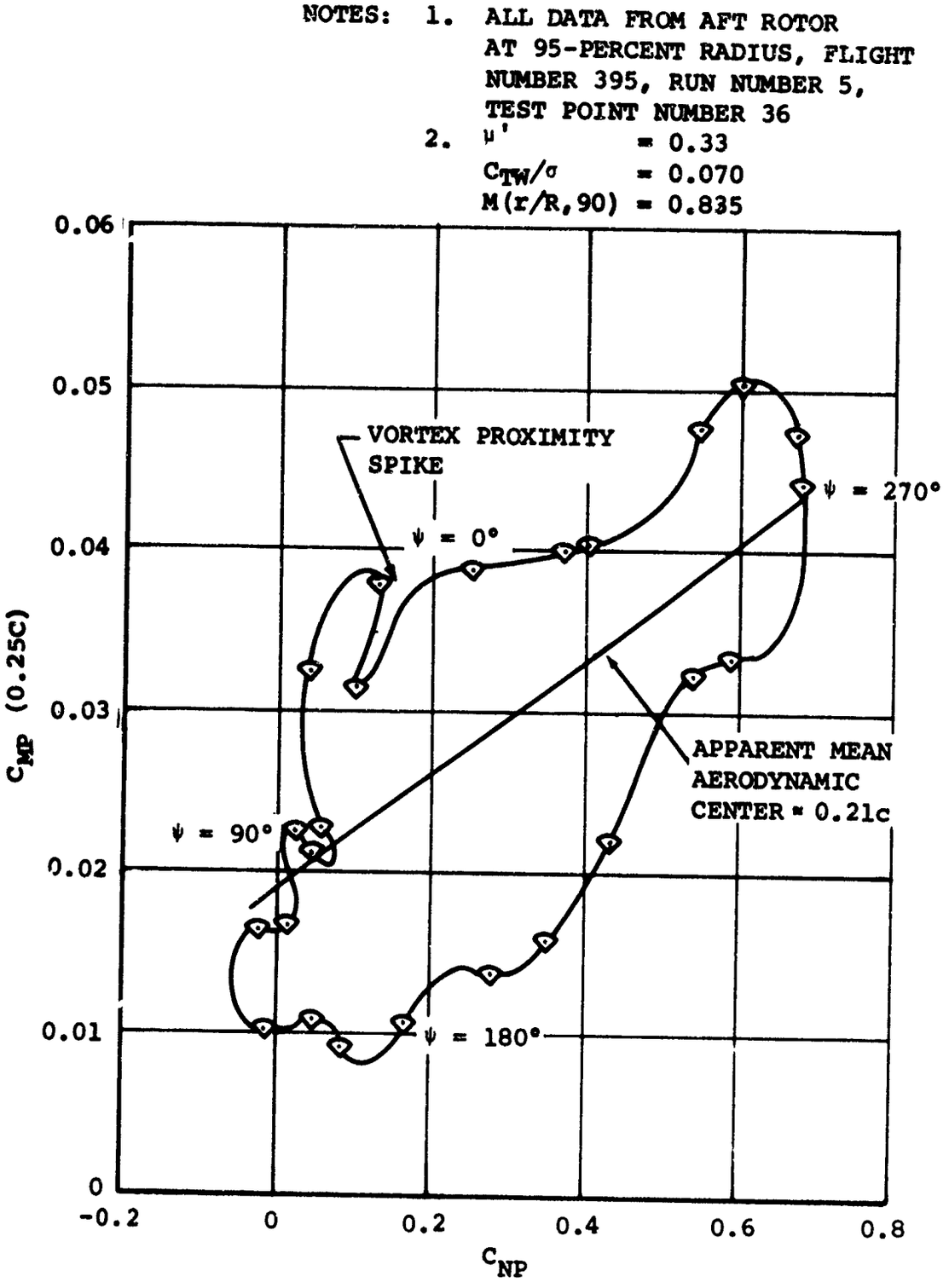

Figure 32. Aerodynamic Damping Indication of Typical Test Point with No Stall or Compressibility Effects.

elliptical shape is inclined, indicating that the mean aerodynamic center is apparently not at the 25-percent chord, but appears to be at the 21-percent chord. This more-forward-than-expected aerodynamic center is also typical of the airloads data, but the magnitude varies somewhat, apparently due to small average airload pressure instrumentation errors. It is believed that the mean aerodynamic center data will be valid for an average of the many data points available and are worthy of additional analysis.

The direction of the manner in which the data progression circumscribes the elliptical shape of Figure 32 is indicative of positive aerodynamic damping. This can be shown from the equation of motion of the blade-torsion/blade-rotation aerodynamic system considered, which can be simplified for this discussion to the following:

$$\left[dC_m/d\alpha\right]\alpha + \left[dC_m/d\dot{\alpha}\right]\dot{\alpha} + \left[\text{smaller unknown terms}\right] (\alpha\dot{\alpha},\ddot{\alpha},\text{etc.})$$
$$= \left[\text{inertia terms, structural spring terms, structural damping}\right]_{(\theta,\dot{\theta},\ddot{\theta})}, \quad (2)$$

where it should be noted that the blade incidence, θ, is not necessarily linearly related to the angle of attack, α. With the usual definitions for the aerodynamic coefficients, the spring term, $dC_m/d\alpha$, is generally positive; for positive damping, $dC_m/d\dot{\alpha}$ is negative. Thus, as α increases, damping reduces the value of C_m, so that for positive damping an ellipse is circumscribed with the data progressing around the ellipse in a counterclockwise manner. Figure 32 shows a similar data progression, indicating that as expected the aerodynamic damping was positive for this case, which had no significant stall, compressibility, or local sweep effects.

It should be noted that rather significant changes in the assumptions of the moment reference axis and the velocities used to form the airload coefficients can be made without influencing the indications of damping. For this report, all data are shown with the pitching moment calculated with respect to the quarter-chord; however, many data points were also calculated with respect to the blade pitch axis (0.20c). This change causes the inclination of the C_N-C_M ellipse without changing the shape of the figure. The use of the tangential component of the velocity, rather than the local resultant velocities based on nonuniform downwash, is illustrated for

some nonstalled forward rotor data in Figure 33. It can be seen that the elliptical figure is stretched considerably by neglecting part of the velocity. A considerably increased $(C_{NP})_{MAX}$ value of 1.26, rather than 0.86, was obtained. Generally, however, the shape of the curve is not particularly distorted by the change in the velocity assumption. There can be seen a higher harmonic positive damping loop on the first-harmonic variation between 210 and 250 degrees azimuth, and there are vortex proximity spikes near the 0- and 90-degree azimuth positions. These vortex proximity effects occur later in the azimuth than is shown in Figure 32, since the data for Figure 33 were obtained at 75-percent radius rather than 95-percent radius. It is concluded that, if an indication of damping is desired without an evaluation of the magnitude of the coefficients, the inflow components of the velocity can probably be neglected; however, values of the coefficients such as $(C_{NP})_{MAX}$ will be significantly in error.

STALL EFFECTS

The aerodynamic evidence of stall is clearly shown in the C_{MP}-C_{NP} relation as illustrated in Figures 34 and 35. Figure 34 is typical of stall at the lower Mach numbers tested and shows a sharp break in the C_{MP}-C_{NP} relation at the maximum normal force coefficient value. Following the moment break, an area is circumscribed in a clockwise manner indicative of negative aerodynamic damping. There are two smaller loops on the main loop, both of which are also traversed in a clockwise manner. The return to a nonstalled C_{MP}-C_{NP} relationship does not occur until after the 0-degree azimuth position is reached. The region of positive damping, from 15 degrees to about 180 degrees, is normal except for the negative damping indication on the advancing blade, which is discussed below.

Blade stall at higher Mach numbers is characterized by an earlier divergence from the normal C_{MP}-C_{NP} relation and by a delayed recovery from stall. A typical test point showing this effect is illustrated in Figure 35. The azimuth from 75 to 165 degrees shows a fairly normal positive damping reflected in the somewhat elliptical variation. At a normal force coefficient of only 0.3, the pitching moment coefficient starts to diverge. The slope of the C_{MP}-C_{NP} relationship remains statically stable (dC_{MP}/dC_{NP} is negative) until just before 270 degrees is reached. A fairly well-defined region of negative damping occurs near this azimuth, but this negative damping is more than balanced by the large region of positive

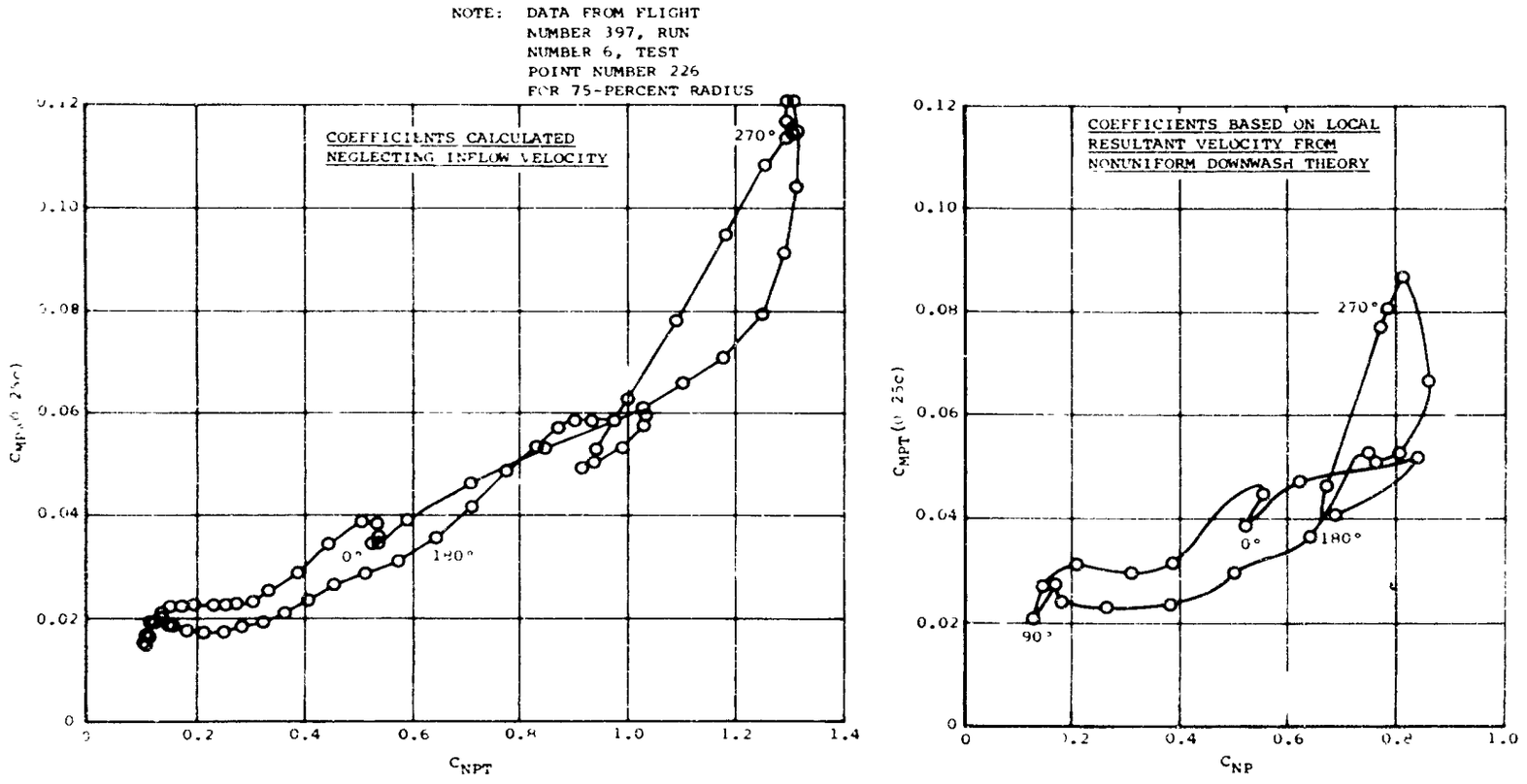

Figure 33. Forward Rotor Airloads Data Showing Absence of Negative Damping Regions and Significance of Local Inflow Velocity Components.

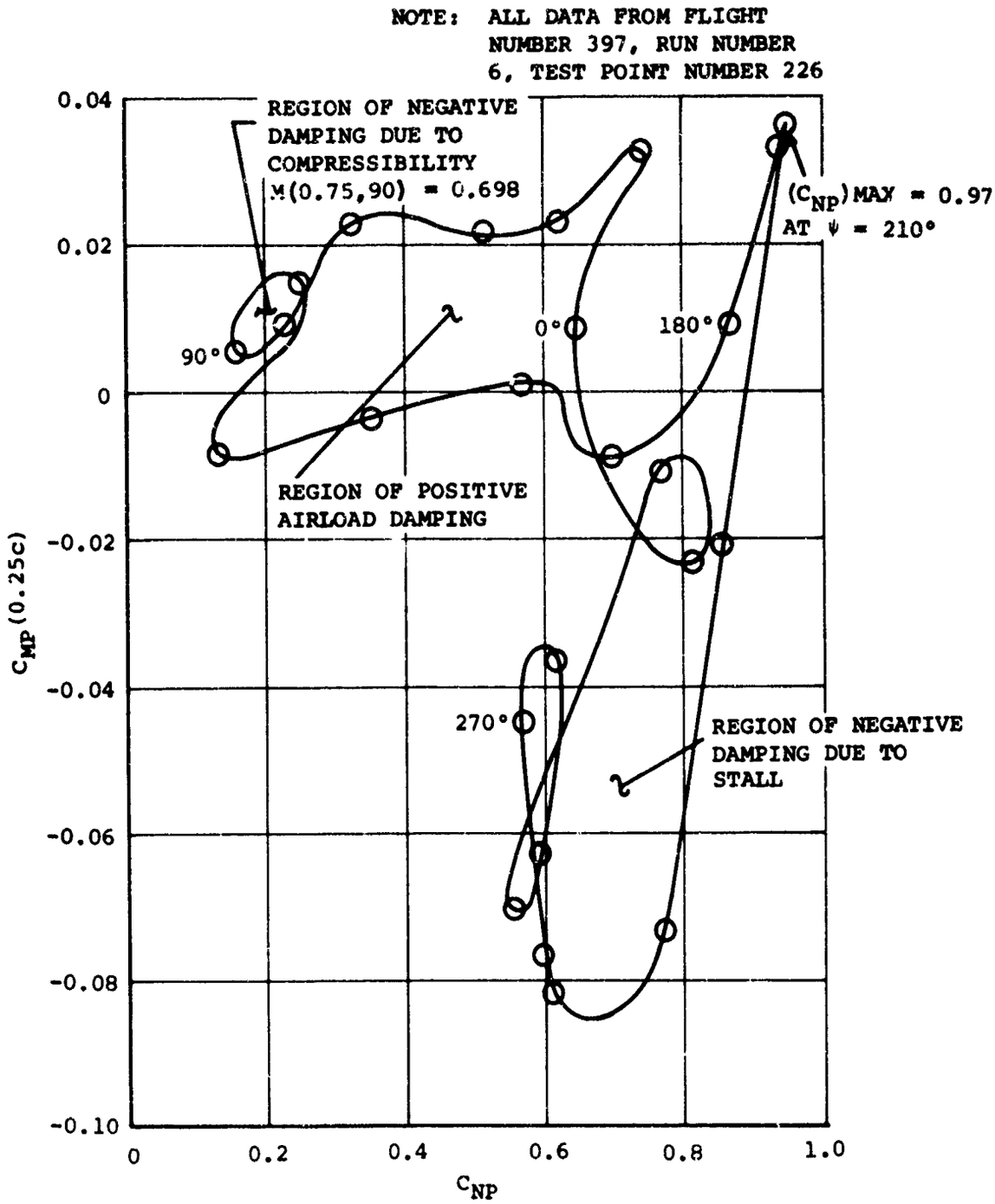

Figure 34. Aerodynamic Pitch Moment Damping at 75-Percent Radius of Aft Rotor for Condition Which Produced Stall and Compressibility Effects.

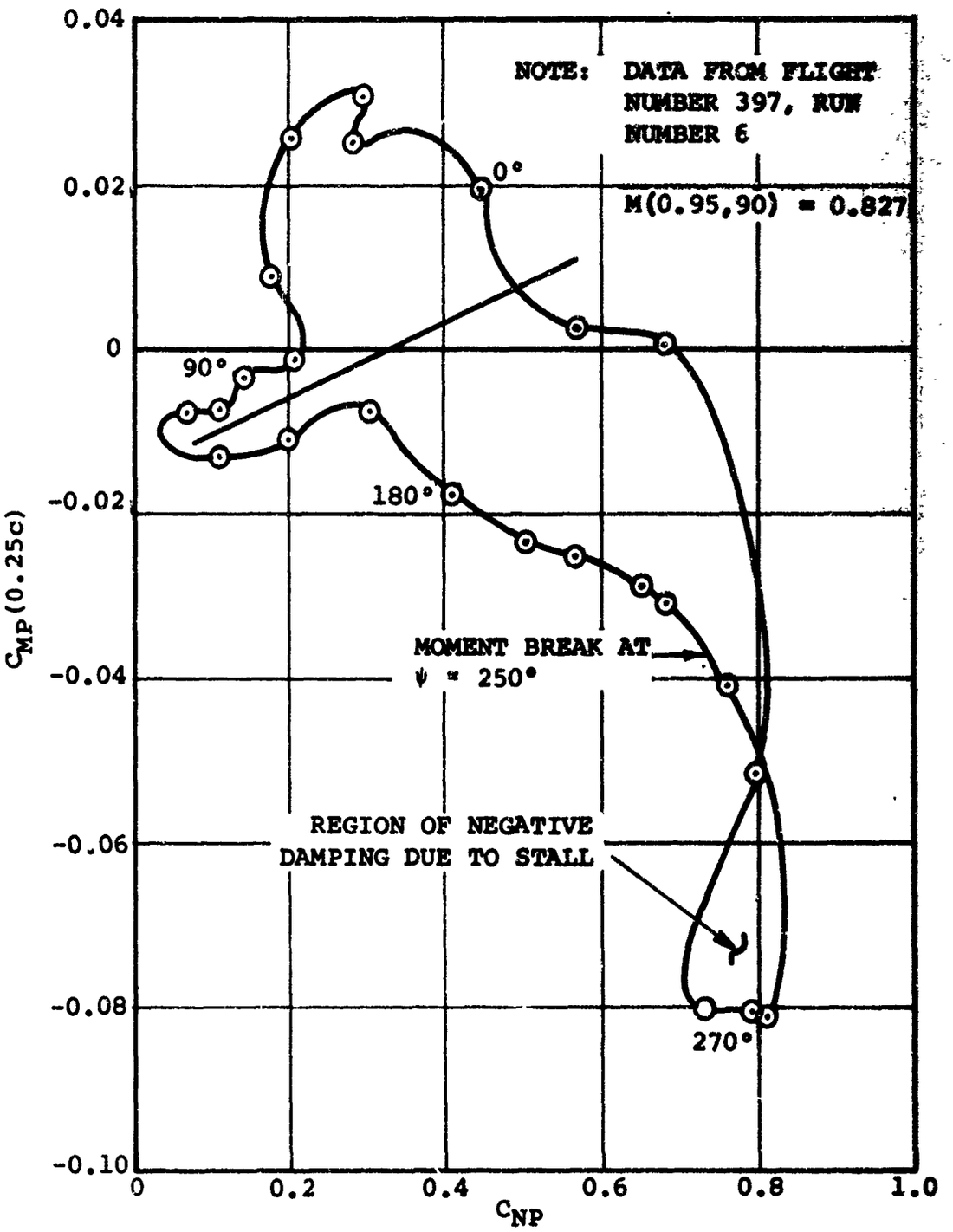

Figure 35. Pitch Moment Damping at 95-Percent Radius of Aft Rotor for Test Point Number 226.

damping which is generated prior to the delayed stall recovery.

The indications of blade stall at the inboard blade stations which experience significant blade sweep angle variations are also shown in the C_{MP}-C_{NP} plots. A curve similar to Figure 34 is obtained for these stations with a moment break, and a negative damping loop is obtained, but the effects of sweep are also imposed. The effects of sweep will be discussed separately.

It was expected that blade stall would increase when both the maximum value of C_{NP} and the local Mach number increased. Summary plots of these parameters for three of the instrumented blade stations are presented as Figures 36, 37, and 38. The test points which show blade stall in the C_{MP}-C_{NP} relation are indicated in these figures by filled symbols. The data are shown to have considerable scatter, indicating that the problem of predicting blade stall is more complicated than a simple $(C_{NP})_{MAX}$-Mach number relationship. Very large values of $(C_{NP})_{MAX}$ are achieved at 55-percent radius without stall, apparently due to the effects of sweep. This sweep benefit is also apparently uncertain, with some stalled points occurring at moderate values of $(C_{NP})_{MAX}$. It is believed that the rates of change of both angle of attack and sweep are also significant parameters of the blade stall prediction problem. Considerably more analysis is apparently required to resolve a consistent criterion for stall.

Within the large, presently unexplained variations of the rather limited stall data, there appears to be a significant influence of the local retreating blade Mach number. The bottom of the scatter of these blade stall data points from Figures 37 and 38 are plotted in Figure 39 and apparently show this effect. A $(C_{NP})_{MAX}$-Mach number relation for stall is shown that is different for the two rotors, but both rotors show a variation similar to the C_ℓ-Mach number relationship for pitch moment divergence of a static two-dimensional airfoil. The static airfoil data are from Figure 3 and were discussed previously. The data of Figure 39 are believed to be a reasonable first-order estimate of the effect of Mach number on blade stall. It appears from these data that rotor blade stall is influenced more significantly by Mach number than is indicated by airfoil section wind tunnel data. The aft rotor data also show stalling at lower values of $(C_{NP})_{MAX}$ than the forward rotor data at Mach numbers below 0.5. This greater sensitivity of the aft rotor to stalling is believed

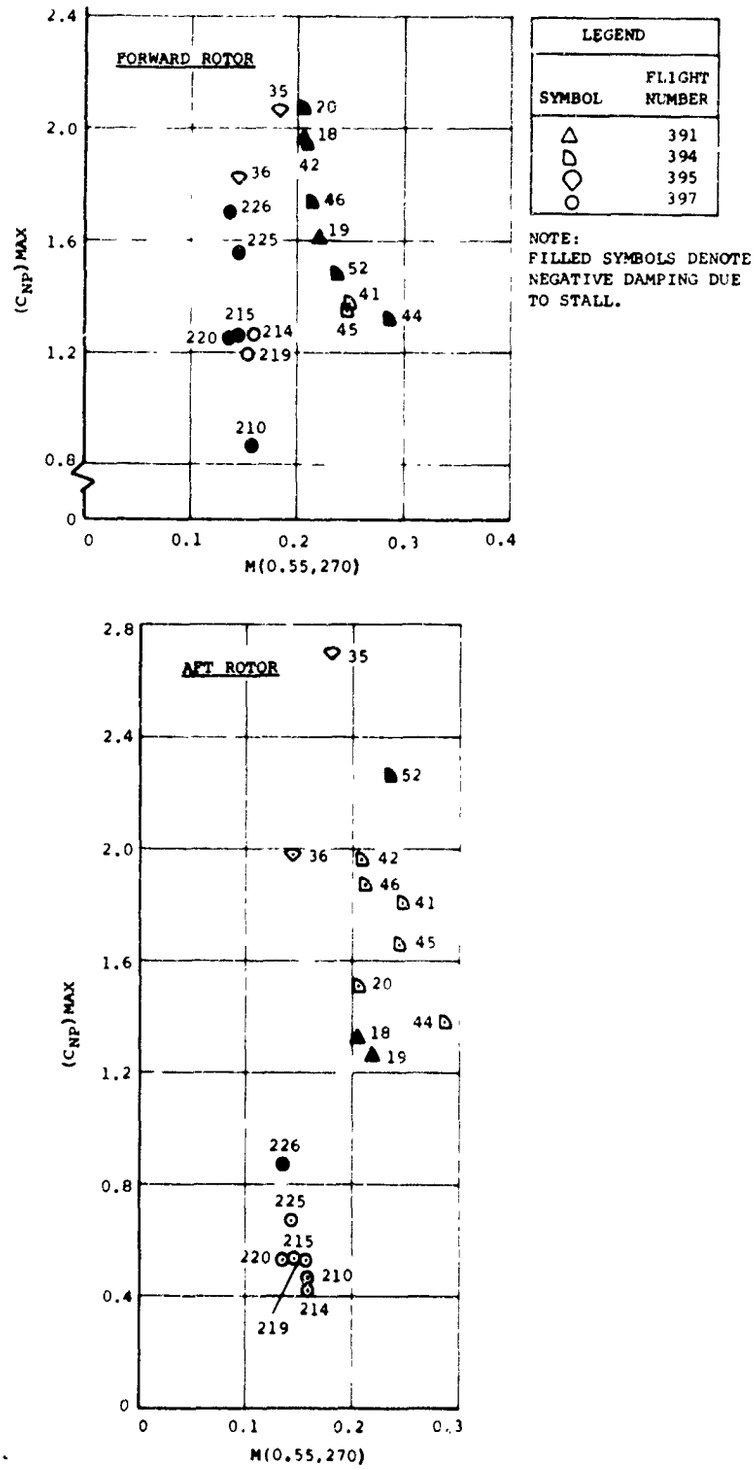

Figure 36. Retreating Blade Section Operating Conditions at 55-Percent Radius.

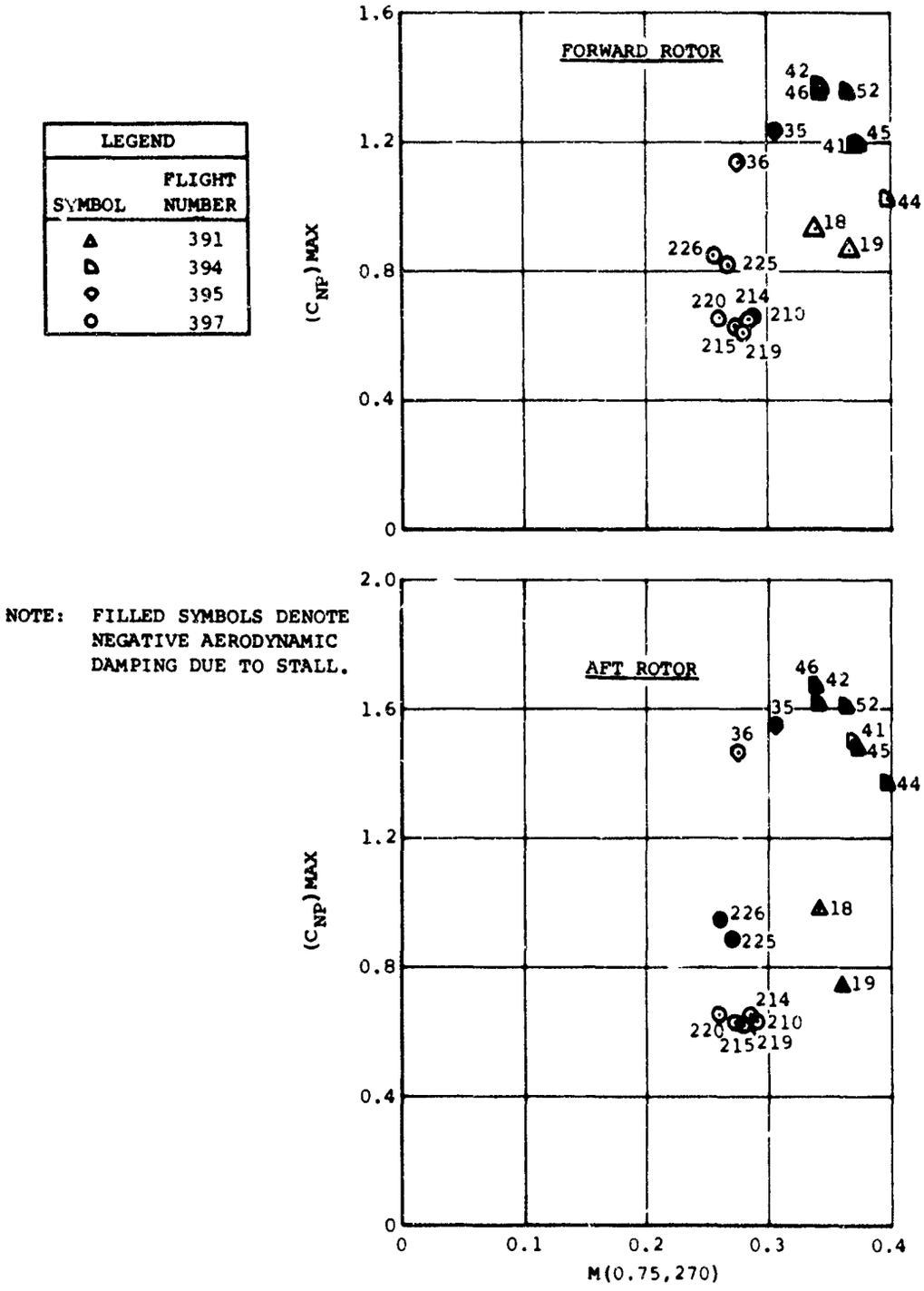

Figure 37. Maximum Normal Force Coefficients Measured at 75-Percent Radius Showing Points with Negative Damping Due to Stall.

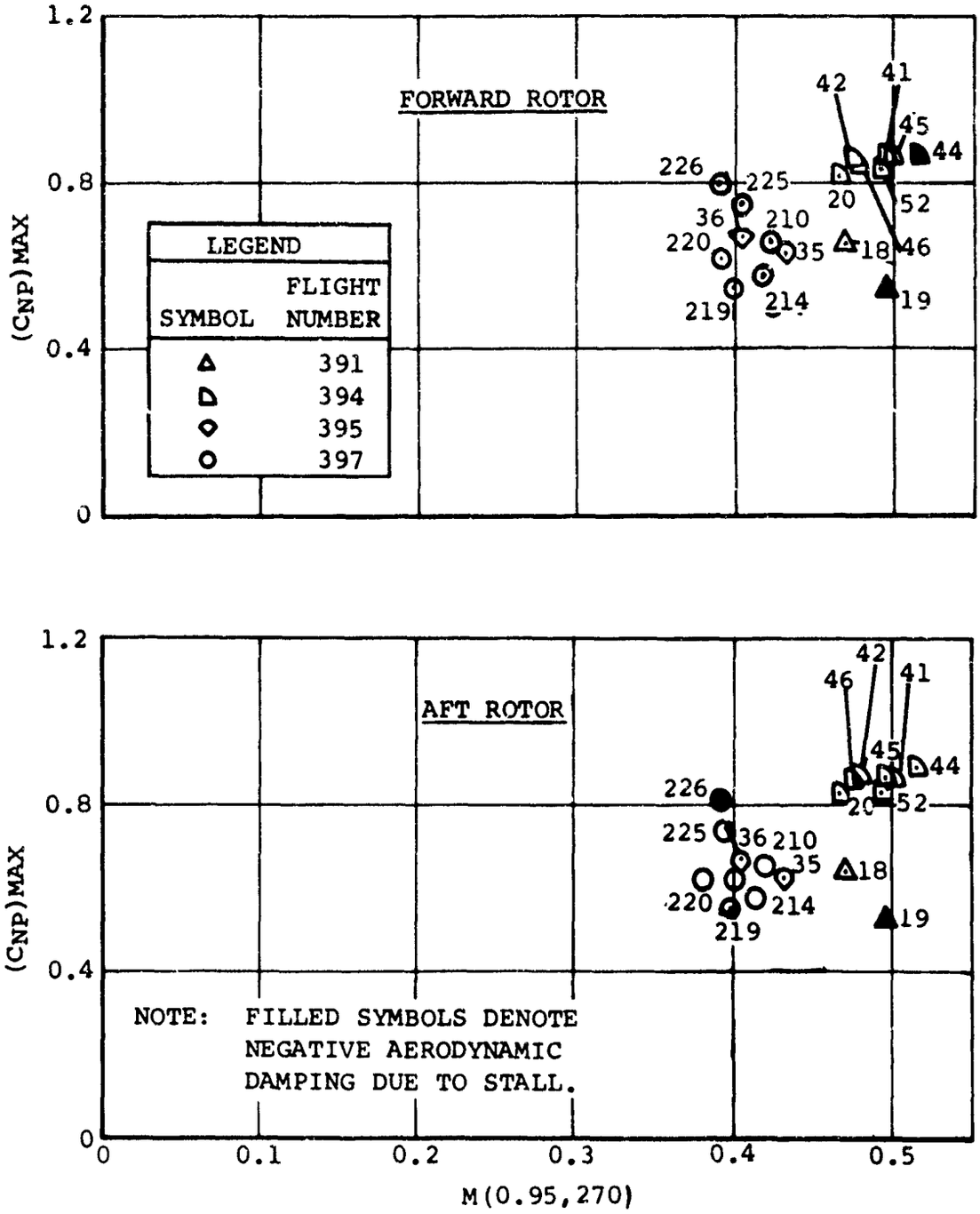

Figure 38. Maximum Normal Force Coefficients Measured at 95-Percent Radius Showing Points with Negative Damping Due to Stall.

NOTES: 1. FLAGGED SYMBOLS DENOTE FORWARD ROTOR DATA.

2. DATA ARE THE SMALLEST VALUES OF $(C_{NP})_{MAX}$ WITH STALL FROM FIGURES 37 and 38.

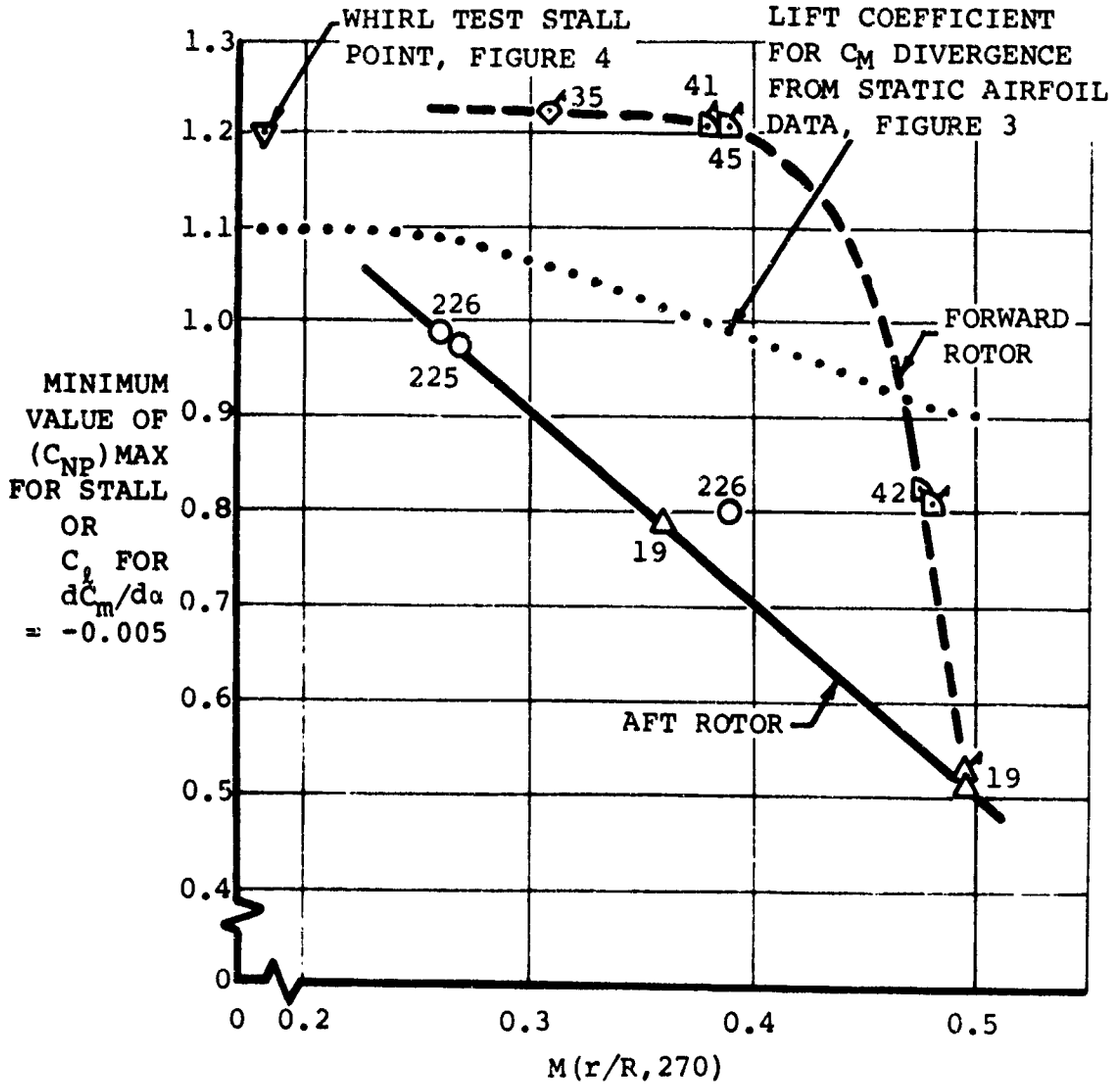

Figure 39. A First-Order Estimate of the Effect of Local Mach Number on Stall.

to be due to the larger radial gradient of the azimuthal average loading on the aft rotor shown in Figure 9. It should be noted that the radial gradient of the aft rotor blade loading is similar to the usual loading gradient of a single rotor.

ADVANCING BLADE COMPRESSIBILITY EFFECTS

There is definite evidence of negative aerodynamic damping on the advancing blade near the 90-degree azimuth position, such as that shown in Figure 34 for many data points. The data of this figure are not actually typical of this phenomenon, since the local advancing Mach number is only about 0.70. For this case, the compressibility effect is made significant by the relatively large C_{NP} values obtained on the advancing blade at the 75-percent radius. A more typical situation is illustrated in Figure 35, with an advancing blade Mach number of 0.83 but with no negative damping shown due to the much lower values of C_{NP} which occurred. An advancing blade section Mach number of about 0.85 generally produced negative damping at small values of C_{NP} and would be considered a critical Mach number for the 0011-1.43 airfoil section of the CH-47A rotor. Substantiation that this phenomenon is a compressibility effect can be obtained from the chordwise pressure distributions, which show a typical transonic pressure variation for points with a negative damping loop on the advancing blade.

These effects of compressibility can be significant in producing excessive blade loads, as shown in Figure 21, and should therefore be studied further. At least, the C_{NP} and Mach number relation required for negative damping on the advancing blade should be defined. Such a study was believed to be beyond the scope of this program.

RADIAL FLOW (LOCAL SECTION SWEEP ANGLE) EFFECTS

The radial component of the helicopter's forward flight velocity produces a local sweep angle at the blade section which is significant. As shown in Figure 40, the sweep angle varies in a predominantly first-harmonic manner with an amplitude of 30 degrees at the 75-percent radius for the relatively high advance ratio (μ'=0.37) illustrated. For a given flight condition, this sweep angle is larger inboard and smaller outboard due to the variation in the relative magnitude of the radial section velocities and the fixed velocity of forward flight. Variations in sweep angle dominate

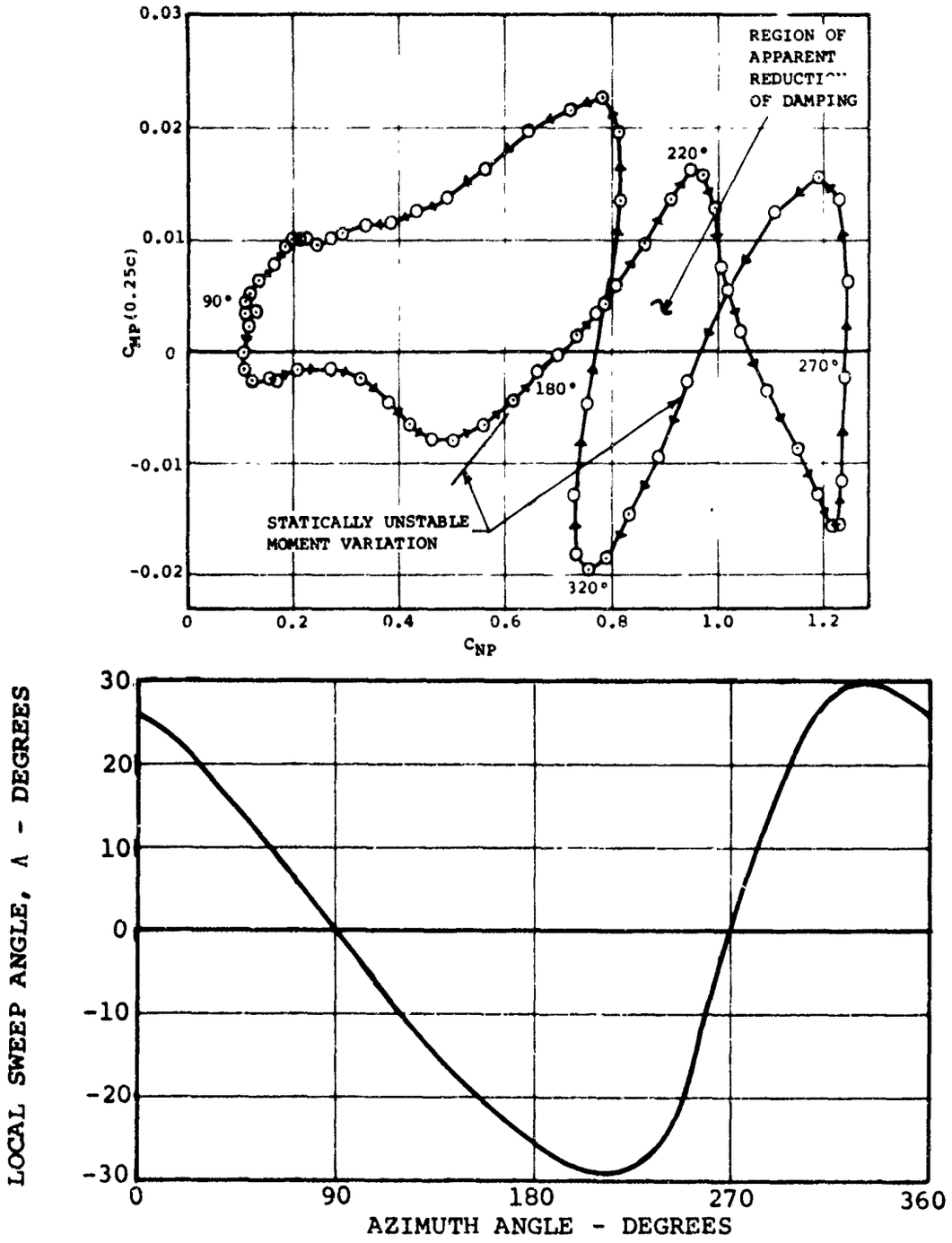

Figure 40. Stall Relief and Reduced Pitch Moment Stability Due to Radial Flow at 75-Percent Radius for the Highest Speed Test Point.

the blade stall of the 55-percent radius data which were mentioned previously. At 75-percent radius and outboard, there is generally little or no effect of sweep, since the advance ratio is usually low. The data for Figure 40 were obtained at a relatively high advance ratio, and the C_{MP}-C_{NP} variation illustrated shows significant effects of sweep. First, there appears to be a delay of stall due to sweep. A $(C_{NP})MAX$ of 1.24 is shown in Figure 40 for aft rotor data, which would be expected from the data of Figure 37 to be a fairly positive indication of stall. The data of Figure 40 do not show the slightest trace of stall. However, Figure 40 also illustrates that sweep effects cause a static instability in the pitching moment with a negative value of dC_{MP}/dC_{NP} shown for two portions of the azimuth. The connection between this negative slope and the sweep angle is shown at the 220- and 320-degree azimuth positions. The sweep angle reverses slope at these two azimuth angles, and this change in slope of the sweep variation is nearly coincident with the change in the slope of the C_{MP}-C_{NP} variation. It appears from these data that a decreasing rate of change of the sweep angle with azimuth is the mechanism which causes the pitch moment instability.

To sum up this section, the data presented are believed to show that the problems which cause high rotor blade loads at high speed can be isolated, but there is much work to be done before the problems due to stall, compressibility, and sweep are resolved. The theoretical prediction of these effects is discussed in the following section, and an approach to the further analysis of these data is presented.

THEORETICAL PREDICTIONS

The state of the art of rotor analysis has not received the proper stimulus from the rotor airloads data which have been available since 1962 (reference 2). These rotor airloads data show significant unexplained phenomena, and therefore the rotor analyses were more easily understood and believed. As discussed in Volume IV of this report, there is now available a large body of airloads data which are in reasonable accord. It behooves the rotorcraft industry to utilize these data. Since present analyses use empirical tables for airfoil performance characteristics, the synthesis of airfoil characteristics from the rotor airloads data is recommended. It is hoped that some guidance in this synthesis can be obtained from the correlations of theoretical predictions of damping, stall, and nonuniform-downwash angle of attack presented in this section.

AERODYNAMIC MOMENT DAMPING PREDICTION

The existence of aerodynamic damping of the first-harmonic pitching moment variation illustrated by the airloads data would generally not be predicted by rotor aerodynamicists, since the wake coupling effects would be neglected. In hovering, the effects of wake coupling on the aerodynamic damping were evaluated by Loewy in 1957 (reference 9). This analysis showed that when the wake spacing was small, the aerodynamic damping was very different from the damping which would be calculated if wake coupling effects were neglected. While this analysis has not been extended to the forward flight case, the results would be expected to be similar. The inclination of the downwash in forward flight tends to keep the wake near the rotor for a few wake revolutions. This results in a wake coupling situation which is similar to hovering but which is complicated by the helical wake. The nonuniform-downwash analyses of references 12 and 17 can probably be modified to calculate the effects of forward flight on pitch moment damping following the hovering analysis. For the present discussion, it is believed that the hovering analysis can be used as a guide. For small spacing (h), for a first-harmonic variation (m=1), and with a small reduced frequency, the quadrature component of the airloads is increased significantly. This is roughly equivalent to a significant increase in the effective reduced frequency as compared to the infinite spacing case.

Comparison of the potential flow aerodynamic damping analysis (reference 1 or the infinite spacing results of reference 9) to the indications of aerodynamic damping from the rotor airloads data requires that an assumption be made as to the effective reduced frequency. The infinite-spacing, first-harmonic reduced frequency obviously should be based on the rotational velocity of the section. That is,

$$k_{1\Omega} = \frac{c\Omega}{2\Omega r} = \frac{c}{2r} \quad . \tag{3}$$

To avoid the selection of an arbitrary larger number or an empirical factor on $k_{1\Omega}$, a reduced frequency based on the forward flight velocity is suggested. This velocity obviously has less theoretical justification, but a good first-order estimate of the damping is provided.

Thus,

$$k_{1V} = \frac{c\Omega}{2V} = \frac{\pi\sigma}{2B\mu} \quad . \tag{4}$$

For test point 36 with an advance ratio of 0.33, the first-harmonic forward-velocity reduced frequency, k_{1V}, is 0.098. The pitching moment at the quarter-chord equations of the theory reduce to

$$C_m = 0.006\alpha - 0.154(\dot{\alpha}/\Omega) \tag{5}$$

$$C_\ell = 5.51\alpha - 1.23(\dot{\alpha}/\Omega) . \tag{6}$$

The assumption that $C_\ell = C_n$ is made, and the relation between C_m and C_n that results is plotted in Figure 41 by making use of the experimental mean aerodynamic center. It is believed that the comparison shown is an excellent first-order approximation. This comparison is believed to be typical of data points which were obtained with small sweep, low Mach number, and without stall.

STALL PREDICTION BY UNIFORM-DOWNWASH THEORY

The uniform-downwash, rigid-blade rotor analysis was selected for comparison with the indications of stall from the airload measurements, since this simple analysis is generally used in contemporary stall criteria. This theory is known to be significantly in error in its prediction of angle of attack and will eventually be abandoned; however, this evolution is

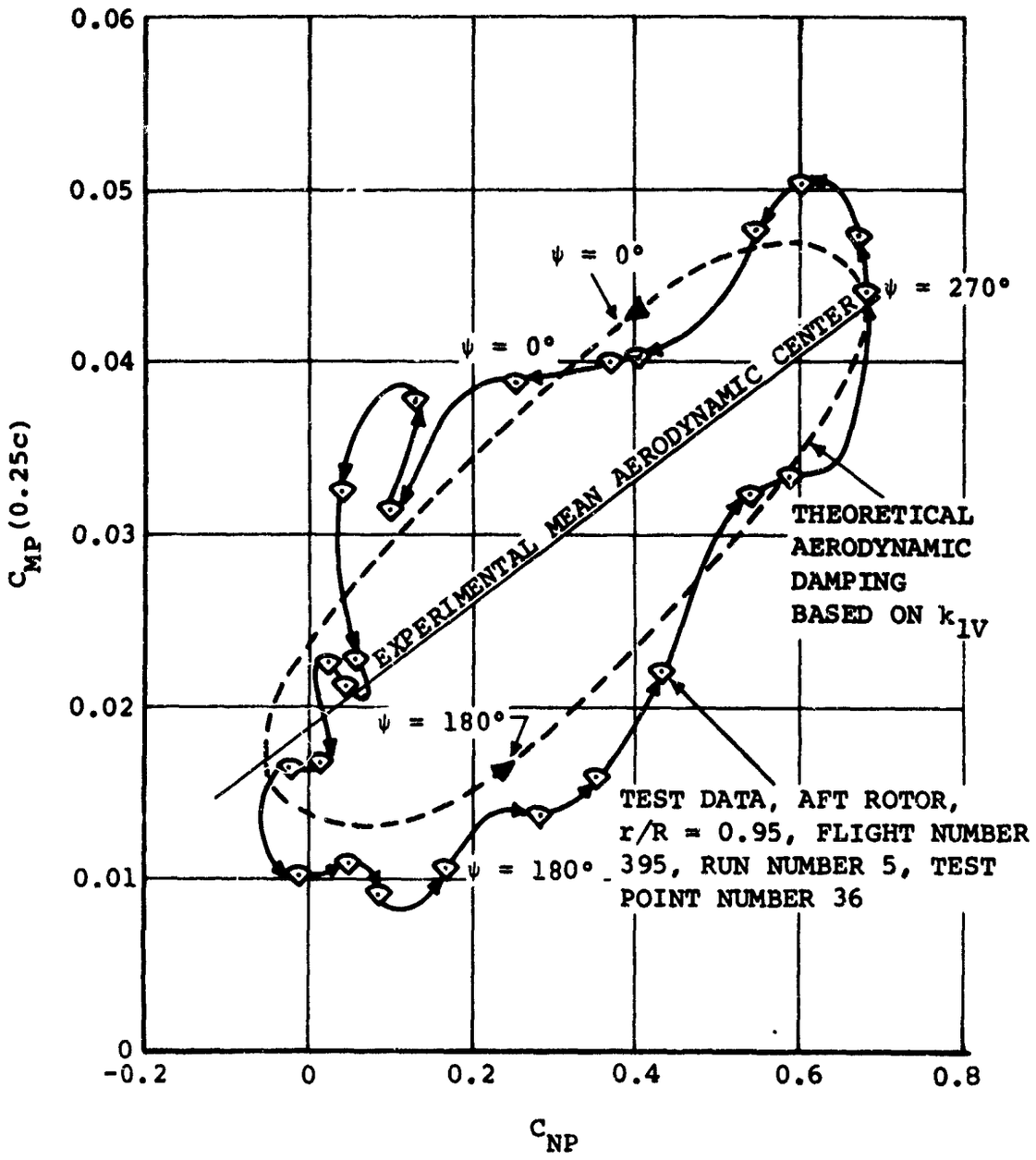

Figure 41. Comparison of Aerodynamic Damping Predicted by Potential Flow Theory and Test Data.

slow. It is expected that the use of a nonuniform-downwash stall criterion will avoid most of the limitations to be discussed.

An initial problem encountered in this comparison was that a representative blade station had to be selected. It was decided that the 75-percent radius station was more likely to indicate more serious consequences of stall, and it was therefore selected. This station is rather far from the blade tip; this situation raised questions as to the applicability of $\approx \alpha$ (1.0,270). It should be noted, however, that for the rotor conditions considered, the difference between $\approx\alpha$(1.0,270) and the angle of attack at the 75-percent radius and 270 degrees is less than one-half of one degree. Nonuniform downwash calculations for these conditions show that the 75-percent radius angle of attack is about 3.5 degrees larger than the uniform-downwash angle of attack. The shift from the tip angle of attack to conditions at the 75-percent radius is therefore significantly less important to this discussion than the initial assumption of uniform downwash. The value of $\approx \alpha$ (1.0,270) was therefore proposed for this evaluation as a barometer of the severity of the operating condition; but as shown below, even this qualitative indication does not apply consistently.

The results of this comparison are shown in Figure 42, using the same stall points presented in Figure 37. It was expected that the maximum normal force coefficients obtained would have a less complicated relation to $\approx\alpha$(1.0,270) than is shown. While it is at present only a supposition that larger values of $(C_{NP})_{MAX}$ indicate more severe blade section operating conditions, it was anticipated that the variations due to gross weight and rpm would be reflected in $\approx\alpha$(1.0,270). From these data, it is concluded that any use of the uniform-downwash angle-of-attack calculations should be made with suspicion. If this theory must be used, the filled symbols of Figure 42 indicate that aerodynamic blade stall usually occurs at angles of attack greater than about 9 degrees. One point of stall shown, which was obtained on the aft rotor with increased rpm, occurred with $\approx\alpha$(1.0,270) of only 6.3 degrees. On the forward rotor, test points without stall were obtained with $\approx\alpha$(1.0,270) values as large as 10.5 degrees. At best, it appears that this theory is inconsistent in its prediction; but if a limit is to be established, a value of 9 degrees appears reasonable. The low value of $\approx\alpha$(1.0,270) has a section retreating blade Mach number of 0.3. It appears from the preceding discussion of Mach number

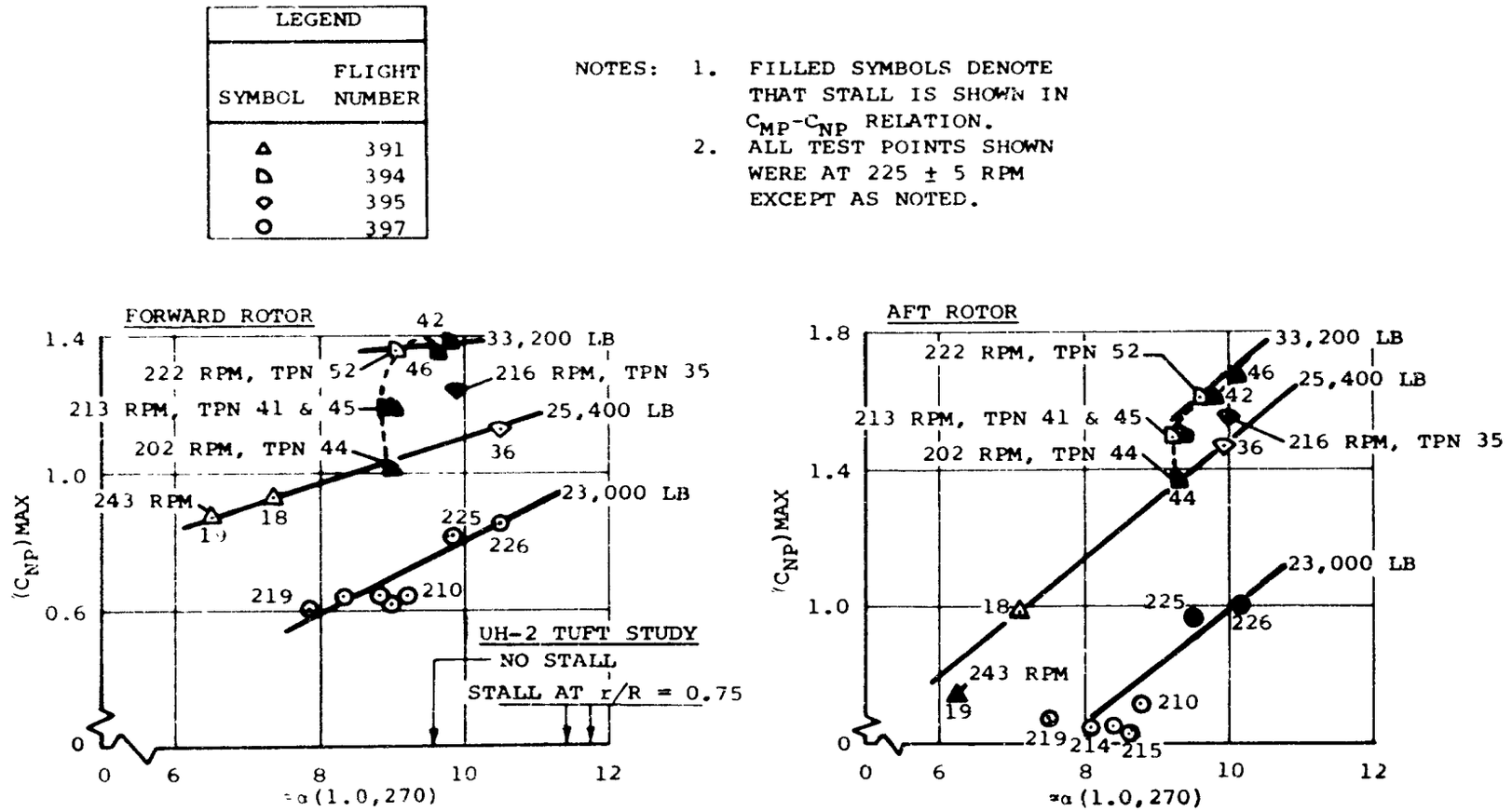

Figure 42. Comparison of Maximum Normal Force Coefficient at 75-Percent Radius to Uniform-Downwash Rigid-Blade Retreating Tip Angles of Attack.

effects that M(0.75,270) should be less than 0.3 for the 9-degree limitation to apply. The rotor blade tuft study of reference 21 is noteworthy in this regard since the general inadequacy of the uniform-downwash theory is graphically illustrated. It appears that the tuft photographs from this reference are in reasonable accord with the airload pressure measurements. The three points obtained have been added to Figure 42. These points indicate that α(1.0,270) greater than 9.6 degrees but possibly less than 11.8 degrees is required for stall at the 75-percent radius. A better criterion for the aerodynamic inception of blade stall effects is obviously required.

PREDICTION OF BLADE SECTION ANGLE OF ATTACK

In a further effort to provide a basis for the synthesis of airfoil data and for aid in the development of a stall criterion, the angle-of-attack distribution for one test condition was calculated using the available nonuniform-downwash theories. This angle-of-attack distribution was compared with the C_{NP} values measured for this test conditon. Since there is little time dependence of lift at the frequencies considered, a linear relation between C_{NP} and angle of attack is expected. Deviations from a linear relation indicate errors in the angle-of-attack prediction. It will be shown that a simplified nonuniform-downwash theory that includes blade bending gives a good prediction of the azimuthal angle-of-attack variations. The lack of proper consideration of tandem rotor interference which has recently been shown precludes the prediction of the azimuthal average angle of attack.

There are presently two nonuniform-downwash theories in use at the Vertol Division. One of these theories, described in detail in reference 4, assumes a rather sophisticated array of vortexes in the downwash flow field but assumes rigid blades. For this report the angle of attack predicted by this theory is defined as α(NUD-R). The second theory has a simpler nonuniform downwash analysis with only a tip and a root vortex but includes blade deflections. The angle of attack from this theory is defined as α(SNUD-E). While this evaluation was being made, it was decided to determine the effect of adding a time delay calculated from potential flow theory to the more accurate of these quasi-static theories. This angle of attack was defined as α_{da} and was added to α(SNUD-E) as follows:

$$\alpha_{da} = \alpha(\text{SNUD-E}) - K_2/K_1 \left[d\alpha(\text{SNUD-E})/d\psi \right] \qquad (7)$$

where K_1 and K_2 were evaluated from potential flow theory at k_{1v}.

The three angle-of-attack distributions which were obtained for the forward rotor at test point 46 are shown in Figure 43. A predominant first-harmonic variation is shown, with the largest higher harmonic variations shown by α(SNUD-E). The rate term of α_{da} tends to smooth the irregularities of this curve. It was expected that the α(NUD-R) would have the smallest oscillations since the wake irregularities are less pronounced and blade bending is not included.

The comparison of these three angle-of-attack distributions with the appropriate C_{NP} data is shown in Figures 44, 45, and 46. α(NUD-R) is shown to overpredict the azimuthal average angle of attack by 1.8 degrees and gives only a fair prediction of the azimuthal waveform. A good prediction of the azimuthal waveform would be indicated if the C_{NP} values fell on a line similar to the theoretical C_n variation shown. The prediction of α(SNUD-E) is much better by contrast. The concave upward shape is eliminated and the local bumps near 90 and 270 degrees azimuth are smaller. The addition of the rate term makes the correlation worse, as shown in Figure 46. It is concluded from this study that blade bending must be included in the calculation of rotor blade angle of attack and that the tip vortex effects of α(NUD-R) are not sufficiently strong. The azimuthal error of α(SNUD-E) for this test point is plotted in Figure 47 and shows that this theory predicts the angle of attack within one degree. This is regarded as excellent agreement for the retreating blade and from an analytical viewpoint; however, the practical significance of the one-degree error shown on the advancing blade can be sizable.

The prediction of the aft rotor angle of attack of a tandem helicopter by the α(NUD-R) theory is somewhat worse than for the forward rotor. This prediction is illustrated in Figure 48 and shows considerable azimuthal variations in the correlation. An average angle-of-attack difference is also shown unexpectedly for this rotor. This difference cannot be explained. It is generally concluded from these data that considerably more work is required before the tandem rotor nonuniform-downwash theories can be used with confidence for detailed analyses.

It has been shown that, with a proper consideration of the effective reduced frequency, the first-harmonic aerodynamic pitch moment damping can be predicted. Predictions of blade

stall by the uniform-downwash theory are inconsistent and inadequate. Angle-of-attack predictions with a simplified nonuniform-downwash elastic-blade theory are within one degree for the forward rotor. Aft rotor predictions by a more sophisticated downwash analysis which assumes rigid blades are poor.

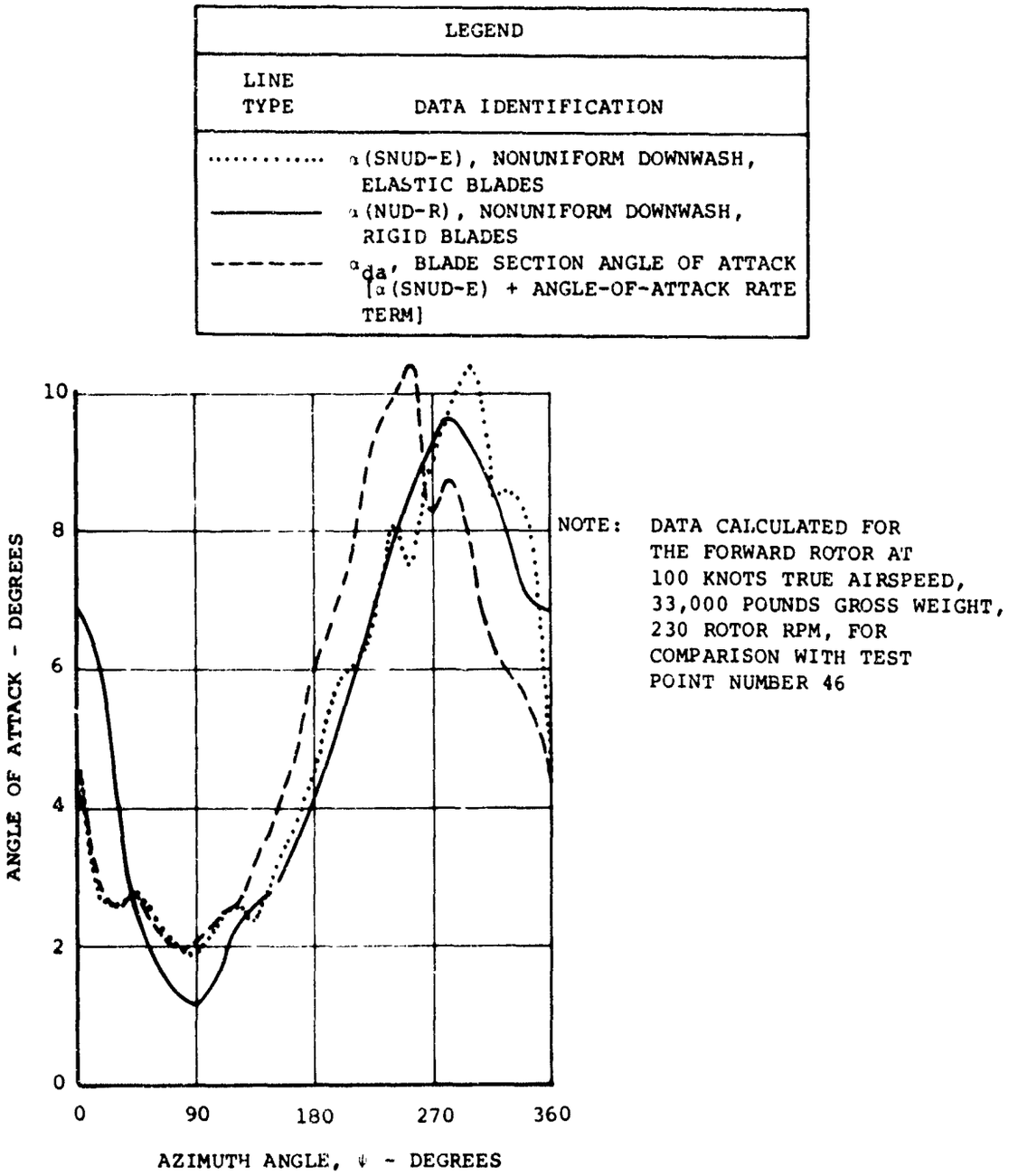

Figure 43. Comparison of Angle-of-Attack Values from Various Theories.

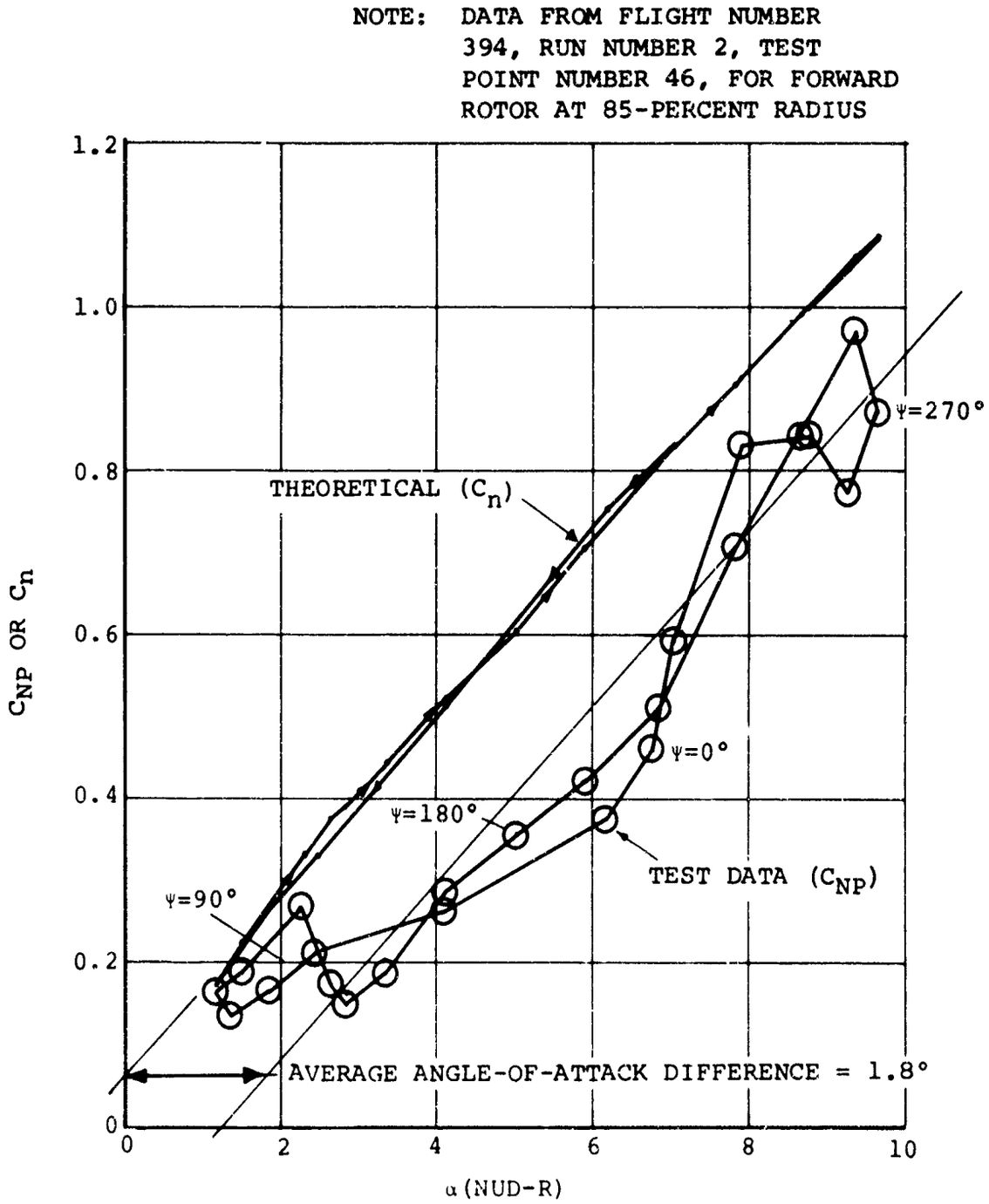

Figure 44. Typical Comparison of Normal Force Coefficient Data to Theoretical Prediction of Nonuniform-Downwash Rigid-Blade Analysis.

NOTES: 1. DATA RECORDED ON FLIGHT NUMBER 394, RUN NUMBER 2, TEST POINT NUMBER 46
2. $\overline{C_{NP}} = 0.46$

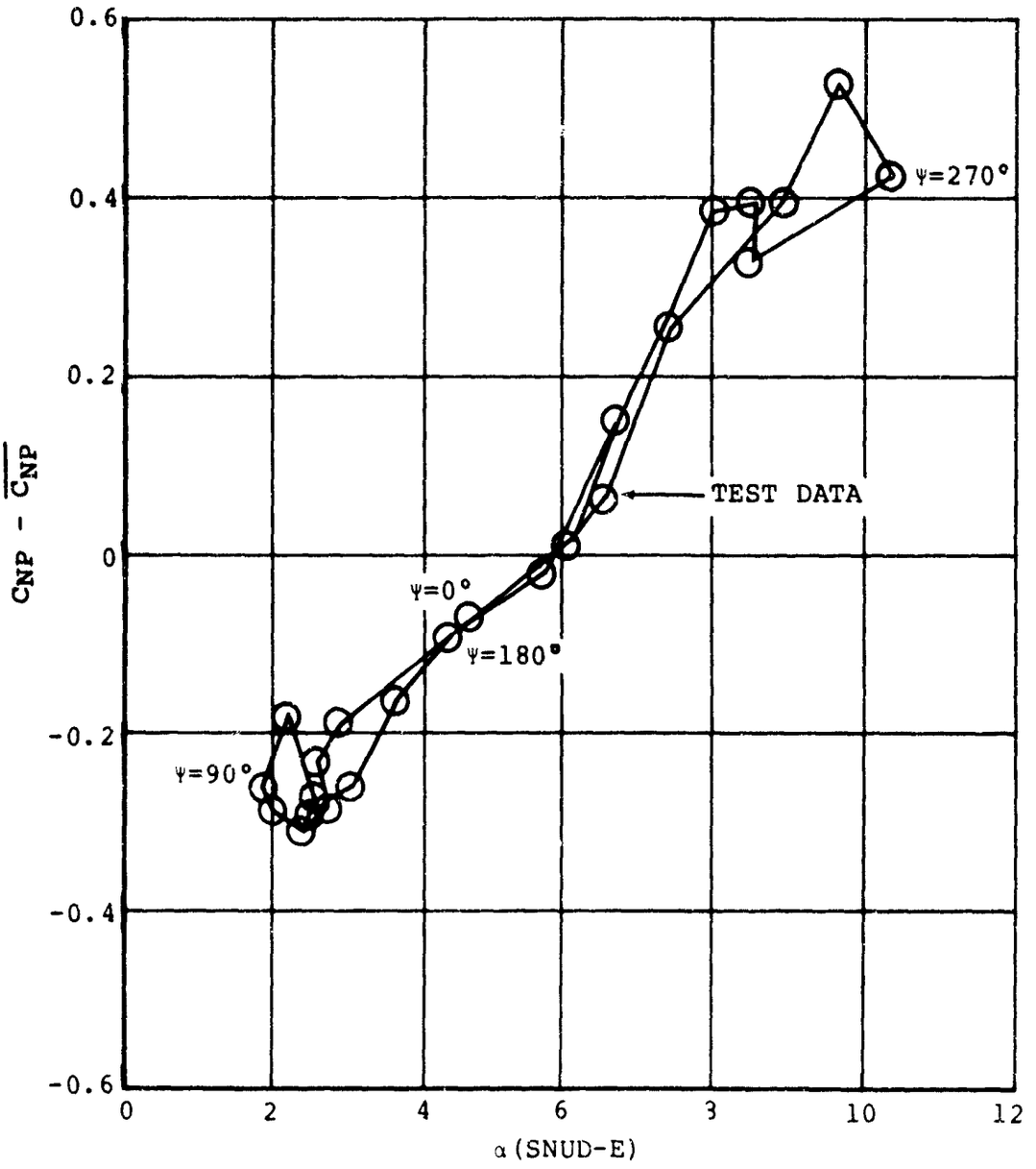

Figure 45. Typical Comparison of Normal Force Coefficient Data to Simplified Nonuniform-Downwash Elastic-Blade Theory.

NOTES: 1. DATA RECORDED ON FLIGHT NUMBER 394, RUN NUMBER 2, TEST POINT NUMBER 46
2. $\overline{C_{NP}} = 0.46$
3. DATA FOR FORWARD ROTOR AT 85-PERCENT RADIUS

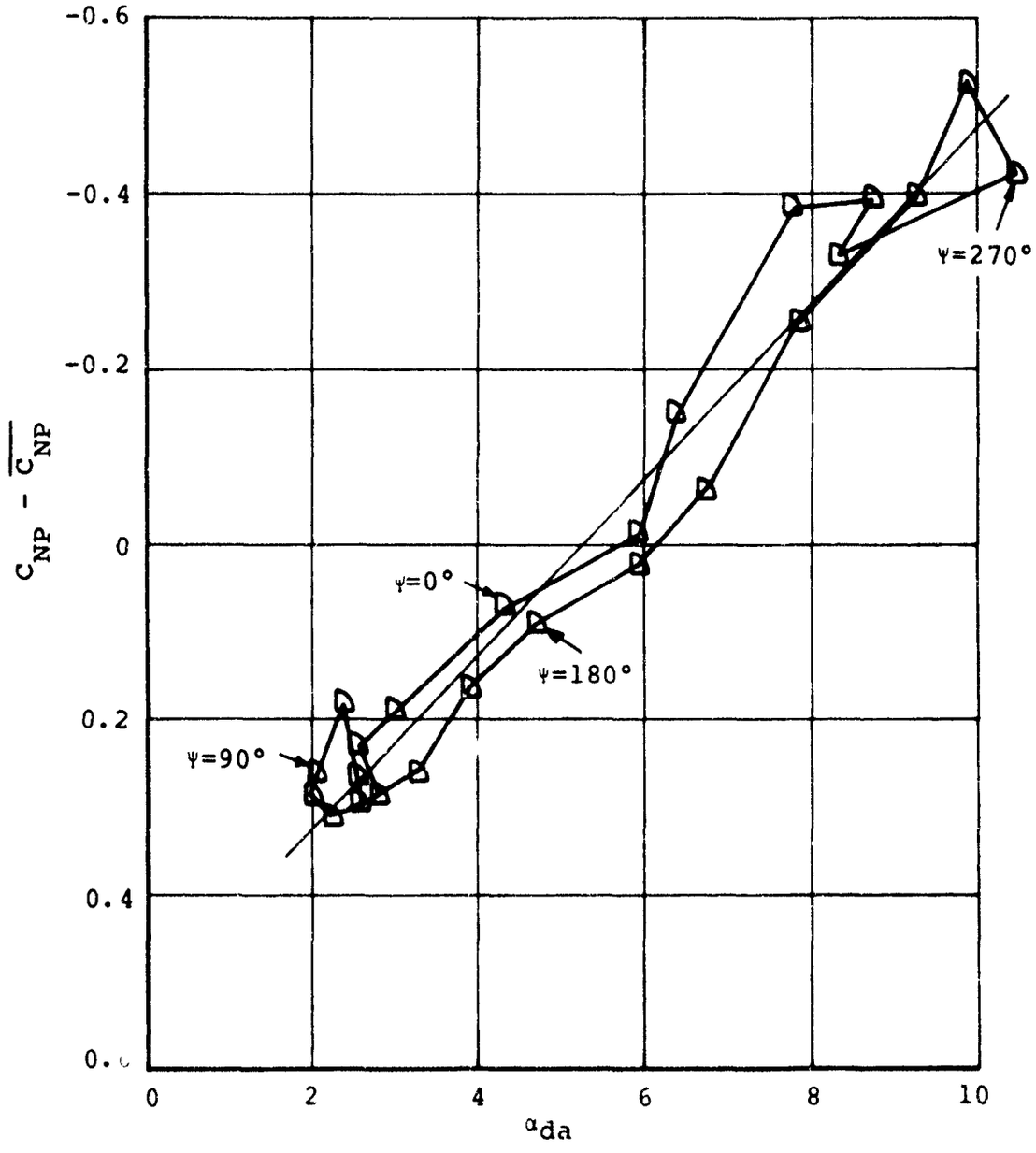

Figure 46. Effect of Adding Time-Dependence Correction to Angle-of-Attack Values from Simplified Nonuniform-Downwash Elastic-Blade Theory.

NOTES:
1. DATA FROM FLIGHT NUMBER 394, RUN NUMBER 2, TEST POINT NUMBER 46
2. THEORETICAL ANGLE OF ATTACK FROM NONUNIFORM-DOWNWASH ELASTIC-BLADE THEORY USING MEASURED CYCLIC TRIM AND FLAPPING ANGLES
3. SLOPE OF C_{NP}-α CURVE ASSUMED TO BE 5.73 PER RADIAN

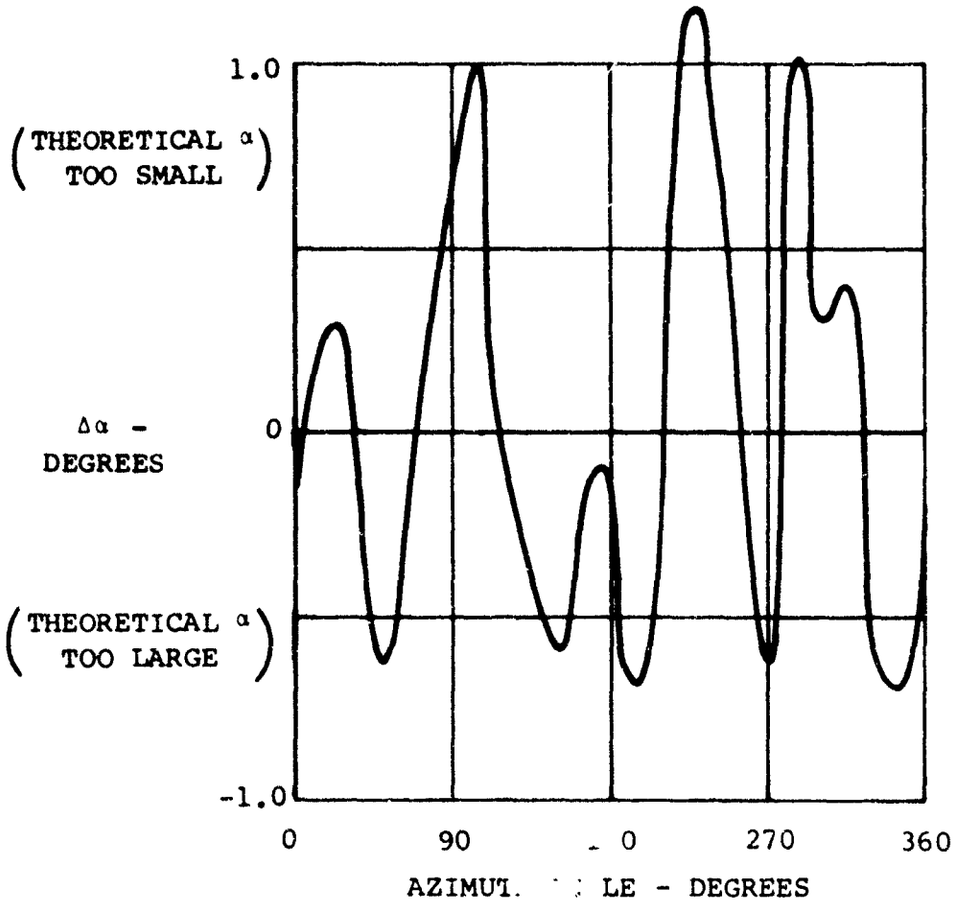

Figure 47. Angle-of-Attack Error of Simplified Nonuniform-Downwash Elastic-Blade Theory.

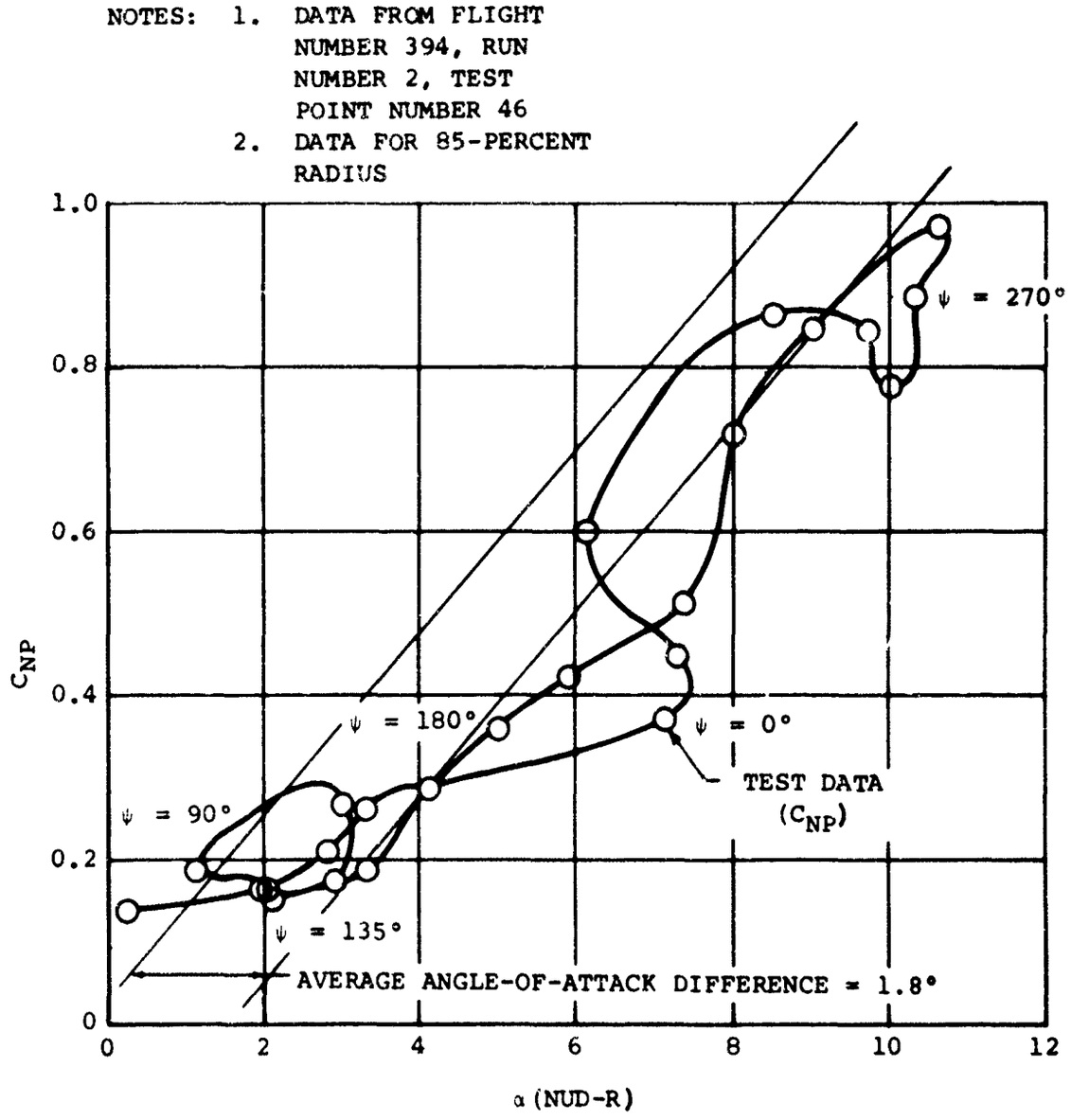

Figure 48. Comparison of Aft Rotor Normal Force Coefficient Data with Nonuniform-Downwash Rigid-Blade Theory.

COMMENTS ON THE SYNTHESIS OF AIRFOIL DATA

The possibility of the synthesis of airfoil data from the airload pressure measurements was suggested in reference 13, and efforts in this regard have continued. The present findings suggest that the approach should be modified somewhat and that this effort can also result in the prediction of the effects of sweep and the negative damping due to stall and compressibility. This effort remains an enormous task with a mandatory requirement for computer data processing, but the resulting increased understanding of rotor aerodynamics which can be produced is believed to be worthwhile.

The recommended approach is outlined in Figure 49. For the tandem rotor airloads data, the steps up to the calculation of the airloads coefficients have been accomplished and are published in reference 3. These data are illustrated in this volume and in Volume IV of this report. This task should also be accomplished for the other available airloads data.

It appears at this juncture that a program is necessary to improve the C_{MP}-C_{NP} relationship. A least-squares fit of a straight line should be made to the C_{MP} and C_{NP} data so that the mean aerodynamic center shift can be subtracted from the C_{MP} values. A statistical analysis of the aerodynamic center data should be made to evaluate this important parameter. It also appears from the data, of the type shown in Figure 32, that the vortex proximity spikes in the C_{MP}-C_{NP} relation should be faired. The prediction of the vortex spikes is probably important, but this is believed to be a separate, more complicated problem. Fairing these data could be accomplished by sequentially fitting circular arcs through every possible three data points between 0 and 120 degrees azimuth. The C_{MP} points which cause a large change in the circular arcs would be replaced by a faired value.

A significant change of philosophy in the synthesis is the recommended abandonment of rotor theory for the prediction of angle of attack. Since C_{NP} is closely related to angle of attack, the use of a theoretical value is unnecessary for the present purposes. While the C_{NP}/angle-of-attack relation probably becomes complicated when the sweep angles and sweep rates are significant, the rotor theories are also of questionable value for these conditions. A significant problem which must be resolved with this approach is that an effective

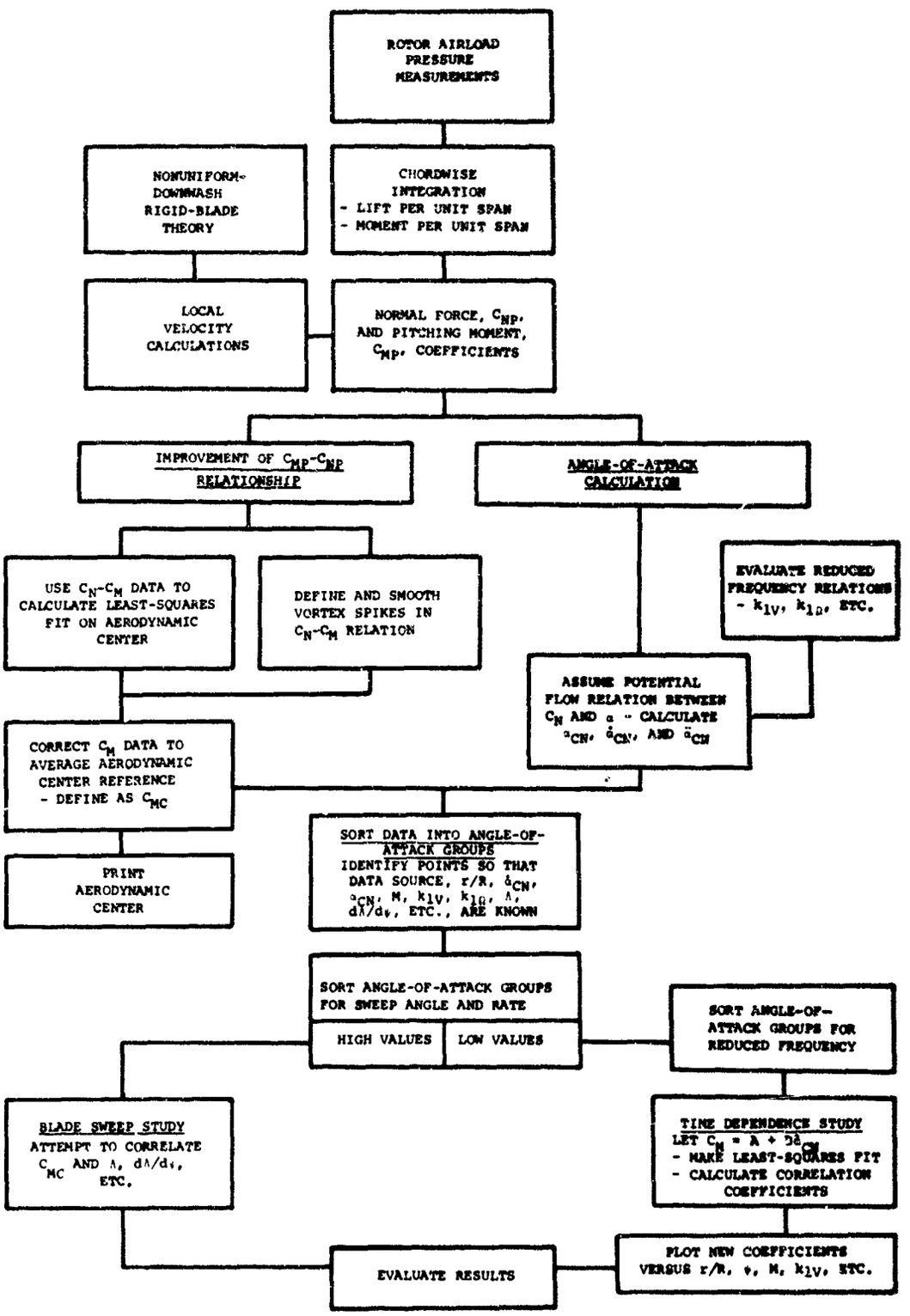

Figure 49. Block Diagram Illustrating Recommended Approach to Airfoil Synthesis from Rotor Blade Airload Pressure Measurements.

reduced frequency relation must be established. It may be found that the mixed motion effects of the higher harmonic variations on the predominantly first-harmonic variation must be considered. As a starting point, it appears that only the first-harmonic phase shift in the C_{NP}/angle-of-attack relation is required.

The next step recommended is to sort the data into angle-of-attack groups. This sorting must include transfer of all data point identification and the parameters of Mach number, angle of attack, angle of sweep, etc., for these points. The angle-of-attack groups should then be sorted for sweep angle and rate. A criterion for sweep angle and/or sweep rate for this sorting must be established; however, as shown in this report, sweep angles of 30 degrees amplitude are large. The large-sweep-angle data should be treated separately. The suggested sweep study cannot be defined at this time other than to suggest that attempts at correlation should be made between C_{MC} and Λ, $d\Lambda/d\psi$, etc.

The small-sweep-angle data should then be sorted into reduced frequency groups. A linear least-squares fit of a constant and the angle-of-attack rate term should then be made to correlate with available data. For the low angle-of-attack data groups, the coefficients, A and B, should be comparable to the potential flow values such as given in equation (7). At high angles of attack, these coefficients should be similar to the stall flutter damping coefficients of reference 5 or 20. If these coefficients do not compare, it is believed either that mixed motion is significant or that the reduced frequency evaluation was in error. Obviously, modifications must be made if this occurs. It is expected that the analysis will be comparable but that the simple C_{MC}-$\dot{\alpha}$ C_{CN} relation proposed gives poor correlation. This relation should then be expanded to include the cross-product terms $\alpha\dot{\alpha}$, $\alpha\ddot{\alpha}$, etc.

The approach to the synthesis of airfoil data suggested is believed to be straightforward, with the largest problems being produced by the large amount of data which must be manipulated. A substantiating theoretical analysis is required to establish an effective reduced frequency, but the first-order estimates presented earlier in this report could be used initially. The remaining tasks are sorting, fitting, and evaluating. This process must be iterative, starting with simple relationships and continually refining the fit. It is not expected that an exact fit will ever be obtained due to the inconsistent nature

of stall and the peculiarities of the unstable rotor wake; however, even the first iteration of this process should provide a significant improvement over the present rotor airfoil data.

CONCLUSIONS

1. Blade stall effects are clearly shown in the rotor airloads pressure measurements when these data are reduced to coefficient form. The most significant effect of stall illustrated by the airloads data is an aerodynamic negative pitch moment damping. Blade section normal force coefficient data do not show a significant change with stall.

2. Practical consequences of blade stall, as reflected in excessive loads or excessive blade motions, are not the same as the aerodynamic evidence of stall. Aerodynamic evidence of stall has been found for many test points well within the boundary of the thrust-coefficient/advance-ratio region of high dynamic loads. These test points were explored thoroughly in the development of the CH-47A helicopter to ensure that the blade loads and motions were satisfactory, and therefore these high-gross-weight low-speed test points were not studied in this program. However, the high-speed light-gross-weight test data obtained show "stall" effects in the rotor loads and motions data. These practical indications of stall (and/or compressibility) are the following:

   a. Blade flapping motion changed slightly with stall. A small increase in the longitudinal first-harmonic amplitude occurred. Eighth-harmonic flapping increased rapidly with stall, apparently due to a significantly increased third-mode flapwise blade bending.

   b. Rotor and hub drag (measured as shaft shear) increased significantly.

   c. Rotor power increased.

   d. Alternating flapwise blade bending at the 85-percent radius doubled.

   e. Chordwise blade bending at the midspan increased.

   f. Blade torsion and the resulting control loads show a significany change in azimuthal waveform due to stall Alternating control loads diverged sharply from the usual speed-squared relationship.

The relationships of aerodynamic stall to the practical manifestations of rotor problems are inadequately defined at the present time; study in this area should continue.

3. Blade stall as determined from the airloads pitching moment data appears to be related to the maximum normal force coefficient which is achieved; this relationship is dependent on Mach number. Aft rotor stalling appears to be more sensitive than that of the forward rotor to variations in the local retreating blade Mach number. The measured boundary values of maximum normal force coefficient and Mach number for rotor blade stalling are similar to static two-dimensional airfoil data.

4. Blade stall appears to be related in a complicated manner to the angle of attack of the retreating blade as calculated assuming rigid blades and uniform downwash. There is a pronounced effect of helicopter gross weight on this relationship, indicating that the blade section angle of attack is not calculated adequately with these simple assumptions. However, to make use of this convenient theory and to ensure that no pitching moment stall effects occur, a limiting angle of attack (based on this theory) of about 9 degrees should be imposed. If the section Mach number at the 75-percent radius of the retreating blade is greater than 0.3, this limitation should be used with particular caution. Practical consequences of stalling can occur if these limitations are exceeded.

5. Compressibility effects on the advancing blade can produce negative aerodynamic damping if the section Mach number exceeds 0.85. Both the forward and aft rotors experience compressibility effects but usually not at the same test point. This difference is believed to be due to the differences in the radial distribution of the blade loading on the two rotors.

6. Rotor blade section sweep appears to produce a significant delay in blade stall. Sweep and/or the rate of change of sweep apparently also tend to reduce aerodynamic damping.

7. Reversed-flow effects are shown to be more significant than expected. The reversed-flow region appears to be about 20 percent of the blade radius larger than the $r/R = -\mu' \sin\psi$ circle. Forward rotor loadings in reversed

flow are considerably different from those of the aft rotor, apparently because of the upwash at the forward rotor produced by the aft rotor.

RECOMMENDATIONS

1. The investigation of blade stall effects based on rotor airloads measurements begun in this report should be continued. A rigorous criterion for stall should be developed. Methods of predicting the magnitude of the negative aerodynamic damping due to stall are required. Time-dependent airfoil coefficient synthesis is recommended.

2. The effects of compressibility should be isolated from the available rotor airloads data. It is shown in this report that compressibility effects can be significant. A criterion for determining when compressibility effects become significant in producing rotor loads is required.

3. A separate study of reversed-flow effects should be made, as the reversed-flow region has been shown to be of greater significance than expected. The stall relief and negative damping due to blade section sweep should be studied and defined.

4. Rotor blade airfoil sections which have dynamic-aerodynamic characteristics at stall which are better suited to rotor operations should be developed. Pitching moment characteristics which give more damping at 5 to 8/rev. frequencies are needed.

5. Rotor blade designs with an increased third-mode flapwise bending frequency should be developed to reduce the coupled effects of stall. Sharply tapered outer blade panels should also be evaluated.

6. Resolution of rotor airloads data to a form which is usable in rotor analyses should follow the approach discussed in the text of this report. This airfoil section data synthesis is a sizable task and should be continued without further delay.

BIBLIOGRAPHY

1. Bisplinghoff, Ashley, and Halfman, Aero-Elasticity, Addison-Wesley Publishing Company, Inc., Reading, Mass., 1955.

2. Burpo, F.B., Measurement of Dynamic Airloads on a Full-Scale Semirigid Rotor, TRECOM Report 62-42, Fort Eustis, Virginia, December 1962.

3. Childs, R.C., and Grant, W.J., Tabular Test Data Summary of Measurements of Dynamic Airloads on a CH-47A Tandem Rotor Helicopter, Boeing Document D8-0387, to be issued.

4. Davenport, F.J., "A Method for Computation of the Induced Velocity Field of a Rotor in Forward Flight, Suitable for Application to Tandem Rotor Configurations," Journal of the American Helicopter Society, Volume 9, Number 3, July 1964.

5. Ham, N.D., and Young, M.I., "Torsional Oscillation of Helicopter Blades Due to Stall," Journal of Aircraft, Volume 3, Number 3, May-June 1966.

6. Harris, Franklin D., Spanwise Flow Effects on Rotor Performance, presented at the USAAVLABS-CAL Symposium on the Aerodynamic Problems Associated with V/STOL Aircraft, June 1966.

7. Henderson, B.O., et al., Rotor Load Correlation Report, Boeing-Vertol Report DYMR-9, December 1965.

8. Laprete, R., Boeing Wind Tunnel Test Number 927 - High Speed Force Tests to Determine Section Characteristics of VR-910M-1 Full Scale Airfoil Sections for Product Improvement of Vertol Division's CH-47, Boeing Document D2-24066-1, March 1966.

9. Loewy, R.G., "A Two-Dimensional Approximation to the Unsteady Aerodynamics of Rotary Wings," Journal of the Aeronautical Sciences, Volume 24, Number 2, February 1957.

10. McCloud, J.L., and McCullough, G.B., Comparison of Calculated and Measured Stall Boundaries of a Helicopter Rotor at Advance Ratios from 0.3 to 0.4, NACA Technical Note D-73, September 1959.

11. Myers, J.S., Subsonic and Transonic Test of VR-557M-1, Seven Partial-Span Helicopter Rotor Blades with a Geometric Aspect Ratio of Three, Boeing Memo Report 2-5352-91, BTWT 646, April 1961.

12. Piziali, R.A., and DuWaldt, F.A., A Method for Computing Rotary Wing Airload Distributions in Forward Flight, TRECOM Report Number TCREC TR 62-44, Fort Eustis, Virginia, November 1962.

13. Pruyn, R., and Alexander, W.T., Jr., The USAAVLABS Tandem Rotor Airloads Measurement Program, paper presented at the Aerodynamic Testing Conference of the American Institute of Aeronautics and Astronautics, Boeing Document D8-0381, September 1966.

14. Pruyn, Richard R., Analysis to Determine an Optimum Rotor for High Speed Helicopters, Kellett Aircraft Corporation Report Number 120A10-1 (Prepared under Navy Contract NOAS 58-718c), December 1958.

15. Purser, Paul E., and Spearman, M. Leroy, Wind Tunnel Tests at Low Speed of Swept and Yawed Wings Having Various Plan Forms, NACA Technical Note 2445, December 1951.

16. Reber, R.M., Flight Test Report - Dynamic Airloads Program, Boeing Document D8-0402, 27 May 1966.

17. Segel, L., A Method for Predicting the Nonperiodic Airloads on a Rotary Wing, AIAA 3rd Aerospace Sciences Meeting Paper 66-17, January 1966.

18. Sissingh, G., Contribution to the Aerodynamics of Rotating-Wing Aircraft, NACA TM 921, 1939.

19. Sweet, Jenkins, and Winston, Wind Tunnel Measurements on a Lifting Rotor at High Thrust Coefficients and High Tip-Speed Ratios, NASA Technical Note TN D-2462, September 1964.

20. Wang, Vaccaro, and DeSanto, A Practical Approach to the Problem of Stall Flutter, New York University OSR Technical Note Number 55-98 (Prepared under Air Force Contract AF 18(600)1372), June 1955.

21. Whitfield, A.A., and Blackburn, W.E., UH-2 Helicopter High-Speed Flight Research Program Utilizing Jet Thrust Augmentation, USATRECOM Technical Report 65-14, Fort Eustis, Virginia, March 1965.

22. Wood, E.R., Hilzinger, K.D., and Buffalano, A.C., An Aeroelastic Study of Helicopter Rotor Systems in High Speed Flight, CAL/TRECOM Symposium on Dynamic Load Problems Associated with Helicopters and V/STOL Aircraft, June 1963.

UNCLASSIFIED

Security Classification

DOCUMENT CONTROL DATA - R & D

(Security classification of title, body of abstract and indexing annotation must be entered when the overall report is classified)

1 ORIGINATING ACTIVITY (Corporate author)
The Boeing Company
Vertol Division
Morton, Pennsylvania

2a. REPORT SECURITY CLASSIFICATION
Unclassified

2b. GROUP
NA

3 REPORT TITLE
IN-FLIGHT MEASUREMENT OF ROTOR BLADE AIRLOADS, BENDING MOMENTS, AND MOTIONS, TOGETHER WITH ROTOR SHAFT LOADS AND FUSELAGE VIBRATION, ON A TANDEM ROTOR HELICOPTER

VOLUME V - INVESTIGATION OF BLADE STALL CONDITIONS

4 DESCRIPTIVE NOTES (Type of report and inclusive dates)
Final Report

5 AUTHOR(S) (First name, middle initial, last name)
Richard R. Pruyn

6 REPORT DATE	7a. TOTAL NO. OF PAGES	7b. NO OF REFS
April 1968	114	22

8a. CONTRACT OR GRANT NO	9a. ORIGINATOR'S REPORT NUMBER(S)
DA 44-177-AMC-124(T)	USAAVLABS Technical Report 67-9E
b. PROJECT NO: Task 1F125901A14604	
c.	9b. OTHER REPORT NO(S) (Any other numbers that may be assigned this report): Boeing Document D8-0382-5
d.	

10 DISTRIBUTION STATEMENT
This document has been approved for public release and sale; its distribution is unlimited.

11 SUPPLEMENTARY NOTES	12. SPONSORING MILITARY ACTIVITY
Volume V of a 5-volume report	U.S. Army Aviation Materiel Laboratories Fort Eustis, Virginia

13 ABSTRACT

This report describes the results of an investigation into helicopter rotor blade stall conditions. The goals of this research were to increase the comprehension of blade stall and to aid in the future design of rotor blades with greater aerodynamic efficiency. The problem of rotor blade stall is discussed, covering areas such as rotor performance limitations, static airfoil section performance, dynamic and aerodynamic effects of the rotor environment, and radial flow effects. The results of the tests are presented and described in detail; they include tests at the high dynamic loads boundary, evidence of stall in rotor loads and blade motion data, coefficients of rotor airloads, and indications of negative aerodynamic damping. The test results are weighed against theoretical methods of prediction for purposes of comparison. The use of airloads measurements in the synthesis of airfoil data is investigated and a method for doing so is provided. The conclusions drawn from these tests are presented and recommendations for future research in this field are given.

DD FORM 1 NOV 68 1473 REPLACES DD FORM 1473, 1 JAN 64, WHICH IS OBSOLETE FOR ARMY USE.

UNCLASSIFIED

Security Classification

14 KEY WORDS	LINK A		LINK B		LINK C	
	ROLE	WT	ROLE	WT	ROLE	WT
IN-FLIGHT MEASUREMENTS						
ROTOR BLADE AIRLOADS						
BLADE STALL						
REVERSED FLOW						
COMPRESSIBILITY						
HIGH DYNAMIC LOADS						
EVIDENCE OF STALL						
COEFFICIENTS OF ROTOR AIRLOADS						
NEGATIVE AERODYNAMIC DAMPING						
STALL EFFECTS						
COMPRESSIBILITY EFFECTS						
RADIAL FLOW EFFECTS						
THEORETICAL PREDICTIONS						
SYNTHESIS OF AIRFOIL DATA						